PHOSPHATE ADSORPTION ONTO GRANULAR FERRIC HYDROXIDE (GFH) FOR WASTEWATER REUSE

vorgelegt von
Diplom-Ingenieur
Alexander Sperlich
aus Berlin

von der Fakultät III - Prozesswissenschaften -
der Technischen Universität Berlin
zur Erlangung des akademischen Grades
Doktor der Ingenieurwissenschaften
- Dr.-Ing. -

genehmigte Dissertation

Promotionsausschuss:

Vorsitzender: Prof. Dr. rer. nat. Wolfgang Rotard
Berichter: Prof. Dr.-Ing. Martin Jekel
Berichter: Prof. Dr. rer. nat. Eckhard Worch

Tag der wissenschaftlichen Aussprache: 08. Juli 2010

Berlin 2010

D 83

ACKNOWLEDGEMENTS

The research presented here was carried out in projects funded by the German Federal Ministry of Education and Research (BMBF) and the European Commission under the 6th Framework Programme, which is gratefully acknowledged.

Prof. Dr.-Ing. Martin Jekel was the supervisor of this work and has always supported me during this research. I thank him for giving me the opportunity to work in his group and opening up many possibilities for me. I was glad to have Prof. Dr. rer. nat. Eckhard Worch in my committee. With his profound knowledge of adsorption, he was always available for discussions on adsorption modeling. Thanks also to Prof. Dr. rer. nat. Wolfgang Rotard for taking over the chair of the thesis committee.

I would also like to thank Sebastian Schimmelpfennig for his enthusiasm and programming skills which resulted in the software FAST. I have fond memories of the time we spent improving FAST, understanding and comparing adsorption models and completing our joint paper. Carsten Bahr and Dr.-Ing. Xing Zheng are acknowledged for making the considerable amount of time we spent sharing the same office very enjoyable. With Carsten, I was fortunate to have a co-worker who was also researching GFH adsorption and always willing to help me out in the lab or by providing the necessary carbohydrates (Gummibärchen etc.) or just by cheering me up. Working with Xing Zheng, I spent some weeks in China and I thank him for making this an unforgettable time for me and for overcoming any problems with the pilot plant in Beijing.

This work would not have been possible without the hard-working and excellent students which I had the pleasure to work with (in alphabetical order): Sabrina Bahnmüller, Benno Baumgarten, Jin Chen, Benito J. Martín Cuevas, Tanja Ratuzny, Mathias Riechel, Alrun Schneider, Stefan Schulz, David Warschke and Christine Wegmann.

In the very beginning of this research, I "inherited" all the experimental setup for adsorption experiments from Dr.-Ing. Arne Genz. I thank him for introducing me to this research and the group, his help and willingness to discuss my results even years after completing his own research. As the project leader, Dr.-Ing. Mathias Ernst has always been covering my back in the research projects and helped me a lot. I always enjoyed the discussions on this work with Prof. Dr. Gary Amy. His comments, suggestions and thought-provoking questions proved very helpful to me. I also wish to thank Anja Sandersfeld and Sebastian Aust for making the FSP-WIB office a very pleasant working environment.

Concentrating on experimental work and modeling was only possible with the help of the hard-working and reliable laboratory staff. Angelika Kersten and Katrin Noack have to be mentioned for the great number of samples which were analyzed for phosphate, but I also wish to thank all the other helping hands in the lab.

For proof-reading the manuscript I especially thank Anja Sandersfeld and Hannelore Meingast. Also, both of them and Karin von Nordheim were of great help solving any administrative issue. I greatly appreciated the help of Werner Däum-

ler, Hans Rietdorf, Thomas Thele and Wolfgang Wichmann whenever something needed to be constructed, repaired or any computer issue needed to be solved.

Dr.-Ing. Wolfgang Driehaus and Wilhelm Depping (GEH Wasserchemie) is thanked for a steady supply with GFH material and helpful discussions on adsorber design and practice. I appreciated the support of Prof. Dr. Zhao Xuan and Dr. Cheng Chuzhou during my stay at Tsinghua University. Thanks also to Berliner Wasserbetriebe for supplying secondary effluent. Many thanks also to Stephan Costabel from the Chair of Applied Geophysics for his help with the BET surface measurements.

Finally, I wish to express my gratitude to all of my co-workers at the Chair of Water Quality Control, who create this special atmosphere which makes working there very enjoyable. The last five years have been a very good time for me. Thank you all very much.

ABSTRACT

Adsorption onto Granular Ferric Hydroxide (GFH), a commercially available, synthetic adsorbent is studied as treatment process for phosphorus removal from wastewater. The objective is to evaluate the suitability of this process alternative for advanced wastewater treatment and reuse. Within this scope, the present work focusses on quantification of competitive adsorption of phosphate and development of a regeneration process that allows multiple application of GFH. Furthermore, breakthrough prediction of GFH fixed-bed columns is assessed.

Adsorption of phosphate in artificial model solutions, natural and waste waters onto GFH was studied in batch and fixed-bed column experiments. Equilibrium isotherms and adsorption edges show that phosphate adsorption is strongly pH dependent. High capacities of up to 24 mg/g P (at pH 6 and an equilibrium concentration of 2 mg/L P) can be reached. Presence of calcium is shown to improve adsorption of phosphate. This is supposed to be the reason for higher capacities in waste and drinking water as compared to DI water and membrane concentrates. The diffuse double layer model can in principle be used to describe phosphate adsorption onto GFH, but fails to describe simultaneous adsorption of phosphate and calcium.

Whereas generally effective for phosphate removal from NF concentrates, GFH adsorption cannot be recommended for membrane concentrate treatment. Since membrane concentrates are often supersaturated with respect to calcium carbonate and/ or calcium phosphate compounds, this can lead to scaling and head loss in the fixed-bed column. Chemical precipitation can effectively remove phosphate and calcium ions and thus reduce the scaling potential of membrane concentrates. This may allow for higher recoveries in the NF/ RO process.

Rapid small-scale column tests (RSSCTs) were shown to be a useful tool for simulation of fixed-bed columns. Isotherm results can be used to provide a rough estimation of operation time, i.e. the ideal breakthrough point of a fixed-bed column, but are of limited use due to the strong influence of mass transfer on the shape of the breakthrough curve. RSSCTs using different empty-bed contact times show that phosphate adsorption kinetics onto GFH are very slow and result in asymptotically shaped breakthrough curves. Analysis of breakthrough data proves that operation of two GFH beds in series can contribute to a more efficient use of the adsorbent.

Breakthrough curves were modeled using the homogeneous surface diffusion model (HSDM) and two of its derivatives, the constant pattern homogeneous surface diffusion model (CPHSDM) and the linear driving force model (LDF). Input parameters, the Freundlich isotherm constants, and mass transfer coefficients for liquid- and solid-phase diffusion were determined and analysed for their influence on the shape of the breakthrough curve. HSDM simulation results predict the breakthrough of phosphate, and the also investigated adsorbates arsenate, salicylic acid, and DOC satisfactorily. Due to a very slow intraparticle diffusion and hence higher Biot numbers, LDF and CPHSDM could not describe arsenate breakthrough correctly. Based on this observation, limits of applicability were defined for LDF

and CPHSDM. When designing fixed-bed adsorbers, model selection based on known or estimated Biot and Stanton numbers is possible.

GFH is stable at high pH and can be efficiently regenerated using 1 M NaOH. Approximately 80 % of the initially bound phosphate can be eluated. However, the incomplete desorption leads to decreasing capacities with each additional use. Multiple uses are thus limited, but at least three operation cycles are feasible. GFH desorption is fast and most of the desorbable phosphate could be eluated using 4 - 6 bed volumes of regenerant. A reuse of the regenerant solution is possible. Despite high phosphate concentrations in the regenerate, 61 - 85 % of the bound phosphate could be desorbed. Phosphate can be recovered from the highly concentrated regenerant stream (up to 3.5 g/L P). Precipitation with lime water resulted in 90 % P removal and a plant available precipitate which might be used as a fertilizer. Regeneration and multiple use of GFH can significantly increase operation times of fixed-bed adsorbers and be an economically favourable option compared to single use.

Laboratory results were confirmed in pilot-scale experiments in Beijing, China which show that selective nutrient removal by adsorption onto GFH after a membrane bioreactor (MBR) can maintain a total phosphorus concentration of < 0.03 mg L^{-1} P, thus preventing eutrophication of artificial lakes.

In conclusion, GFH adsorption is an effective and promising treatment technique to remove phosphorus from waste and surface waters. Economic use is limited to special applications where near zero effluent concentrations are required. Regeneration and serial operation prolonge operation times of fixed-bed columns and decrease the specific adsorbent costs.

ZUSAMMENFASSUNG

Gegenüber den herkömmlichen Verfahren zur Phosphatentfernung kann es bei bestimmten Fragestellungen der Abwasserwiederverwendung sinnvoll sein, Phosphat bis auf ganz geringe Restkonzentrationen zu entfernen. Dies kann beispielsweise bei der Wiederverwendung von Abwasser in Landschaft gestaltenden künstlichen Gewässern der Fall sein. Dass Eisenhydroxide hohe Adsorptionskapazitäten für Phosphat zeigen, ist seit langem bekannt.

Ziel der vorliegenden Arbeit ist es, die Phosphatadsorption an kommerziell verfügbare Adsorbentien auf Eisenbasis hinsichtlich der Eignung für die weitestgehende Abwasserreinigung und Abwasserwiederverwendung zu bewerten. Im Mittelpunkt der Untersuchungen steht Granuliertes Eisenhydroxid (GEH), das vor allem in der Arsenentfernung eingesetzt wird. Zentrale Fragestellung ist die Quantifizierung der konkurrierenden Adsorption von Abwasserinhaltsstoffen und der damit einhergehenden Kapazitätsverluste und die Entwicklung eines Regenerationsverfahrens, dass die Wiedernutzung des Adsorbens ermöglicht. Schließlich soll eine Methodik zur Vorhersage des Durchbruchs von Festbettadsorbern mittels mathematischer Modelle erarbeitet werden.

Laborversuche mit Abwasser, natürlichen Wässern und Modelllösungen zeigen eine starke pH-Abhängigkeit der Adsorption von Phosphat an GEH. Hohe Beladungen von bis zu 24 mg/g P (bei pH 6 und einer Gleichgewichtskonzentration von 2 mg/L P) werden erreicht. In Abwasser und Trinkwasser werden höhere Beladungen beobachtet als im reinen System (vollentsalztes Wasser). Als Grund wird die Anwesenheit von Calcium vermutet, die die Adsorption von Phosphat an GEH deutlich verbessert. Eine modellhafte Beschreibung der Adsorption mittels des Doppelschichtmodells ist prinzipiell möglich, eine Simulation der simultanen Adsorption von Phosphat und Calcium gelingt jedoch nicht.

Obwohl mittlere Phosphatbeladungen im Membrankonzentrat beobachtet werden, ist die Adsorption an GEH nicht geeignet für die Aufbereitung von Membrankonzentrat. Übersättigte Konzentratlösungen führen zu Ausfällungen und Druckverlust in den Festbettfiltern. Mittels chemischer Fällung können Phosphat und Calcium effektiv entfernt und das Scalingpotential deutlich verringert werden, was eine Erhöhung der Ausbeute in der Hochdruckmembranfiltration ermöglicht.

Kleinfilterversuche (Rapid small-scale column tests - RSSCT) sind ein wichtiges Hilfsmittel zur Simulation von Festbettadsorbern. Mittels Isothermenversuchen kann der ideale Durchbruch von Festbettfiltern berechnet werden, dessen Aussagekraft jedoch aufgrund des großen Einflusses der Kinetik auf die Form der Durchbruchskurve begrenzt ist. Kleinfilterversuche zeigen, dass die Kinetik der Adsorption von Phosphat an GEH sehr langsam ist und zu asymptotisch geformten Druchbruchskurven führt. Anhand von Durchbruchsdaten konnte zudem gezeigt werden, dass die Reihen-Wechsel-Schaltung von Festbettadsorbern eine bessere Ausnutzung des Adsorbens ermöglicht.

Experimentell aufgenommene Durchbruchskurven lassen sich mit dem Oberflächendiffusionsmodell (HSDM) und zwei abgeleiteten Modellen, CPHSDM und LDF, darstellen. Der Einfluss der experimentell bestimmten Modelleingabeparameter wie der Freundlich-Isothermenkonstanten und der Stoffübergangskoef-

fizienten der Film- und Korndiffusion auf die Form der Durchbruchskurve wurde analysiert. Der Durchbruch von Phosphat und den ebenfalls untersuchten Adsorbaten Arsenat, Salicylsäure und DOC konnte mit dem HSDM zufriedenstellend wiedergegeben werden. Durch den sehr langsamen inneren Stofftransport treten höhere Biot-Zahlen auf, bei denen LDF und CPHSDM den Durchbruch nicht korrekt vorhersagen können, wie für Arsenat beobachtet wurde. Anhand dieser Ergebnisse wurden Anwendungsgrenzen für LDF und CPHSDM definiert und gezeigt, dass eine Modellauswahl mittels bekannter oder abgeschätzter Biot- und Stanton-Zahlen möglich ist.

GEH ist auch bei hohen pH-Werten stabil und eine Regeneration mittels NaOH ist möglich. Etwa 80 % des anfangs adsorbierten Phosphats können eluiert werden. Die unvollständige Desorption führt zu Kapazitätsverlusten mit jeder Wiedernutzung, deren Anzahl dadurch begrenzt ist. Es sind mindestens drei Betriebszyklen ohne Wechsel des Materials möglich. Die Desorption von Phosphat ist schnell und der Hauptteil des gebundenen Phosphats kann innerhalb der ersten 4 - 6 Bettvolumen eluiert werden. Die gebrauchte Natronlauge kann wiederverwendet werden. Trotz dadurch auftretender hoher Phosphatkonzentrationen in der Regeneratlösung, können 61 - 85 % des gebundenen Phosphats desorbiert werden. Eine Phosphorrückgewinnung aus der konzentrierten Lauge (bis zu 3.5 g/L P) ist möglich: mittels chemischer Fällung durch Zugabe von Kalkmilch können ca. 90 % des Phosphats entfernt werden. Das Präzipitat ist pflanzenverfügbar und kann als Dünger genutzt werden. Die Regeneration und Mehrfachnutzung von GEH erhöht die Standzeiten der Adsorber deutlich und ermöglicht einen kostengünstigeren Einsatz des Verfahrens.

Die Ergebnisse der Laborexperimente zur Adsorption und Regeneration wurden durch Pilotversuche auf einer Kläranlage in Peking (China) bestätigt. Durch selektive Nährstoffentfernung mittels Adsorption an GEH anschließend an einen Membranbioreaktor kann eine Ablaufkonzentration von < 0.03 mg L^{-1} P Gesamtphosphor sicher eingehalten werden. Dadurch kann die Eutrophierung künstlicher Seen verhindert werden.

Zusammenfassend ist festzustellen, dass die Adsorption an GEH für die Phosphorentfernung aus Abwasser und Oberflächenwasser geeignet ist. Ein ökonomisch sinnvoller Einsatz beschränkt sich auf Anwendungen, in denen sehr geringe Restkonzentrationen benötigt werden. Regeneration und Reihen-Wechsel-Schaltung verlängern die Standzeiten der Adsorber und verringern die spezifischen Materialkosten.

CONTENTS

LIST OF FIGURES

LIST OF TABLES

ACRONYMS

ATP Adenosine Triphosphate

BES N,N-Bis(2-hydroxyethyl)-2-aminoethanesulfonic Acid

BET Brunauer-Emmett-Teller Isotherm

BF Bank Filtration

BNR Biological Nutrient Removal

BOD_5 Biological Oxygen Demand

BTC Breakthrough Curve

BV Bed Volumes

BXH Beixiaohe

CAS Conventional Activated Sludge

CD Constant Diffusivity Approach

CD-MUSIC Charge Distribution and Mult-Site Complexation Model

CMBR Completely-mixed Batch Reactor

COD Chemical Oxygen Demand

DCBR Differential Column Batch Reactor

DDL Diffuse Double Layer Model

DFHSDM Dispersed-flow Homogeneous Surface Diffusion Model

DFPSDM Dispersed-flow Pore and Surface Diffusion Model

DI De-ionized Water

DNA Desoxyribonucleic Acid

DOC Dissolved Organic Carbon

DW Drinking Water

EBCT Empty-bed Contact Time

EBPR Enhanced Biological Phosphorus Removal

EXAFS Extended X-ray Absorption Fine-structure Spectroscopy

FAST Fixed-bed Adsorption Simulation Tool

FS FerroSorp

FT-IR Fourier Transformed Infrared Spectroscopy

GAC Granular Activated Carbon

GFH Granular Ferric Hydroxide

GW Ground Water

HLR Hydraulic Loading Rate

HSDM (Plug-flow) Homogeneous Surface Diffusion Model

KMP Potassium Magnesium Phosphate

LC Laboratory-scale Column

LC-OCD Liquid Chromatography with Organic Carbon Detection

LEM Local Equilibrium Model

LDF Linear Driving Force Model

MAP Magnesium Ammonium Phosphate

MBR Membrane Bioreactor

MES 2-(N-morpholino)ethanesulfonic Acid

MWCO Molecular Weight Cut-off

NF Nanofiltration

NOM Natural Organic Matter

OECD Organisation for Economic Co-operation and Development

P Phosphorus

PAC Poly-aluminium Chloride

PD Proportional Diffusivity Approach

PDE Partial Differential Equation

PEST Parameter Estimation Tool

PSDM (Plug-flow) Pore and Surface Diffusion Model

RO Reverse Osmosis

RSSCT Rapid Small-scale Column Test

SCM Surface Complexation Model

SFBR Short Fixed-bed Reactor

SP Soluble Phosphorus

SSF Slow Sand Filtration

SRP Soluble Reactive Phosphorus

SUP Soluble Unreactive Phosphorus

TAPS (N-Tris(hydroxymethyl)methyl-3-aminopropanesulfonic Acid

TDP Total Dissolved Phosphorus

TDS Total Dissolved Solids

TMP Trans-membrane Pressure

TP Total Phosphorus

UF Ultrafiltration

U.S. EPA United States Environmental Protection Agency

$UV_{254/436}$ UV Absorption at 254/ 436 nm

WCF Water Conversion Factor

WWTP Wastewater Treatment Plant

LIST OF NOTATION

$A_{0..4}$	coefficients of CPHSDM	-
Bi	Biot number, $Bi = k_L r_P c_0/(D_S \rho_P q_o)$	-
c	liquid-phase concentration	M/L^3
c_0	influent liquid-phase concentration	M/L^3
c^*	liquid-phase concentration at exterior adsorbent surface	M/L^3
D_g	solute distribution parameter, $D_g = \rho_B q_0/(\epsilon_B c_0)$	-
D_S	surface diffusion coefficient	L^2/t
$EBCT$	empty-bed contact time, $EBCT = m/(\rho_B Q)$	t

Ed	diffusivity modulus, $Ed = St/Bi$	-
K_F	Freundlich isotherm coefficient	$(L^3/M)^n$
k_L	liquid-phase mass transfer coefficient	L/t
L	length of fixed-bed	L
m	mass of adsorbent	M
n	Freundlich isotherm exponent	-
N	number of simulated data points	-
q	solid-phase concentration	M/M
q_0	solid-phase concentration in equilibrium with influent liquid-phase concentration, $q_0 = K_F \cdot c_0{}^n$	M/M
q^*	solid-phase concentration at exterior adsorbent surface	M/M
$\bar{q}$	average solid-phase concentration	M/M
Q	fluid flow rate	L^3/t
r	radial coordinate	L
r_P	radius of adsorbent grain	L
R	dimensionless radial coordinate, $R = r/r_P$	-
ΔR	discretisation grid width for dimensionless radial coordinate	-
St	modified Stanton number, $St = k_L m/(r_P \rho_P Q)$	-
St_{min}	minimum Stanton number required to establish constant pattern	-
t	time coordinate	t
T	dimensionless time coordinate, $T = t/(EBCT\epsilon_B D_g)$	-
ΔT	discretisation grid width for dimensionless time coordinate	-
v_F	superficial filter velocity, hydraulic loading rate (HLR)	L/t
X	dimensionless liquid-phase concentration, $X = c/c_0$	-
X^*	dimensionless liquid-phase concentration at exterior adsorbent surface	-
$\Delta\bar{X}$	arithmetic mean of absolute differences between model simulations	-
Y	dimensionless solid-phase concentration, $Y = q/q_0$	-
Y^*	dimensionless solid-phase concentration at exterior adsorbent surface	-

z	axial coordinate	L
Z	dimensionless axial coordinate, $Z = z/L$	-
ΔZ	discretisation grid width for dimensionless axial coordinate	-
α	Courant number of filter PDE (6.3), $\alpha = D_g \Delta T/\Delta Z$	-
β	numerical stability number of filter PDE (6.3), $\beta = 3StD_g\Delta T$	-
γ	Courant number of intraparticle PDE (6.6), $\gamma = Ed\Delta T/\Delta R^2$	-
ϵ_B	bed porosity	-
ρ_P	density of adsorbent grain	M/L^3
τ	packed-bed (effective) contact time, $\tau = EBCT/\epsilon_B$	t
	Subscribes	
i	index of grid cell for time coordinate	-
j	index of grid cell for axial coordinate	-
k	index of grid cell for radial coordinate	-

1 GENERAL INTRODUCTION

Advanced phosphorus removal to near zero levels cannot be achieved by traditional biological nutrient removal and chemical precipitation processes, but will become increasingly important for a number of different applications such as wastewater reuse in artificial lakes, advanced wastewater treatment due to increasingly stringent regulation on phosphorus discharge, as well as restoration of eutrophic surface water bodies.

In this study, phosphate adsorption onto Granular Ferric Hydroxide (GFH), a commercially available ferric hydroxide adsorbent was investigated for its suitability in wastewater reuse applications. GFH has been developed 1990-1994 and is mainly applied for removal of arsenic from water [36, 35, 38]. Given that ferric hydroxides have been known for high affinities for phosphate adsorption, phosphate was identified as a major competitor for arsenic adsorption and the potential use of GFH for phosphate removal was proposed.

As early as 1997, GFH was used in the restoration of Lake Plötzensee [63, 70]. In pilot-scale operation, severe problems due to algae growth on the adsorbent material occured. As a consequence, high head loss was observed and frequent backwash was required, which led to abrasion because of the low mechanical strength of the adsorbent. In these very early trials, the GFH production process was still under development and an increase of the mechnical strength was targeted.

In 2002, a screening of several commercial adsorbents for phosphorus removal in fresh and sea water aquariums was done, and the GFH-based product RowaPhos showed the highest adsorption capacities [75].

Within the framework of a larger research project on decentralized wastewater treatment using membrane bio-reactors (MBR), GFH and activated alumina were tested as a polishing step for MBR filtrates in laboratory-scale [57, 61]. Results showed pH-dependent high phosphate adsorption capacities for GFH and no significant effect of competition by other organic or inorganic compounds. In conclusion, pilot operation was recommended to study breakthrough characteristics and GFH fixed-bed operation in larger scale.

The present study was initiated through the joint Chinese-German project "Sustainable water concept and its application for the Olympic Games 2008". Within this project, GFH phosphate removal from wastewater and subsequent water reuse in an artificial lake was tested. Next to this pilot study, extensive laboratory studies were done to quantify competitive adsorption of phosphate and wastewater constituents and its effect on operation times of fixed-bed adsorbers. A regeneration process for GFH which enables the multiple application of GFH has been investigated. Using mathematical models, a methodology for breakthrough prediction of fixed-bed adsorbers has been developed.

In chapter 2, available literature on phosphate adsorption onto ferric hydroxide surfaces is reviewed. An overview is given on phosphorus chemistry and occurrence, the fundamentals of adsorption, modeling of fixed-bed systems, and regeneration.

The equilibrium of the adsorption of phosphate onto GFH is investigated in chapter 3. The influence of water composition and competition of drinking water and wastewater constituents is assessed in isotherm experiments. For comparison, two alternative adsorbents are tested. Column experiments are used to simulate breakthrough of fixed-bed adsorbers under different water qualitity and operational conditions.

In chapter 4, the diffuse double layer (DDL) model is tested to describe the adsorption equilibrium data. Formation of three mononuclear phosphate surface complexes is hypothesized and equilibrum constant are determined. The interaction of phosphate and calcium adsorption is investigated and description by the DDL model tested.

In chapter 5, focus is shifted towards the treatment of membrane concentrates. Due to the rejection of polyvalent anions by nanofiltration and reverse osmosis membranes, high concentrations of phosphate occur in membrane concentrates. Treatment to i) increase the recovery of the membrane filtration and minimize the volume of the concentrate stream, and ii) increase the concentrate quality to enable discharge into surface water bodies are evaluated. Within the latter scope, GFH adsorption is tested as a polishing step for membrane concentrates.

Breakthrough prediction of GFH fixed-bed filters is addressed in chapter 6. Adsorbate and matrix specific constants describing adsorption equilibrium and mass transfer are determined for arsenate, phosphate, salicylic acid, and groundwater DOC. Breakthrough curves are experimentally determined and modeled using the homogeneous surface diffusion model (HSDM) and two of its derivatives, the constant pattern homogeneous surface diffusion model (CPHSDM) and the linear driving force model (LDF). The input parameters are analyzed for their influence on the shape of the breakthrough curve and limits of model applicability are determined.

Chapter 7 provides a detailed evaluation of regeneration and multiple application of GFH and comparison to an alternative adsorbent. Due to the potential creation of a toxic and hardly disposable concentrate stream, regeneration of arsenic loaden adsorbent material is neither investigated nor desired. However, if GFH adsorption is used for phosphate or DOC removal, regeneration can increase operation time and cost effectiveness. A regenerant solution containing phosphate is not toxic and could be safely disposed off. The main objective of this study is to quantify the efficiency of phosphate desorption and address the question whether multiple application results in a loss of adsorption capacity. Kinetics of desorption and recovery of phosphorus from the regenerate stream is also evaluated.

Chapter 8 focusses on pilot-scale operation of GFH adsorption columns for advanced wastewater treatment and reuse. A sustainable water concept developed for different applications of municipal water reuse is tested in a pilot-scale study in Beijing's wastewater treatment plant Beixiaohe. The selective phosphate removal from a membrane bio-reactor effluent and reuse in an artificial lake is investigated.

2 LITERATURE REVIEW

2.1 CHEMISTRY, OCCURRENCE AND ENVIRONMENTAL RELEVANCE OF PHOSPHORUS

2.1.1 *Chemistry and natural occurrence*

Phosphorus (P), having the atomic number 15 and an atomic weight of 30.97376 is the eleventh most abundant element in the earth's crust and widely present in rocks, soils, waters and in living organisms. Phosphorus compounds play a crucial role in life processes, forming the backbone of the DNA and being involved in metabolic energy transfer as ATP and related compounds, yet are also among the most toxic substances known, used as chemical warfare agents and as pesticides. There are more than 100,000 known phosphorus compounds of which the majority contain linkages to oxygen, carbon, nitrogen and metals. Under most conditions, naturally occuring phosphorus is exclusively combined with four oxygen molecules, forming the phosphate oxyanion [18].

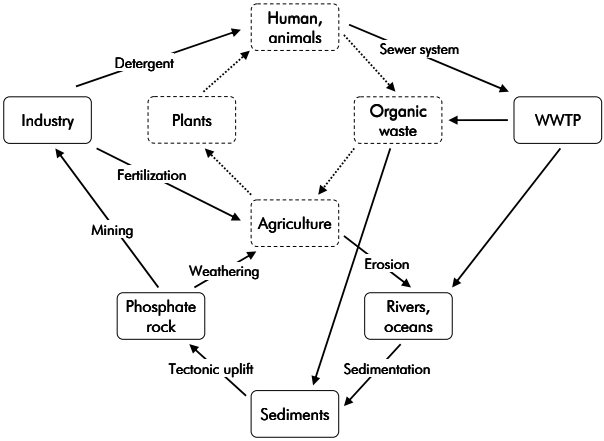

Figure 1: Geological and biological (land) phosphorus cycle including anthropogenic influence, aquatic cycle not shown [22]

Phosphorus in natural and waste waters is distributed between various physical compartments, including: a dissolved fraction comprising both inorganic and organic P species; a colloidal fraction associated with both inorganic colloids

such as clays and organic macromolecules including humic and fulvic acids; a particulate component including P species adsorbed to particle surfaces or retained in the particle matrix and also a biological constituent associated with aquatic organisms such as algae or bacteria [30].

In nature, phosphorus passes through several interconnected cycles. The geological cycle of phosphorus includes erosion, transport to the oceans, sedimentation, tectonic uplift and alteration of phosphate-containing rocks into plant-available phosphate in soils. The cycle time is several million years [22, 50, 118]. Besides the geological cycle, phosphorus is cycled as part of the food chain on land and in aquatic systems, with cycle times ranging between a few weeks and up to one year [22, 118]. The global P cycle has been modified extensively with modern human (agricultural, urban and industrial) practices. As a result, fluxes of P have doubled during the past several centuries [118] due to a high rate of extraction of P from mineral deposits followed by widespread use in fertilizers and detergents. Figure 1 illustrates the geological and biological phosphorus cycles including anthropogenic influences.

To measure the phosphorus content in waters, operational definitions are used, i.e. the various commonly measured P fractions are not identical to the known specific physical or chemical components of P in natural and waste waters. Figure 2 summarizes the operationally defined P fractions. Soluble and particulate phosphorus are differentiated by filtration through a 0.45 µm membrane filter. Since this fractionation is solely operational, the filtrate may not fully represent the dissolved P fraction but contain significant quantities of P containing colloidal material.

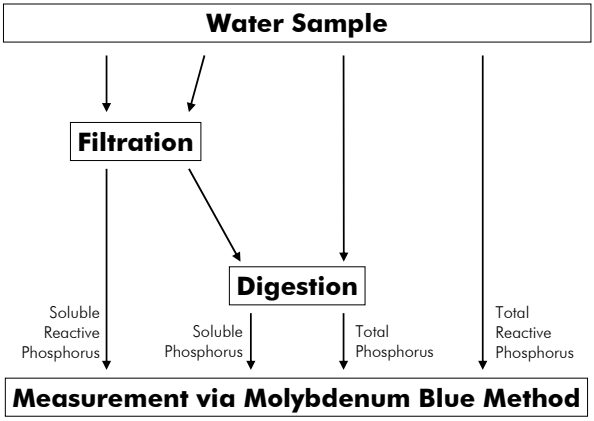

Figure 2: Phosphorus forms

Soluble Reactive Phosphorus (SRP) is measured by reacting with acidic molybdate to form 12-phosphomolybdic acid, which on reduction forms the strongly coloured phosphomolybdenum blue species which can be determined spectrophotometrically. SRP consists largely of the inorganic orthophosphate and is the fraction of total phosphorus which is directly available for uptake by bacteria and algae. Historically, SRP has been called dissolved inorganic phosphate or simply orthophosphate. The term reactive is used to indicate that the phosphorus in the SRP fraction is not solely inorganic, but could include any other form of phosphorus that reacts with the reagents. Some organic P forms have been found to hydrolize and react with ammonium molybdate, while (inorganic) polyphosphates do not react. Nevertheless, the commonly used term orthophosphate is used for SRP in the experimental part of this work.

Soluble Phosphorus (SP) is measured after digestion of the sample, usually by acid oxidation (e.g., using potassium persulfate [1]), to decompose the dissolved and some colloidal P species to inorganic monomeric phosphate. SP is also termed Total Dissolved Phosphorus (TDP).

The difference between SRP and SP concentrations is known as Soluble Unreactive Phosphorus (SUP). This fraction contains filterable phosphorus forms that do not react with the phosphorus reagents under the time and conditions of the test. The compounds in the SUP fraction are mainly organic forms of phosphorus and chains of inorganic phosphorus molecules, i.e. polyphosphates. The organic fraction is reported to be hard to remove during wastewater treatment [108].

The Total Phosphorus (TP) fraction incorporates all filterable and particulate forms and is the variable that should be studied for biomass management in surface waters [20]. There exists a correlation between TP and chlorophyll, i.e. biomass, and several models have been developed to predict phytoplankton density in surface waters. A widely used statistical model has been established by Vollenweider and Kerekes [120] and allows classifications of natural lakes according to their trophic status.

Figure 3 shows the aqueous speciation of phosphoric acid (orthophosphate). In the pH range of most natural waters and wastewaters (pH 6 - 9.5), the monovalent ($H_2PO_4^-$) and the divalent (HPO_4^{2-}) form are the dominating species. For the dissociation of phosphoric acid, the equilibrium constants are $pK_{a1} = 2.12$, $pK_{a2} = 7.21$, and $pK_{a3} = 12.67$ (ionic strength of zero, T=25°C). Speciation and charge of the anionic adsorbate phosphate influence the adsorption onto metal oxide surfaces, i.e. phosphate removal is pH dependent.

2.1.2 *Eutrophication*

The pollution of surface waters by phosphates is the main cause for eutrophication and was recognized as a problem in the middle of the twentieth century. Phosphorus is an essential plant nutrient and excess quantities of it result in extensive growth of phytoplankton, macroalgae, and higher plants. In some cases, this includes harmful algal blooms and depletion of dissolved oxygen that subsequently results in the decline of aquatic life [48, 20]. A survey on the extent of the problem on a global level has found that in Europe 53 % of lakes and reservoirs are eutrophic. The proportions for Africa, South East Asia, North and South america are 28 %, 54 %, 48 %, and 41 %, respectively [73]. Point sources (e.g., from municipal wastewater treatment plants, industrial and some agricultural) account

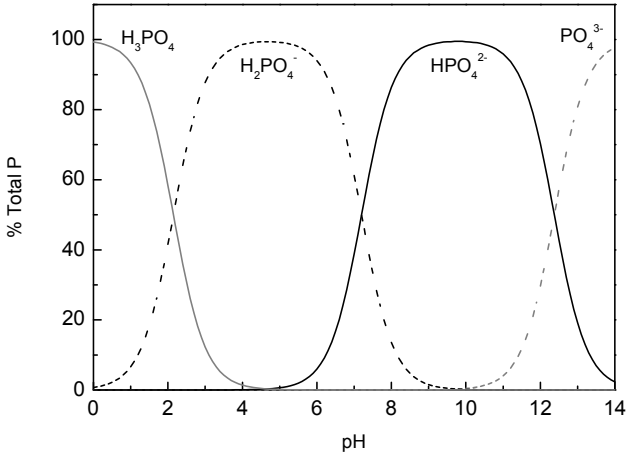

Figure 3: Aqueous speciation of phosphorus as function of pH

for more than half of the phosphorus discharged in Europe. The principal sources of phosphorus in wastewater originate from human excreta and, in some countries, from the use of detergents. Phosphorus release to surface waters has led to legislations, such as the European Union Urban Wastewater Directive [45], designed to remove phosphorus from domestic and industrial wastewater. Consequently, phosphorus removal has become more widely employed in wastewater treatment and emissions of phosphorus from sewage into surface waters, across Europe, have typically fallen by 30-60 % since the mid-1980's [41], with considerable variations across the continent. Similar control measures have been implemented in the U.S.A. and Japan. E.g., the U.S. EPA has established a maximum contaminant level for phosphorus to be $<$20 µg/L in rivers and streams and in lakes and reservoirs during summer growing season [42, 43].

While sewage discharges are gradually tackled, the relative importance of diffuse phosphorus sources, such as agriculture and soil erosion will increase. Despite improvements in discharge and surface water quality in recent years, phosphorus pollution remains a significant issue in developed countries. Developing countries have also severe eutrophication problems driven by increasing fertilizer use, as well as very poor treatment of urban wastewater from increasing populations [48].

2.1.3 *Phosphorus removal technologies*

Today, the most widely applied phosphorus removal processes are chemical and biological phosphorus removal. The principle of chemical P removal from wastewater is to transfer dissolved phosphates into particulate form by producing chemical precipitates of low solubility from the addition of di- and tri-valent metal ions or

lime. The formed precipitates and particulate phosphates are usually removed by solid separation processes such as sedimentation, flotation or filtration [108, 21]. Polyphosphates and organic phosphorus may take part in adsorption reactions, but only to a limited extent and thus represent the partly removable phosphorus fraction. The proportions of easily vs. partly removable phosphorus fractions influences process performance and achievable levels of residual phosphorus in the effluent, which are also governed by the raw water quality, type and dose of precipitant, location of dose application, chemical speciation, mixing conditions, process configuration, and the target water quality. The process is robust and flexible and phosphorus removal of more than 90 % is achievable under optimized conditions. Extensive information in this subject area is available [108, 92] and therefore only briefly covered in this work.

The phenomenon of biological phosphate removal was first recognized by Greenberg et al. [62] who proposed that under certain conditions activated sludge had the ability to accumulate phosphate in excess of that required for balanced microbial growth. In later years, this was frequently referred to as 'luxury' phosphate uptake and its exploitation appeared to provide the basis of a biological alternative to chemical precipitation for phosphate removal from wastewater. Ultimately, this led to the development of the enhanced biological phosphate removal (EBPR) process. EBPR can be achieved through the activated sludge process by recirculating sludge through anaerobic and aerobic conditions. This is achieved by configuring the treatment system such that an anaerobic zone is added upstream of the traditional aerobic phase. A specialized group of microorganisms known as polyphosphate accumulating organisms is able to gain a selective advantage by taking up carbon sources such as volatile fatty acids under anaerobic conditions and storing them intracellularly as carbon polymers. The energy required for these biotransformations is mainly generated by the cleavage of polyphosphate, which is intracellularly stored. Ultimate phosphate removal from the system is achieved by the wastage of phosphate-rich excess sludge. Many different process configurations exist where both P and nitrogen removal are combined, which is also referred to as biological nutrient removal [108]. When operated successfully, the EBPR process is a relatively inexpensive and environmentally sustainable option for phosphate removal. However, the stability and reliability of EBPR can be a problem and disturbances and prolonged periods of insufficient P removal have been observed at full-scale plants [13, 114]. Research is underway to overcome these problems and to gain a more detailed process understanding. Recent advances have been discussed by Oehmen et al. [87]. When operated under favourable conditions, EPBR plants are able to remove 80-90 % of influent phosphate. Table 1 shows typical effluent concentration ranges after different stages of wastewater

treatment. For comparison, annual average values of two wastewater treatment plant effluents which were used in this work are shown.

Table 1: Typical effluent concentration ranges after wastewater treatment [mg/L]

	TP	COD	BOD_5	NH_4-N	Data source
Untreated wastewater	4-12	250-800	110-350	12-45	Asano [3]
CAS[1]	4-10	40-80	5-25	1-10	Asano [3]
Activated sludge with BNR	1-2	20-40	5-15	1-3	Asano [3]
MBR	<0.3[2]	<10-30	<1-5	<1-5	Asano [3]
WWTP Berlin-Ruhleben[3]	0.33	43	3.1	0.43	SenStadt [97], Moeller and Burgschweiger [85]
WWTP Beixiaohe, Beijing[3]	2-3	41	12	20	BDG [10]

[1] CAS is defined as activated sludge treatment with nitrification
[2] With coagulant addition
[3] Annual average

Although less frequently used in large-scale phosphorus removal from wastewater, a great number of adsorbents have been studied and used in a variety of phosphorus removal applications as diverse as wastewater treatment, maintenance of potable water supplies and constructed wetlands [34]. In general, adsorbents with a significant phosphate uptake capacity are enriched in Ca, Fe and/ or Al [39, 76]. Table 17 shows a summary of phosphorus adsorbents which have been tested in laboratory studies or in applications as diverse as phosphate removal via constructed wetlands, from natural and wastewaters, as reactive capping or barriers in aquatic systems or as soil amendment to assist in phosphate fertilizer retention. Given the great variety of potential adsorbents, the choice of adsorbent depends on the application. Criteria for adsorbent choice include adsorption capacity, cost, stability in terms of phosphorus retention (e.g., under variable pH or redox conditions) and practicality of implementation (e.g., use in fixed-bed systems or as powder/ slurry). Table 2 shows some typical scenarios for phosphate removal and considerations for adsorbent choice. It is important to note that there exists a trade-off between phosphorus load and the desired residual phosphate concentration. For treatment of CAS effluents, the adsorbent of choice is cheap. High phosphorus loads result in low operation times and thus high adsorbent consumption in fixed-bed systems. In this scenario, phosphate adsorption has to compete with the conventional alternative of chemical and biological P removal, since only moderate target concentrations are required.

A near to complete removal of phosphate is necessary for special applications such as restoration of surface water bodies, treatment of swimming pool waters or wastewater reuse for scenic impoundment, as well as in regard to increasingly stringent regulations on phosphorus discharge and in surface waters [11, 65, 42, 43, 97]. The required levels either cannot be reached using the traditional techniques or require high dosages of coagulant and a higher complexity of operation (e.g., two-stage coagulation). In these scenarios, characterized by low phosphorus loads and low target concentrations, the use of engineered adsorbent with high phosphate adsorption capacity is the preferential treatment alternative. GFH is an engineered, commercially available adsorbent which is approved for drinking water application. Consequently, this work focusses on the potential application of GFH in effluent polishing or swimming pool application and the experimental conditions (concentration range, pH) are chosen accordingly.

Table 2: Application and choice of adsorbents modified after Douglas et al. [34]

Application	System characteristics	Criteria for Choice
Secondary/ tertiary effluent	High throughput and load, moderate residual P concentration	Primarily low cost, large reduction on P but not necessarily to very low concentration → natural or waste/ by-product adsorbents
Effluent polishing after chemical or biological P removal (e.g. for non-potable wastewater reuse)	Low load , very low target concentration	High capacity → engineered adsorbents
Swimming pool water, especially nature-oriented outdoor pools	Very low load, low target concentration	High capacity, no significant human health/ ecotoxicological effects → engineered adsorbents
Surface water restoration - lake or impounded river	Generally low load in summer and low residual surface water P concentration except when mixed with anoxic bottom water	No significant human health/ ecotoxicological effects, Stability under anoxic conditions, playoff between low-moderate cost and moderate-high adsorption capacity

2.1.4 *Phosphorus recovery*

In a sustainable society renewable resources should substitute non-renewable sources wherever possible. Where this cannot be done, recovery, reuse and recycling of non-renewable resources should be implemented [46].

Phosphorus is an essential, but limited and non-renewable resource for which there is no substitute. Almost all P used by society is mined from a comparatively small number of commercially exploitable deposits in the world. The annual total production is some 20 million tonnes of P, derived from approximately 140 Mt of rock concentrate [72]. Different estimates suggest that global P reserves last approximately 60-240 years, depending on exploitation rate, phosphate rock quality and processing [106]. Since the quality of rock phosphate depends also on its concentration of harmful substances such as cadmium and uranium [117], increasing costs for processing of rock phosphate are expected [4]. Due to the above mentioned facts, there are increasing efforts to recycle phosphorus contained in wastewater. As mineral fertilizers for agricultural production account for 80 % of the global P consumption [106], direct use as fertilizer or further use in the fertilizer industry is the most promising reuse option. With common wastewater treatment processes, phosphorus removed from the liquid phase is transferred to the sewage sludge. The use of sewage sludge in agriculture has been controversially discussed for many years. Due to health and environmental concerns, this use is declining and some countries have given up the practice [106].

In recent years, several techniques for phosphorus recovery from wastewater have been developed. In general, phosphorus recovery is possible from the liquid phase, the sewage sludge and the sludge ash, respectively. Recovery from the liquid phase is particularly successful from phosphorus-rich process water or side streams. A comprehensive overview on current technologies for phosphorus recovery is given in Cornel and Schaum [22]. The authors conclude that based on estimated recovery costs of 3600 to 8800 Euro/t P, recovered phosphorus is, up to today, more expensive as mined phosphorus. However, this might change in the future due to decreasing P deposits and political incentives.

2.2 ADSORPTION OF PHOSPHATE ONTO FERRIC HYDROXIDE SURFACES

2.2.1 *Fundamentals of adsorption*

Adsorption is a mass transfer process in which substances present in a liquid phase are accumulated on a solid phase and thus removed from the liquid. Whereas absorption means that the molecules are accumulated *in* the phase, in adsorption the accumulation takes place at the boundary layer between solid and liquid phase. The solid phase onto whose surface the target compound is adsorbed is referred to as the adsorbent (e.g., GFH, activated carbon). The target compound (e.g., phosphate) is called the adsorbate [84]. During the adsorption process, dissolved species are transported into the porous adsorbent particle by diffusion and are then adsorbed onto the extensive inner surface of the adsorbent. For a detailed overview of adsorption theory, the studies of Sontheimer et al. [99] and Kümmel and Worch [77] are recommended.

Depending on the type of interaction between adsorbate and adsorbent surface, chemisorption and physical adsorption can be differentiated. Chemisorption typically shows bonding energies above 200 kJ/mol. Here, the adsorbate reacts with the surface to form a covalent or an ionic bond. Physical adsorption is a rapid process caused by nonspecific binding mechanisms such as van der Waals forces and results in bonding energies of 4 - 40 kJ/mol. Generally, physical adsorption is less specific for which compounds adsorb to surface sites, has weaker forces and energies of bonding, operates over longer distances (multiple layers), and is more reversible [27]. In contrast to the adsorption of organic adsorbates from water (polar solvent) onto a nonpolar adsorbent (activated carbon), where van der Waals forces are predominating, adsorption of ionic species (e.g., phosphate) onto iron oxide surfaces is mostly driven by electrostatic attraction, which is highly dependent on pH and ionic strength.

The affinity of the adsorbate for an adsorbent is quantified using adsorption isotherms, which are used to describe the amount of adsorbate that can be adsorbed onto an adsorbent at equilibrium and are usually a function of the liquid-phase concentration. To develop isotherms, a known quantity of adsorbate in a fixed volume of liquid is exposed to various dosages of adsorbent. After sufficient time, the adsorption equilibrium is reached an the adsorption equilibrium capacity can be calculated from a mass balance:

$$q^* = \frac{L}{m} \cdot (c_0 - c^*) \tag{2.1}$$

where L is the volume of liquid, m is the mass of adsorbent used, c_0 is the initial, and c^* the equilibrium adsorbate concentration. It is important to differentiate between adsorption of a single and of multiple compounds. In the latter case, the different adsorbates will compete for adsorption sites and the adsorption equilibrium as well as the isotherm can be significantly different than without competition. In a multi-component system, the initial concentration of the target adsorbate influences the resultant isotherm.

In order to describe the adsorption equilibrium mathematically, different models exist, differing in complexity and in the number of parameters necessary. Of practical relevance are mainly two-parametric isotherms, in particular those formulated by Langmuir [79] and Freundlich [51].

The Langmuir adsorption isotherm is used to describe the equilibrium between surface and solution as a reversible chemical equilibrium between species (Langmuir 1918). The adsorbent surface consists of fixed individual sites where adsorbate molecules can be chemically bound. It is assumed that the reaction has a constant free-energy change (ΔG_{ads}) for all sites and a maximum of one adsorbate molecule can be bound to each site (monolayer coverage). The following expression for the adsorption equilibrium capacity can be derived:

$$q^* = q_{max} \cdot \frac{K_L \cdot c^*}{1 + K_L \cdot c^*} \tag{2.2}$$

K_L is the Langmuir coefficient and q_{max} is the maximum surface concentration, indicating a monolayer coverage. To derive the model parameters q_{max} and K_L, equation 2.2 can be linearized. The Langmuir equation assumes a homogeneous structure of the adsorbent surface, i.e. all adsorption sites are energetically equal. That is why the Langmuir equation is in most cases only applicable for small concentration ranges, since the surface of GFH, for example, is of a heterogeneous nature.

The Freundlich [51] isotherm was originally proposed as an empirical eqution to describe data for heterogeneous adsorbents:

$$q^* = K_F \cdot c^{*n} \tag{2.3}$$

The Freundlich parameters K_F and n have to be determined in batch experiments, using logarithmic regression of the data and the linearized form of the Freundlich equation.

The Freundlich isotherm is generally better suited to describe adsorption in aqueous solutions than the Langmuir isotherm. It has been shown that the Freundlich equation can be derived from the Langmuir equation if a logarithmic decrease of the differential adsorption enthalpy with increasing solid-phase concentration is assumed, corresponding to the behavior of a heterogeneous adsorbent surface. It is important to note that the Freundlich equation can only be used to describe experimental data within a limited concentration range where the constants are valid. To describe adsorption outside of this range, other isotherms have to be derived in experiments within other concentration ranges.

Various extensions to the Freundlich equation as well as other approaches have been developed. For multicomponent adsorption, the ideal adsorbed solution theory (IAST) has been developed, which describes multicomponent equilibria based on single-solute isotherms. More information can be found in Sontheimer et al. [99].

Surface complexation models (SCM) represent a fundamentally different approach to describe adsorption equilibria. SCMs describe adsorption as a complexation reaction between adsorbate and adsorbent surface, analogously to equilibrium reactions in solution. The following dissociation reactions can be formulated for the ferric hydroxide surface ($\equiv$ denotes the surface):

$$\equiv FeOH_2^+ \rightleftharpoons \equiv FeOH + H^+ \qquad K_{a1}^S = \frac{[\equiv FeOH][H^+]}{[\equiv FeOH_2^+]} \tag{2.4}$$

$$\equiv FeOH \rightleftharpoons \equiv FeO^- + H^+ \qquad K_{a1}^S = \frac{[\equiv FeO^-][H^+]}{[\equiv FeOH]} \tag{2.5}$$

The equilibrium constants K_a^S are termed apparent or conditional acidity constants and can be obtained by combining acid/base titration data with site density.

The acidity constants are not constant, but depend on the surface charge, i.e. on the degree of ionization of the OH groups and on the ionic strength of the solution. Intrinsic acidity constants, $K^S_{a\,int}$, represent the dissociation of surface hydroxyl groups at zero surface charge and cannot be measured directly. They can be calculated from the experimentally accessible conditional constants, $K^S_{a\,cond}$, either by extrapolation to a situation of zero surface charge, or by fitting the experimental data to an appropriate SCM to compute the electrostatic component:

$$K^S_{a\,int} = K^S_{a\,cond} \cdot \exp\left(\frac{-zF\phi_0}{RT}\right) \tag{2.6}$$

where z is the charge of the adsorbed species; F is the Faraday constant and ϕ_0 is the surface potential. For iron oxides, the values of the pK_as usually fall between 5 and 10, but with considerable variation in the values for different samples of a particular oxide [23]. Teermann [109] evaluated GFH titration data and reported (intrinsic) acidity constants of 6.3 (pK^S_{a1}) and 9.4 (pK^S_{a2}).

Since the surface potential ϕ_0 (Equation 2.6) cannot be measured directly, SCMs include different description of the electrical double layer at the oxide/ solution interface and the locations of the various adsorbing species. The main SCMs are the constant capacitance [68], the diffuse double layer (DDL) [40, 107], the triple layer [28], the four layer [16] and the CD-MUSIC [67] models. By relating adsorption to such parameters as the number of reactive surface sites, the intrinsic acid/base constants for each type of surface site and the complexation constants for the adsorbed species, SCMs produce isotherms with a sounder physical basis than do empirical equations such as the Freundlich equation [23].

2.2.2 *Current state of research*

Ferric (hydr)oxide surfaces have been known for their strong interaction with arsenate and phosphate ions in solution, which leads to favourable adsorption characteristics and high capacities [23]. A number of natural and engineered adsorbent media are commercially available, most of them for arsenate removal. For example, granular ferric hydroxide (GFH) has been developed in 1990-1994 [38]. Currently, more then 1600 small plants in West Bengal and approximately 400 full scale treatment plants for arsenic removal are operated worldwide using GFH as adsorbent [9]. Compared to the removal of arsenate for drinking water production, phosphate removal using GFH is less often practiced.The general efficiency of GFH for advanced phosphorus removal using GFH has been shown [57], but more information is needed on GFH adsorption capacity as a function of pH and water composition.

Due to a well defined crystal structure, widespread occurrence in nature and ease of synthesis in the lab, hydrous ferric oxide, goethite and hematite have often been used as model adsorbents, with phosphate being the most widely investigated inorganic ligand [40, 80, 89, 111, 115]. Phosphate is generally believed to form strong inner-sphere complexes with the ferric (hydr)oxide surface [23]. Spectroscopic studies (FT-IR, EXAFS) have not provided an entirely consistent picture of the exact structure of the formed surface complexes. Whereas various researchers have presented evidence for the formation of bidentate, binuclear surface complexes [90, 94, 111], other investigations support monodentate surface complex formation [56, 93, 81].

Due to the specific binding at the ferric (hydr)oxide surface, phosphate is a strong competitor for other anions. Phosphate has been shown to suppress the adsorption of arsenate [69, 82], sulfate [54] and NOM [56]. The presence of cations in solution may affect phosphate adsorption i) directly, through the formation of ternary surface complexes and ii) indirectly by changing the electrostatic properties of the surface. Calcium has been shown to improve phosphate adsorption onto ferric (hydr)oxide surfaces. Yao and Millero [129] used the triple layer model to describe adsorption of phosphate on manganese dioxide in seawater. The enhanced phosphate adsorption in the presence of calcium could not be described with the model and the postulated surface complexes. It was concluded that calcium-phosphate species might be adsorbed at the surface and ternary surface complexes were suggested. Gao and Mucci [53] reported that competitive adsorption of phosphate in seawater could be predicted using the constant capacitance model with the inclusion of ternary complexes. The addition of calcium was found to increase adsorption on the goethite surface, slightly at pH < 8.5 and extensively at pH > 9. However, there is no consensus about the formation of ternary calcium phosphate surface complexes. Rietra et al. [94] studied the simultaneous adsorption of phosphate and calcium on goethite and modeled the data with CD-MUSIC. They conclude that no ternary complexes were formed, but that the increase was due to electrostatic effects.

Despite the abundance of literature on phosphate adsorption onto ferric hydroxide surfaces, only very few studies are available on akaganeite or GFH. Chitrakar et al. [19] studied adsorption from seawater onto synthetic akaganeite and goethite and reported high affinities and selectivity towards phosphate. The formation of inner-sphere complexes was concluded. Deliyanni et al. [29] synthesized nanocrystalline akaganeite and reported high capacities for phosphate. FT-IR spectroscopy revealed the inner-sphere complex formation and indications for a monodentate, mononuclear Fe-P surface complex. Recently, Genz [56] proposed to describe phosphate adsorption onto GFH by three mononuclear surface complexes, which had earlier been proposed for the adsorption of phosphate onto goethite [93]:

$$\equiv FeOH + PO_4^{3-} + 3H^+ \quad \rightleftharpoons \quad \equiv FePO_4H_2 + H_2O \tag{2.7}$$

$$\equiv FeOH + PO_4^{3-} + 2H^+ \quad \rightleftharpoons \quad \equiv FePO_4H^- + H_2O \tag{2.8}$$

$$\equiv FeOH + PO_4^{3-} + H^+ \quad \rightleftharpoons \quad \equiv FePO_4^{2-} + H_2O \tag{2.9}$$

Whereas the phosphate adsorption capacity is essentially the same per unit surface area for synthetic and natural goethites, there is no clear correlation between surface area and phosphate adsorption capacity for hematite. It has been found that adsorption capacity depends on crystal morphology [23]. Given the fact that GFH is a commercial adsorbent media and only poorly crystallized, variations in capacity due to material inhomogeneity cannot be ruled out.

2.3 BREAKTHROUGH PREDICTION OF FIXED-BED ADSORBERS

In water and wastewater treatment, granular adsorbents are commonly applied in fixed-bed columns. One critical aspect of the design of a fixed-bed adsorber involves characterization of the effluent concentration profile as a function of throughput (i.e., the volume processed or the time of operation). This profile, commonly termed the breakthrough curve (BTC), represents the specific combination

of equilibrium and rate factors that control process performance in a particular application. The dynamic behavior of a fixed-bed adsorber can be visualized in terms of an active mass transfer zone that moves through the bed as a function of mass loading and saturation of the adsorbent, as shown in figure 4. The mass transfer zone is the length of the bed needed for the adsorbate to be transferred from the fluid into the adsorbent. The time when the front of the mass transfer zone appears in the effluent and the effluent concentration exceeds the treatment objective is called breakthrough. The time when the effluent concentration equals the influent is called the point of exhaustion, since the bed is no longer able to remove any adsorbate. The shape of the breakthrough curve depends on several factors, including the physical and chemical properties of both the adsorbate and the adsorbent, the particular rate limiting mechanisms involved, the depth of the bed, and the velocity of flow. If mass transfer is fast, no adsorbate will appear in the effluent prior to complete exhaustion of the bed and the adsorbent material will be at equilibrium with the influent concentration. Slow mass transfer leads to flat breakthrough curves, i.e. a portion of the bed is still unused although adsorbate is present in the column effluent. Analysis of fixed-bed column breakthrough data can be used to evaluate design parameters and optimize column operation. To predict breakthrough behavior, mass transfer models have been developed for adsorption onto granular activated carbon (GAC), which consider the sequence of external (film) diffusion, intra-particle (pore or surface) diffusion and an internal surface reaction [99].

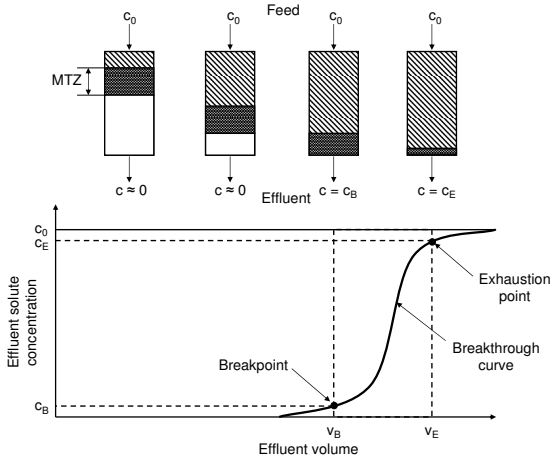

Figure 4: Mass transfer zone and breakthrough curve development in different operation stages of a fixed-bed column

In general, all of these models combine mathematical descriptions of the adsorption equilibrium and adsorption kinetics with a mass balance over a differential element of the adsorber, which includes description of the advective flow. Many

of these models describe adsorption kinetics as a combination of external film diffusion and intra-particle diffusion and are hence called dual-resistance models. Usually, fixed-bed models consist of a set of partial differential equations which, depending on their complexity, have to be solved either analytically or numerically. Table 3 shows available models to describe the dynamic behavior of fixed-bed columns and their main characteristics. According to Sontheimer et al. [99], the plug-flow homogeneous surface diffusion model (HSDM) is the most appropriate choice for single components of small molecular weight, since pore diffusion is usually a small part of the intraparticle mass transport flux and axial dispersion is unimportant for typical adsorber operation. In this work, the HSDM and two of its derivatives, the constant pattern homogeneous surface diffusion model (CPHSDM) and the linear driving force model (LDF) are tested on their applicability for breakthrough prediction of GFH fixed-bed adsorbers. These models were chosen for their good documentation, reports on successful breakthrough curve modeling as well as for available simulation software [99, 64, 127]. The HSDM neglects dispersion as relevant mass-transfer step, which is reasonable considering flow rates of 5 - 20 m/h in GFH application [122]. For intraparticle diffusion, only surface diffusion was included for the sake of simplicity. The PSDM, which in contrast to HSDM, describes intra-particle diffusion in the liquid-filled pores (pore diffusion) and not adsorbed onto the solid-phase (surface diffusion) might also be suited to describe a GFH fixed-bed system, but is not investigated in this work.

Table 3: Fixed-bed adsorption models that describe adsorber dynamics and their specific mass transfer mechanisms modified after Sontheimer et al. [99]

Model abbreviation	Model name	Film transfer	Dispersion	Surface diffusion	Pore diffusion	Other comments
HSDM	(Plug-flow) Homogeneous surface diffusion model	X		X		
CPHSDM	Constant pattern homogeneous surface diffusion model	X		X		HSDM model solutions are approximated; Assumptions: fully established mass transfer zone, favorable adsorption
HSDM/ LDF	Linear driving force model	X		X		Intraparticle diffusion is described as linear relationship
PDM	Plug-flow pore diffusion model	X			X	
PSDM	Plug-flow pore and surface diffusion model	X		X	X	
DFPSDM	Dispersed-flow pore and surface diffusion model	X	X	X	X	
DFHSDM	Dispersed-flow homogeneous surface diffusion model	X	X	X		
LEM	Local equilibrium model					Negligible mass transfer resistances; only advection is described

2.3.1 *Homogeneous surface diffusion model*

The Homogeneous Surface Diffusion Model (HSDM) consists of two partial differential equations (PDE), describing the mass transport through the adsorber (filter equation) and into the adsorbent grain (intraparticle equation). The following assumptions are incorporated in the HSDM: plug-flow conditions in the bed, linear liquid-phase mass transfer, solid-phase mass transfer only by surface diffusion, constant hydraulic loading rate and diffusion coefficients, spherical adsorbent grains, and the use of the Freundlich isotherm to describe the adsorption equilibrium. More details can be found in Sontheimer et al. [99].

A mass balance over an infinitesimal element of the filter leads to equation (2.10), where the first term represents the mass in the void fraction (pores), the second term reflects solute entering and exiting the element by advective transport, and the last term represents the sink, i. e., the mass of solute adsorbed by the adsorbent grains.

$$\epsilon_B \frac{\partial c}{\partial t} + v_F \frac{\partial c}{\partial z} + 3(1-\epsilon_B)\frac{k_L}{r_P}(c - c^*) \quad = \quad 0 \tag{2.10}$$

Intraparticle transport is described according to Fick's second law and is given in radial coordinates by:

$$\frac{\partial q}{\partial t} \quad = \quad D_S \left(\frac{\partial^2 q}{\partial r^2} + \frac{2}{r}\frac{\partial q}{\partial r} \right). \tag{2.11}$$

Both equations require intial and boundary conditions, which can be found in chapter 6. The adsorption equilibrium is considered in the boundary condition for the particle surface of equation 2.11. At the exterior adsorbent grain surface, the mass transported into the grain equals the mass transported the stagnant liquid film:

$$\left.\frac{\partial q}{\partial r}\right|_{r=r_P} \quad = \quad \frac{k_L}{\rho_P D_S}\left(c - c_{r=r_P}\right) \tag{2.12}$$

Using the Freundlich isotherm (Equation 2.3), this transforms into:

$$\left.\frac{\partial q}{\partial r}\right|_{r=r_P} \quad = \quad \frac{k_L}{\rho_P D_S}\left[c - \left(\frac{q_{r=r_P}}{K_F}\right)^{\frac{1}{n}}\right] \tag{2.13}$$

In this boundary condition, filter and intraparticle PDE are coupled by the Freundlich equation. Due to the non-linear character of the coupling, a numerical solution is required which results in a substantial computational effort. In an attempt to provide user-oriented tools to predict breakthrough, derivatives have been developed which need less computational effort. Hand et al. [64] presented the constant pattern homogeneous surface diffusion model (CPHSDM), which uses numerically derived solutions for the HSDM and a simple algebraic equation to approximate the model solution. The linear driving force model (LDF) uses a linear approximation for the intraparticle diffusion rate, which was first proposed by Glueckauf [59]. This results in a reduced amount of computation and an increased calculation speed. More information on HSDM, CPHSDM, and LDF can be found in chapter 6.

2.3.2 *Parameter estimation*

Input parameters for models describing the dynamic behavior of fixed-bed systems include adsorption equilibrium parameters (e.g., for HSDM the Freundlich parameters K_F and n), kinetic parameters (e.g., for HSDM the film diffusion coefficient k_L and the surface diffusion coefficient D_S) and operational parameters (EBCT, flow rate, filter depth, grain size). If not known, these parameters have to be experimentally determined. Alternatively, a number of empirical correlations to estimate them has been developed.

The film diffusion coefficient, k_L, is often calculated from one of a number of empirical correlations distinguished by a functional relationship between the dimensionless Reynolds (Re), Schmidt (Sc), and Sherwood (Sh) numbers, the latter being related to the film diffusion coefficient by:

$$Sh = \frac{k_L \cdot d_P}{D_L} \tag{2.14}$$

where d_P is the adsorbent particle diameter, D_L is the bulk liquid diffusivity of the adsorbate and Re and Sc are defined as:

$$Re = \frac{d_P \cdot \nu_F}{\epsilon_B \cdot \nu} \tag{2.15}$$

$$Sc = \frac{\nu}{D_L} \tag{2.16}$$

where ν_F / ϵ_B is the interstitial velocity, and ν is the kinematic viscosity of the fluid. Amongst others, Gnielinski [60], Wilson and Geankoplis [126], Ohashi et al. [88] have proposed empirical correlations for external mass transfer. The liquid diffusivity which is required for these correlation, depends on molecular size and can be calculated using correlations of Wilke and Chang [124], Worch [128], amongst others. For small molecules, tabulated values of the diffusion coefficient are available. If the molecular size is known, the diffusivity can be estimated using the Stokes-Einstein equation:

$$D_L = \frac{\overline{k}T}{6\pi\eta r_{SE}} \tag{2.17}$$

in which $\overline{k}$ is the Boltzmann constant and r_{SE} the Stokes-Einstein molecular radius.

Experimental determination of the external (film) and internal (surface diffusion) mass transfer coefficients is possible by model calibration to rate data from experiments carried out in completely mixed batch, short fixed-bed or differential column batch reactors. Detailed information can be found in Sontheimer et al. [99].

2.3.3 *Dimensionless numbers*

Dimensionless numbers are used to summarize the partly interdependent input parameters into independent, dimensionless parameters which describe the system completely. Depending on the mass transfer processes included, the definitions of the dimensionless numbers vary slightly. The dimensionless groups used in HSDM are the solute distribution parameter, D_g, the Biot number, Bi, the modified Stanton number, St, and the diffusivity modulus, Ed.

The solute distribution parameter, D_g, is defined as the ratio of the mass of adsorbate in the solid phase to the mass of adsorbate in the liquid phase under equilibrium conditions:

$$D_g = \frac{\rho_B q_0}{\epsilon_B c_0} \tag{2.18}$$

The Biot number compares the external mass transfer rate to the internal mass transfer rate:

$$Bi = \frac{k_L r_P c_0}{D_S \rho_P q_o} \tag{2.19}$$

The Stanton number relates the solute liquid phase mass transfer rate to the solute mass transfer rate by advection:

$$St = \frac{k_L m}{r_P \rho_P Q} \tag{2.20}$$

The diffusivity modulus, Ed, is equal to the ratio of St to Bi and represents the ratio of the solute transfer rate by intraparticle diffusion to the solute transfer rate by advection:

$$Ed = \frac{St}{Bi} = \frac{D_S D_g \tau}{r_P^2} \tag{2.21}$$

where τ is the packed-bed contact time of the column. For constant pattern conditions, the mass transfer zone will remain constant in shape as it moves through the fixed-bed after it is established. In this case, Ed and St can be viewed as measures of bed length relative to the length of the mass transfer zone [64].

2.3.4 *Rapid small-scale column tests*

An alternative procedure to predict breakthrough curves are rapid small-scale column tests (RSSCT), which have been developed for the adsorption of organic micropollutants onto GAC [26, 25, 24]. In the RSSCT concept, the dispersed-flow homogeneous pore surface diffusion model (Table 3) is used to scale down the full-scale adsorber to a RSSCT and maintain perfect similarity between RSSCT and full-scale performance, i.e. identical breakthrough curves. This can be achieved by setting the dimensionless groups that describe mass transfer and adsorption in the small-scale column equal to those for the large scale column.

The relationship between the empty-bed contact time of the full-scale column ($EBCT_{LC}$) and the empty-bed contact time of the RSSCT column ($EBCT_{SC}$) is obtained by equating the diffusivity modulus of the full-scale column and the RSSCT:

$$Ed_{SC} = Ed_{LC} \tag{2.22}$$

Using the dimensionless number definition (Equation 2.21), this equation can be solved for the ratio of the packed-bed contact times of full-scale and RSSCT column, τ_{SC}/τ_{LC}:

$$\frac{\tau_{SC}}{\tau_{LC}} = \left(\frac{r_{P,SC}}{r_{P,LC}}\right)^2 \cdot \left(\frac{D_{S,LC}}{D_{S,SC}}\right) \tag{2.23}$$

Under the assumption that the adsorption capacity and physical properties of the adsorbents and bed do not depend on particle size, the RSSCT scaling equations for EBCT can be obtained. Specifically, the solute distribution parameter, D_g, is assumed to be constant in the RSSCT and full-scale processes, which is only valid if equilibirum capacity, bed void fractions, particle densities, and influent concentrations are equal. Different scaling equations are used, depending on which assumption is made about the effective surface diffusivity. The constant diffusivity (CD) approach is used when the effective surface diffusivity is independent of particle size, and hence identical for full-scale and RSSCT columns and it follows:

$$\frac{EBCT_{SC}}{EBCT_{LC}} = \frac{\tau_{SC}/\epsilon}{\tau_{LC}/\epsilon} = \left(\frac{r_{P,SC}}{r_{P,LC}}\right)^2 \tag{2.24}$$

The proportional diffusivity (PD) approach assumes that the effective surface diffusivity is linearly proportional to the particle radius, and surface diffusion is the controlling mechanism. The scaling equation is:

$$\frac{EBCT_{SC}}{EBCT_{LC}} = \frac{r_{P,SC}}{r_{P,LC}} \tag{2.25}$$

The scaling equation for hydraulic loading is obtained by equating the Stanton numbers of the full-scale column and the RSSCT, which leads to:

$$\frac{v_{F,SC}}{v_{F,LC}} = \frac{r_{P,LC}}{r_{P,SC}} \tag{2.26}$$

If the PD approach is used, the from equation 2.26 resulting design requires the length of the RSSCT to be equal to the length of the full-scale process, which might be undesirable in terms of head-loss and necessary total influent volume. A lower hydraulic loading rate can be chosen, as long as the effects of dispersions are limited, which is the case if $Re \cdot Sc$ is in the mechanical dispersion region from 200 to 200,000 [26]. The resulting scaling equation is:

$$\frac{v_{F,SC}}{v_{F,LC}} = \frac{r_{P,LC}}{r_{P,SC}} \cdot \frac{Re_{SC,\,min}}{Re_{LC}} \tag{2.27}$$

Since RSSCTs use a smaller adsorbent grain size and column diameter it is possible to perform RSSCTs in a fraction of the time, and with a fraction of the water used in pilot studies. It has been shown that RSSCTs provide a powerful alternative to both modeling as well as time-consuming laboratory and pilot studies of GFH fixed-bed columns. The CD approach has been found to be more suitable for GFH adsorption than the alternative proportional diffusivity approach [101].

2.4 REGENERATION

If adsorption is thought of as surface complexation reaction (Equation 2.7- 2.9), a high concentration of OH^- ions shifts the equilibrium so that less adsorbate is bound to the surface. Also the surface acid/base reaction is shifted more towards negatively charged species, which hinders adsorption of anions such as phosphate. Consequently, a pH increase due to the use of caustic agents such as NaOH shifts the adsorption equilibrium and can result in desorption of the adsorbed solute. If the adsorption capacity can be regained in this process, the adsorbent will be regenerated.

In several studies, sodium hydroxide (NaOH) solution has been shown as suitable regenerant for metal oxide adsorbents as well as hybrid anion exchange resins: Donnert and Salecker [33] reported regeneration of activated alumina for phosphate adsorption by 0.5 M NaOH. Zhu and Jyo [131] used a zirconium loaded phosphoric acid chelating resin for phosphate removal. More than 90 % of the removed phosphate could be eluted within 20 bed volumes using 0.5 M NaOH. Phosphate adsorption behaviour was not adversely affected by repeated adsorption/desorption cycles. Chitrakar et al. [19] used synthetic akaganeite for selective phosphate adsorption from seawater and regenerated with 0.1 M NaOH. Almost no loss in capacity after up to 12 adsorption/ desorption cycles was reported. Recently developed hybrid anion exchangers containing hydrated ferric oxide nanoparticles were reported to remove phosphate and showed much higher capacities than the parent material [14, 83]. Solutions of 2 - 4 % (0.5 - 1 M) NaOH and 2 % NaCl were found very effective to desorb phosphate and $>$ 95 % phosphate was desorbed after 12 bed volumes of regenerant [83]. Genz et al. [57] studied phosphate adsorption from MBR effluents onto GFH and activated alumina followed by regeneration with 0.6 M NaOH and reported no decrease in capacity after three adsorption/ desorption cycles. A high regenerant to bed volume ratio (100 : 1) was used and a non-desorbable P fraction was supposed in long-term operation.

3

PHOSPHATE ADSORPTION ONTO GRANULAR FERRIC HYDROXIDE: ISOTHERM AND FIXED-BED COLUMN STUDIES

Alexander Sperlich[1] and Martin Jekel[1]

AS PREPARED FOR WATER SCIENCE & TECHNOLOGY

ABSTRACT

Adsorption of phosphate in artificial model solutions, natural and waste waters onto granular ferric hydroxide (GFH) was studied in batch and fixed-bed column experiments. Physical characterization and grain size analysis of the adsorbent media reveal high specific surface areas independent of grain size and variations of density and water content over the different grain size fractions. Equilibrium isotherms show that phosphate adsorption is strongly pH dependent. High capacities of up to 24 mg/g P (at pH 6 and an equilibrium concentration of 2 mg/L P) can be reached. Presence of calcium was shown to improve adsorption of phosphate. This is supposed to be the reason for higher capacities in waste and drinking water as compared to DI water and membrane concentrates. Two alternative commercially available adsorbents (FerroSorp and Bayoxide E33) were tested and showed approx. only 50 % of the capacity of GFH at pH 7. Rapid small-scale column tests (RSSCTs) were shown to be a useful tool for simulation of fixed-bed columns. Isotherm results can be used to provide a rough estimation of operation time, i.e. the ideal breakthrough point of a fixed-bed column, but are of limited use due to the strong influence of mass transfer on the shape of the breakthrough curve. RSSCT using different empty-bed contact times show that phosphate adsorption kinetics onto GFH are very slow and result in asymptotically shaped breakthrough curves. Analysis of breakthrough data proves that operation of two GFH beds in series can contribute to a more efficient use of the adsorbent.

3.1 INTRODUCTION

3.1.1 *Aim of the study*

Ferric (hydr)oxide surfaces have been known for their strong interaction with arsenate and phosphate ions in solution, which leads to favourable adsorption characteristics and high capacities [23]. A number of natural and engineered adsorbent media are commercially available, most of them for arsenate removal. For example, granular ferric hydroxide (GFH) has been developed in 1990 - 1994 [38]. Currently, more then 1600 small plants in West Bengal and approximately 400 full scale treatment plants for arsenic removal are operated worldwide using GFH as adsorbent [9]. Compared to the removal of arsenate for drinking water

1 Technische Universität Berlin

production, phosphate removal using GFH is less often practiced. Phosphorus needs to be removed from waste waters to prevent the eutrophication of the receiving surface water bodies. Therefore techniques such as chemical precipitation and biological phosphorus removal are employed in most cases. Compared to these techniques, adsorption might be used to reach very low effluent concentrations in special applications, where sufficient dilution of the water cannot be guaranteed (e.g., water reuse applications, surface water restoration). The general efficiency of GFH for advanced phosphorus removal has been shown [57, 104], but more information is needed on GFH adsorption capacity as a function of pH and water composition. The objective of this study is to quantify the adsorption capacity of GFH for phosphate removal, to assess the competitive adsorption in natural waters and waste waters and to identify the major functions of adsorption capacity.

3.1.2 *Fixed-bed column studies*

The effluent concentration profile of a fixed-bed column is known as breakthrough curve and provides information on operation time and thus adsorption equilibrium. However, the shape of the breakthrough curve is influenced by mass transfer. If mass transfer is fast, no adsorbate will appear in the effluent prior to complete exhaustion of the bed and the adsorbent material will be at equilibrium with the influent concentration. Slow mass transfer leads to flat breakthrough curves, i.e. a portion of the bed is still unused although adsorbate is present in the column effluent. Analysis of fixed-bed column breakthrough data can be used to evaluate design parameters and optimize column operation.

To predict breakthrough behavior, mass transfer models have been developed for adsorption onto granular activated carbon (GAC), which consider the sequence of external (film) diffusion, intra-particle (pore or surface) diffusion and an internal surface reaction [99]. It has been shown that these models can be used for GFH adsorption [103]. Besides isotherm parameters such as the Freundlich constants (K_F and n), these models require the input of mass transfer coefficients, which have to be experimentally determined. Intra-particle diffusion into the GFH grains was found to be very slow, resulting in an asymptotic shape of the breakthrough curve and limited applicability of simplified mass transfer models [103]. An alternative procedure to predict breakthrough curves are rapid small-scale column tests (RSSCT), which have been developed for the adsorption of organic micropollutants onto GAC [26]. In the RSSCT concept, mathematical models are used to scale down the full-scale adsorber to a RSSCT and maintain perfect similarity between RSSCT and full-scale performance, i.e. identical breakthrough curves. This can be achieved by setting the dimensionless groups that describe mass transfer and adsorption in the small-scale column equal to those for the large scale column. Since RSSCTs use a smaller adsorbent grain size and column diameter it is possible to perform RSSCTs in a fraction of the time, and with a fraction of the water used in pilot studies. It has been shown that RSSCTs provide a powerful alternative to both modeling as well as time-consuming laboratory and pilot studies of GFH fixed-bed columns [101]. In this study, RSSCTs were used to test the breakthrough behavior of phosphate in different model waters and waste waters. RSSCTs were also used to evaluate specific design variables, such as empty-bed contact time (EBCT) and bed operation in series. For scaling RSSCTs, the effective surface diffusivity was assumed to be independent of particle size. This constant diffusivity approach

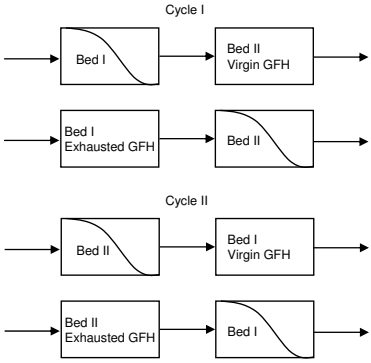

Figure 5: Operation of two beds in series [27]

[24] has been found to be more suitable for GFH adsorption than the alternative proportional diffusivity approach [101].

Fixed-bed adsorption columns can be operated as two (or multiple) beds in series to achieve a higher utilization of the adsorbent material and hence longer bed lives. When breakthrough occurs, the first bed (lead column) contains only exhausted adsorbent material, whereas some capacity is left in the second bed (lag column). The first bed is then replaced with fresh adsorbent material and the second bed is switched to the influent (Figure 5) and becomes the lead column. The second operation cycle starts and operation continues until the effluent from the first bed, now lag column, exceeds the treatment objective.

Assuming that the loading on the first and second column is the same as in cyclic operation, it is possible to calculate the specific throughput for two beds in series based on breakthrough data of two columns in non-cyclic operation. A mass balance for one operation cycle yields:

$$Q \cdot c_0 \cdot t_C = Q \left(c_0 t_C - \int_0^{t_0} c_1 \, dt \right) + Q \int_0^{t_0} c_2 \, dt \tag{3.1}$$

where Q is the volumetric flow rate, co the influent concentration, c1 the effluent concentration from column 1, c_2 the effluent concentration from column 2, t_C is the cycle time and t_0 is the operation time of a non-cyclic column study until the effluent exceeds the treatment objective. The mass fed for cyclic operation equals the mass retained on the first column plus the mass in the effluent of the second column. The adsorbate in the second column can be ignored, since it would be equal to the mass that was in the first column at startup [27]. Using this equation, RSSCT data can be used to quantify the advantages of operation in series.

3.2 MATERIALS AND METHODS

3.2.1 *Adsorbent media*

GFH was obtained from the producer (GEH Wasserchemie, Osnabrück, Germany). GFH is a poorly crystallized iron(III) oxide-hydroxide and consists predominantly of akaganeite (β-FeOOH). The $pH_P ZC$ (point of zero charge) is reported to be between 7.5 and 8.0 [96, 109]. The water content was determined to be approx. 45 %. A grain size distribution analysis as well as bed density measurement was conducted according to EN 12902. Virgin GFH material was sieved in wet conditions using a set of standard testing sieves (0.2 - 2.0 mm). Particle density was measured by adding small amounts of GFH into a cylinder and measuring the displacement of DI water.

FerroSorp Plus, supplied by Zeolith Umwelttechnik GmbH (Waldsassen, Germany), is a granular adsorbent media based on ferric hydroxide. Manufacturer's (HeGo Biotec GmbH, Berlin, Germany) data specify a grain size range of 0.5 - 2.0 mm and a water content of 10 - 15 %. An adsorption capacity for phosphate to be reached under optimal operational conditions of 12 - 16 g/kg P is stated by the manufacturer.

Bayoxide E33 (Lanxess AG, Leverkusen, Germany) is a synthetic ferric hydroxide, which is goethite (β-FeOOH). Manufacturer's specifications indicate a grain size range of 0.5 - 2.0 mm, a water content of 20 %. A specific surface area of 120 - 200 m^2/g is reported.

All results are presented on a dry mass basis after drying at 105°Cfor 12 h and subsequent cooling in a desiccator.

3.2.2 *Surface area measurements*

Specific surface area was determined with a Micromeritics Gemini 2360 surface area analyzer (Micromeritics, Norcross, GA, USA) using the BET method [17]. All samples were dried and degassed before analysis. The statistical measurement uncertainty was 0.5 %.

3.2.3 *Batch experiments*

3.2.3.1 *Isotherms*

Adsorption isotherms were developed using < 63 µm (ground) GFH. The air-dried material which was used had a water content of approx. 22 %. For comparison, two isotherms were developed using air-dried, ground FerroSorp (water content 7.3 %) and Bayoxide E33 material (water content 4.8 %).

Model solutions were prepared using de-ionized (DI) water and NaCl to set an ionic strength of 10 mmol/L. Different concentrations of phosphate were set by adding KH_2PO_4 (analytical reagent grade chemicals).

To study the pH dependence of phosphate adsorption, different initial concentrations (0.5 - 4 mg/L P) were used. The liquid-to-mass ratio varied in the range of 3-25 L/g. Since competitive adsorption can be neglected in these systems, variation of the L/m-ratio should lead to the same results as using different initial concentrations. Constant pH-conditions were achieved by adding 2 mM of one

Table 4: Batch isotherm experiments

Water matrix	Adsorbent	pH	L/m [L/g]	Data source
DI	GFH	6.2 ± 0.1	$3.1 - 23.7$	this study
DI	GFH	7.1 ± 0.2	$3.2 - 25.7$	this study
DI	GFH	8.1 ± 0.2	$3.2 - 12.8$	this study
DI + Calcium	GFH	7.0 ± 0.2	$3.2 - 25.0$	this study
DW	GFH	7.0 ± 0.2	$3.2 - 25.7$	this study
MBR effluent	GFH	7.2 ± 0.1	$3.2 - 16.2$	this study
NF concentrate of DW	GFH	7.3 ± 0.1	$2.5 - 49.6$	Sperlich et al. [105]
NF concentrate of 2ndary effl.	GFH	7.2 ± 0.1	$2.5 - 47.7$	Sperlich et al. [105]
DI	FerroSorp	7.2 ± 0.1	$2.2 - 11.0$	this study
DI	Bayoxide E33	7.2 ± 0.1	$0.6 - 9.3$	this study

of the biological buffer substances MES (2-(N-morpholino)ethanesulfonic acid, pK_A = 6.1), BES (N,N-Bis(2-hydroxyethyl)-2-aminoethanesulfonic acid, pK_A=7.1) and TAPS (N-Tris(hydroxymethyl)methyl-3-aminopropanesulfonic acid, pK_A=8.4), all Sigma-Aldrich. The adsorption of these buffer substances onto GFH was determined in batch experiments (not described here) and found to be negligible. After preparation of the model water, the pH was adjusted to 6, 7 and 8, respectively, using HCl or NaOH.

To study the influence of water composition and competitive adsorption, isotherms were developed in Berlin drinking water (DW) , wastewater and an artificial model solution with specific addition of 0.9 mM $CaCl_2$. In the artificial model solution and Berlin DW batches, an initial concentration of 2 mg/L P was set. The initial phosphate concentration in wastewater (MBR effluent from Beijing's wastewater treatment plant Beixiaohe) was 3.9 mg/L P. In these experiments, the isotherms were developed by variation of the L/m-ratio (3-25 L/g), i.e. different quantities of GFH material were added.

All experiments were conducted at room temperature (20 $\pm$1°C). Isotherms were developed by filling 250 mL glass bottles with the test solution and pre-weighed masses of the adsorbent. The bottles were shaken for 96 h. Preliminary tests indicated that equilibrium has been reached after this time. Upon equilibration, samples were filtered (0.45 µm) to remove the adsorbent.

For comparisons, isotherms developed in membrane concentrate solution were evaluated, which are described in Sperlich et al. [105]. An overview on batch isotherm experiments is shown in Table 4.

3.2.4 *Fixed-bed column studies*

Initially, two laboratory-scale column (LC) studies were performed using columns with a diameter of 25 mm and a dry mass of 45.6 g and 53.9 g of GFH, respectively, corresponding to a media depth of approx. 15 cm. The EBCT was adjusted to 3.0 and 3.3 min by experimental conditions. A medium grain size range of 0.8 - 1 mm was used. LC 1 was operated using DI water with an initial concentration of 2 mg/L P until breakthrough (after approx. 1 month and 900 L water fed).

Table 5: GFH fixed-bed column studies

Experiment type	Water matrix	pH	c_0 [mg/L P]	Grain size fraction [mm]	EBCT [min]	$EBCT_{large,\ CD}$ ($EBCT_{large,\ PD}$) [min]
LC 1	DI	7-8	2.2 ± 0.1	$0.8 - 1$	3.3	-
LC 2	DW	7-8	2.0 ± 0.1	$0.8 - 1$	3.0	-
RSSCT 1	DW	7-8	2.2 ± 0.1	$0.2 - 0.4$	0.45	3.2(1.2)
RSSCT 2	DW	7-8	2.2 ± 0.1	$0.2 - 0.4$	0.9	6.4(2.4)
RSSCT 3	DW	7-8	2.1 ± 0.1	$0.1 - 0.2$	0.6	17.1(3.2)
RSSCT 4	MBR effluent	7-8	3.0 ± 0.8	$0.1 - 0.2$	1.1	31.3(5.9)
RSSCT 5	NF concentrate	8.5	0.7 ± 0.1	$0.2 - 0.4$	0.4	2.6(1.0)

LC 2 was operated with DW and an equal initial concentration of 2 mg/L P until breakthrough occurred (after approx. 1.3 months). A total of 1,400 L was fed to the fixed-bed column.

Using significantly less water (100 - 180 L) and time (approx. 1 week) a number of RSSCTs were performed. To test the RSSCT concept, the LC design was scaled down using the constant diffusivity approach (RSSCT 1) and the proportional diffusivity approach (RSSCT 3). RSSCT 1 - 3 were scaled to test the influence of EBCT on the shape of the breakthrough curve. In RSSCT 4 and 5, competitive adsorption of waste water constituents was tested using MBR effluent and NF concentrate of secondary effluent.

A summary of the performed breakthrough experiments is given in Table 5. For RSSCTs, the theoretical EBCT of the large scale column, $EBCT_{large}$ (assuming a grain size of 0.8 mm, constant diffusivity scaling, proportional diffusivity approach in brackets) is given.

3.2.5 *Analyses*

Orthophosphate was determined using a flow injection analyzer (FIAstar 5000 Analyzer, FOSS Analytical, Denmark) according to ISO 15681-1. The standard deviation was determined to be 4.8 % at a mean concentration of 0.016 mg/L P and 0.77 % at 3.8 mg/L P with a detection limit of 3 µg/L. For pH measurement a WTW pH 340 with a Sentix 41 electrode (WTW, Germany) was used. Calcium was determined by atomic absorption spectroscopy (Varian SpectrAA-300, VARIAN, USA) at a wavelength of 422.7 nm according to DIN 38406-E3-1. DOC was analysed by thermal-catalytic oxidation using a High-TOC analyser (Elementar Analysensysteme, Germany).

3.3 RESULTS AND DISCUSSION

3.3.1 *Physical characterization of GFH*

Figure 6 shows the grain size distribution of GFH material and the specific surface area determined for the different fractions. The uniformity coefficient ($\frac{d_{60}}{d_{10}}$) is approx. 3.5. The average measured specific surface area (BET) of the sieved GFH media was $241 \pm 8\ m^2/g$. Although the specific surface area varied for the different grain size fractions, no trend can be observed and the specific

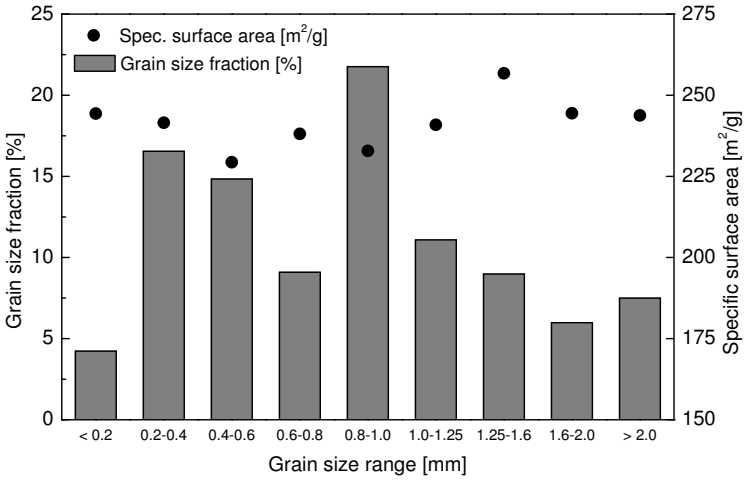

Figure 6: Specific surface area and mass fraction of different grain size fractions

surface area is not a function of grain size. Since this variation is larger than the measurement uncertainty of the BET specific surface area (0.5 %), it might be explained by the heterogeneity of the adsorbent media and hence due to the production process. This confirms Driehaus' results [36], who reported slightly higher values (280 m^2/g) independent of particle size.

Compared to the sieved media, the specific surface area measured for ground GFH material was slightly higher (251 m^2/g). The determined values confirm data reported from previous investigations (Table 6). Very similar values have been reported by Badruzzaman et al. [8] and Saha et al. [96], whereas older investigations by Teermann [109] and Driehaus [36] showed slightly higher values for the granular material. Significantly lower values for ground material [109] could not be confirmed. The specific surface area of FerroSorp media was determined to be 147.5 m^2/g, which is in the range of the reported values for Bayoxide E33 but significantly lower than the specific surface area of GFH.

Figure 7 shows that the density of the bed, the particle density, the water content and the bed porosity are not constant for the different grain size fractions. The bed density is decreasing with increasing particle size, which can be explained by the increasing homogeneity of the material, since the median size increases in relation to the constant grain size interval. On the other hand, the density of the bigger particles is higher, whereas their water content is lower. These aspects have to be considered when experiments with sieved material are performed. The observed variations in water content forbid the use of average values for water content or manufacturer's data for isotherm or breakthrough experiments. Instead, the water content should be experimentally determined for each of the sieved fractions used in the experiment. When comparing data for adsorption capacity, data should be

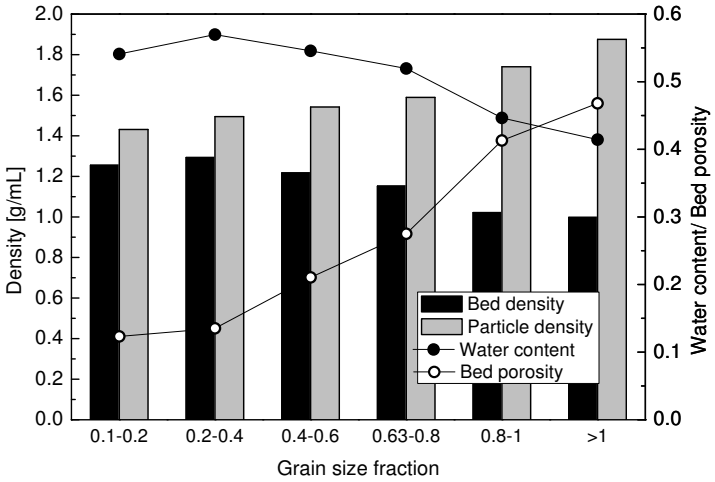

Figure 7: Density, water content and bed porosity for different GFH grain size fractions

given on a dry mass basis to avoid confusion due to different water content of the material.

Teermann [109] determined 0.76 mmol/g of active surface sites for GFH material, which corresponds to a theoretical maximum capacity of 23.6 mg/g P, if mononuclear surface complexes are assumed. Considering the determined value for specific surface area (241 m^2/g), 0.76 mmol/g of active surface sites [109] corresponds to 1.9 sites/nm^2. Assuming that the number of surface sites is directly related to adsorption capacity, the determined standard deviation for the BET measurements of the different fractions (7.8 m^2/g) can then be used to calculate a solid-phase concentration of 0.76 mg/g. This value can be considered as variation due to material heterogeneity for any solid-phase concentration calculated from mass balances in isotherm or breakthrough experiments.

3.3.2 *Batch experiments*

3.3.2.1 *Isotherms*

Figure 8 a) shows the capacity of GFH for phosphate adsorption in DI water depending on pH. At pH 7, approx. 18 mg/g P are reached at an equilibrium concentration of 1 mg/L P. A lower pH value of 6 leads to slightly higher solid-phase

concentrations, whereas at pH 8 significantly lower solid-phase concentrations (approx. 12 mg/g P at 1 mg/L P) are observed.

Table 6: Physical characterization of GFH

Data source	Grain size fractions	BET specific surface area [m^2/g]	Grain size fraction [% by weight]	Water content [%]	Particle density of the moist adsorbent [g/mL]	Bed (bulk) density, moist [g/mL]
Teermann [109]	ground	178	-	-	-	-
this study	ground	251	-	22	-	-
Teermann [109]	granular (as received)	292	-	-	-	-
Saha et al. [96]	granular (as received)	250-350	-	43-46	1.59	1.32
Driehaus [36]	granular (as received)	280±4	-	59±8	-	-
Wasserchemie [122]	granular (as received)	>220	-	40-45	1.5-1.7	1.05-1.2
Badruzzaman et al. [8]	sieved (average)	235±8	-	≈50	-	1.02-1.18
this study	sieved (average)	241±8	-	51±6	1.61±0.17	1.16±0.12
	<0.2	244.3	4.2	54[1]	1.43[1]	1.25[1]
	0.2-0.4	241.5	16.5	57	1.49	1.29
	0.4-0.63	229.4	14.8	55	1.54	1.22
	0.63-0.8	238.1	9.1	52	1.59	1.15
	0.8-1.0	232.9	21.8	45	1.74	1.02
	1.0-1.25	240.9	11.1			
	1.25-1.6	256.8	9.0	41[2]	1.88[2]	1.00[2]
	1.6-2.0	244.5	6.0			
	>2.0	243.8	7.5			

[1] determined for the grain fraction 0.1-0.2 mm
[2] determined for the grain fraction > 1.0 mm

The adsorption of phosphate onto GFH is believed to be dominated by complexation between surface groups and the adsorbing molecules. Depending on pH, the GFH surface sites react as acid or base, resulting in a pH-dependent surface charge causing electrostatic interactions with the surrounding aqueous phase [98]. Below its pH_{PZC} of 7.5 - 8.0, GFH is a positively-charged adsorbent. Phosphate is an anionic adsorbate in monovalent ($H_2PO_4^-$) and divalent (HPO_4^{2-}) form (pK_{a1} = 2.15; pK_{a2} = 7.1; pK_{a3} = 11.5). Above pH 7.1, the more negative, divalent HPO_4^{2-} will be the dominating phosphate species in solution. Also, the surface charge of GFH becomes more negative with increasing pH, resulting in more neutral and negatively charged groups on the surface. This explains the sharper decrease in adsorption capacity from pH 7 to 8 compared to the less pronounced decrease from pH 6 to 7.

Figure 8 b) shows the influence of the water matrix on GFH adsorption capacity at pH 7. The addition of 0.9 mM Ca^{2+} leads to significantly higher solid-phase concentrations compared to the reference isotherm (pH 7, DI water). Adsorption of positively charged calcium ions onto the GFH surface shifts the pH_{PZC} to higher values, thus improves the adsorption of phosphate. Also, calcium might facilitate double-layer adsorption of phosphate. Phosphate isotherm experiments

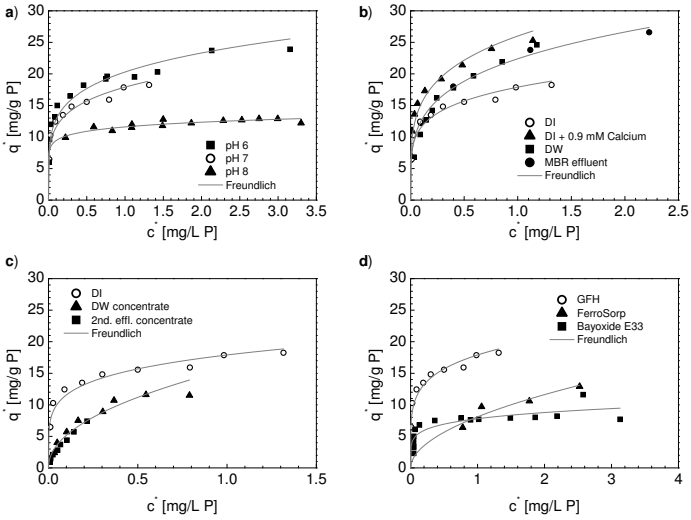

Figure 8: Batch isotherms developed for a) GFH at different pH values in DI water, b) GFH at pH 7 in different model solutions, c) GFH at pH 7 - 8 in membrane concentrates [105], d) GFH, FerroSorp and Bayoxide E33 in DI water

using Berlin drinking water also show higher capacities than in DI water, but slightly less than the calcium spiked DI water. Calcium concentrations in Berlin drinking water were significantly higher (2.5 mM), but competition of other water constituents such as DOC (approx. 4.5 mg/L) has to be taken into account. Isotherms with MBR effluent from Beijing's waste water treatment plant Beixiaohe (DOC approx. 6.4 mg/L) show very similar capacity.

Compared to the reference isotherm (DI water, pH 7), isotherms of NF concentrate of secondary effluent and DW [105] show lower capacities (Figure 8 c). Competition of high concentrations of DOC present in the NF concentrates, the high ionic strength and lower initial phosphate concentrations lead to lower solid-phase concentrations. Although higher concentrations of calcium are also present, this cannot compensate for DOC competition.

Figure 8 d) shows phosphate adsorption isotherms for FerroSorp and Bayoxide E33 under identical conditions (DI water, pH 7). The results show that GFH shows significantly higher capacities for phosphate adsorption (approx. twice as high solid-phase concentrations). This is in accordance with the significant lower specific surface areas of these adsorbents.

All isotherm results were evaluated using the Langmuir [79] and Freundlich [51] equations. The determined isotherm constants are summarized in Table 7. As can be seen from the coefficients of determination, both models can be used to describe the adsorption of phosphate onto GFH. The Langmuir isotherm appears to be slightly better suited to describe the equilibrium data. To be consistent with fixed-bed modeling studies which use Freundlich isotherm data as input parameters, the Freundlich constants were used for calculation of the ideal breakthrough point.

In summary, GFH adsorption is pH dependent, resulting in a significant decrease in capacity in the relevant pH range between 6 and 8 (DI water). Compared to the theoretical maximum capacity of 23.6 mg/g P calculated from surface area and assuming mononuclear surface complex formation, adsorption capacity at pH 6 is in the range of this value, indicating that the maximum capacity might have been reached. Adsorption of phosphate from DW and waste water (MBR effluent) is improved compared to the single adsorbate system. This can be attributed to the presence of calcium which outweighs competition of DOC and could indicate multilayer coverage or formation of ternary surface complexes (e.g., calcium-phosphate surface complexes). At pH 7, equilibrium solid-phase concentrations in the range of the theoretical maximum capacity are observed. Adsorption of phosphate from NF concentrate is decreased compared to the single adsorbate system.

Table 7: Isotherm model parameter: Freundlich and Langmuir coefficients

Water matrix	Adsorbent	pH	Freundlich parameters			Langmuir parameters		
			K_F *	n	R^2	q_m	K_L	R^2
				[-]		[mg/g]	[L/mg]	
DI	GFH	6.2 ± 0.1	20.3	0.20	0.91	23.9	9.3	0.99
DI	GFH	7.1 ± 0.2	17.9	0.19	0.93	18.4	18.9	0.99
DI	GFH	8.1 ± 0.2	11.6	0.09	0.81	13.0	10.3	0.99
DI + Calcium	GFH	7.0 ± 0.2	26.0	0.23	0.91	25.7	20.2	0.99
DW	GFH	7.0 ± 0.2	24.2	0.35	0.98	26.7	6.3	0.99
MBR effluent	GFH	7.2 ± 0.1	22.4	0.25	0.99	28.5	5.4	1.00
NF concentrate of DW	GFH	7.3 ± 0.1	15.6	0.48	0.94	13.9	7.2	0.99
NF concentrate of 2ndary effl.	GFH	7.2 ± 0.1	18.9	0.62	0.98	10.1	9.6	0.91
DI	FerroSorp	7.2 ± 0.1	8.1	0.52	0.87	20.1	0.7	0.92
DI	Bayoxide E33	7.2 ± 0.1	7.8	0.17	0.69	8.7	14.9	0.96

* $[L^n/(g \times mg^{n-1})]$

3.3.3 *Fixed-bed column studies*

Phosphate breakthrough curves for GFH adsorption in different water matrices are shown in Figure 9. The ideal (stoichiometric) breakthrough was calculated from Freundlich isotherm constants and is shown for comparison (Table 4).

Figure 9 a) shows phosphate breakthrough in identically scaled laboratory-scale columns for DI water and DW. The lower capacities observed in isotherms using DI water are confirmed by the column results. The stoichiometric breakthrough according to isotherm results matches quite well.

Figure 9 b) compares laboratory-scale DW data to DW RSSCT operated with different EBCTs. Obviously, breakthrough data of RSSCT 1 (corresponding EBCT using constant diffusivity scaling) capture the shape of the laboratory-scale breakthrough curve quite well, although the breakthrough occurs slightly later. RSSCT 3, which was scaled using the proportional diffusivity approach, shows a steeper, more sigmoidal breakthrough curve which does not follow the laboratory-scale breakthrough curve (LC 2). In conclusion, the constant diffusivity scaling is better

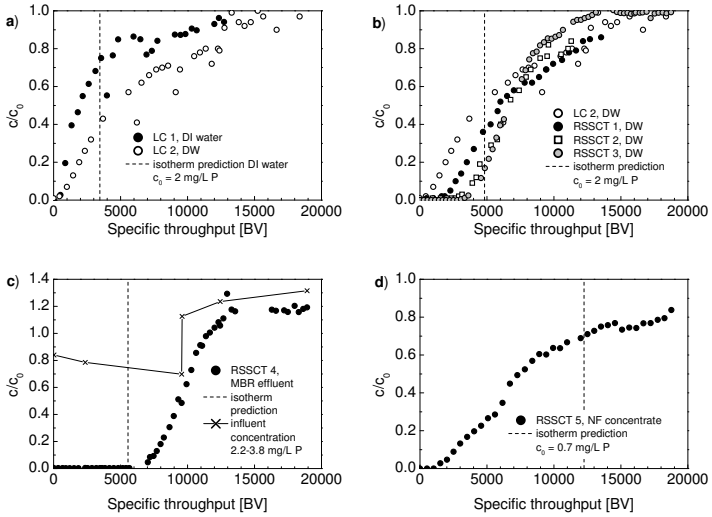

Figure 9: Phosphate breakthrough in GFH fixed-bed columns operated in different water matrices and corresponding isotherm prediction: a) DI water vs. DW, pH 7 - 8, b) DW, pH 7 - 8 c) MBR effluent, d) NF concentrate

suited to describe phosphate breakthrough onto GFH than the proportional diffusivity scaling, confirming earlier results for arsenate adsorption onto GFH [101]. The RSSCT breakthrough curves operated with different EBCTs under otherwise identical conditions (RSSCT 1 - 3, DW, pH 7 - 8, c_0 = 2 mg P/L) also show the strong influence of mass transfer on the shape of the breakthrough curve. The RSSCT columns which were scaled using higher values of the EBCT (RSSCT 2 - 3) show a more sigmoidal breakthrough curve compared to the asymptotical shape of the lower EBCT column (RSSCT 1). Theoretically, the stoichiometric breakthrough point should match the barycenter of the breakthrough curve. Thus, for drinking water, the isotherm data slightly underpredict the adsorbents capacity.

Figure 9 c) shows breakthrough data determined for MBR effluent along with the influent concentration, which was normalized to the average influent concentration. Obviously, biological activity in the waste water storage tank led to a decreasing influent concentration and a sudden increase of influent concentration, when the feed water was changed (at approx. 10,000 BV). The ideal breakthrough point calculated from isotherm data using the average influent concentration underpredicts the operation time of the fixed-bed column significantly, which can be explained by the varying influent concentration and bacterial growth in the storage tank. The high EBCT used for scaling the RSSCT is reflected in the steep shape of the breakthrough curve.

In Figure 9 d), the calculated ideal breakthrough is tested against RSSCT data from experiments using NF concentrate [105]. A reasonable isotherm prediction is shown and a strong influence of adsorption kinetics is indicated by the flat breakthrough curve. The influence of mass transfer on the shape of the breakthrough

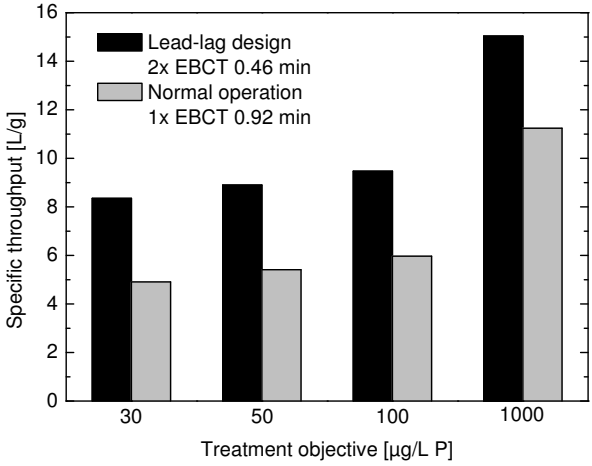

Figure 10: Calculated specific throughput for operation of two GFH fixed-beds in series (lead-lag design)

curve is discussed in detail in Sperlich et al. [103]. In this study, the focus was set on adsorption capacity.

In summary, isotherm results are in good agreement with fixed-bed data. Consequently, isotherms can be used to provide a reasonable, but rough estimation of operation time by calculating the ideal breakthrough point. However, GFH breakthrough curves are strongly influenced by mass transfer and corresponding operational parameters such as EBCT, which leads to a flat, asymptotical shape of the breakthrough curve at lower EBCTs. In these cases, prediction of breakthrough using isotherm data is very inaccurate. The implications for prediction of breakthrough curves are discussed in Sperlich et al. [103].

Analysis of breakthrough data from RSSCT 1 and 2 (Figure 9) helps to quantify the improvement in utilization of the adsorbent when used in series. Since RSSCT 2 was operated with an EBCT twice as high as RSSCT 1, the breakthrough profiles represent the breakthrough profile of the second (lag) and the first (lead) column in series operation, respectively. The specific throughput was calculated for treatment objectives of 30, 50, 100 and 1000 µg/L P using Eq. 3.1 and integration of the breakthrough curves. Figure 10 shows that operation of fixed-beds in series allows significant higher specific throughputs, ranging from 134 to 175 % compared to normal operation and depending on the treatment objective. Consequently, better utilization of the adsorbent material can improve bed life and might reduce operation cost, especially if low effluent concentrations are needed. However, the saved adsorbent costs have to be compared to the extra costs for additional vessels and piping.

3.4 CONCLUSIONS

- Physical characterization of GFH shows a high specific surface area of 241 ± 8 m^2/g independent of grain size.
- Variations of particle density, bed density and water content were observed for different grain size fractions and have to be considered when sieved material is used.
- High capacities for phosphate adsorption onto GFH were determined. Under the chosen experimental conditions (pH 7, DI water) GFH outperforms the alternative adsorbents FerroSorp and Bayoxide E33 by a factor of approximately two.
- GFH is suitable to remove phosphate from waste water. Capacities in drinking and waste water are approximately 25 % higher than in DI water (at pH 7 - 8, c^* = 1 mg/L P).
- Competitive adsorption of DOC is compensated by the presence of calcium which improves phosphate adsorption.
- Batch equilibrium data are in agreement with capacities observed in fixed-bed column experiments and can provide a rough estimation of column breakthrough.
- RSSCT account for slow mass transfer and can simulate larger pilot and laboratory scale columns experiments.
- Analysis of column breakthrough data shows that operation of two GFH columns in series results in a 134 - 175 % more efficient use of the adsorbent as compared to single column operation.

4 SURFACE COMPLEXATION MODELING

4.1 INTRODUCTION

SCMs can be used to describe the adsorption equilibrium. Their advantage over isotherm models is that they can be used to predict adsorption equilibria under different pH, water quality, and experimental (e.g., liquid-to-mass ratio used) conditions, if the model is valid and the surface complexation constants known. Ideally, this allows the calculation of isotherms based on water quality data. Despite this enormous potential, SCMs are still more a topic of scientific debate, rather than applied in practice, due to a number of problems. First, the equilibrium constants for surface complexes formed by any adsorbate/adsorbent combination have to be known. For complex waters the number of complexes formed in solution and at the surface is much higher than in artificial model solutions. Up to now, most studies have been on simpler, artificial systems. Usually, the formed surface complexes are hypothesized and batch equilibrium data are fitted to derive the constants. Evidence for the formation of a specific surface complex can only be provided by spectroscopic methods. Nevertheless, information about phosphate surface complex formation on iron oxide surfaces varies widely in both the specific complexes formed and the constants determined [23]. Furthermore, a number of different SCMs exist and there is no consensus about their applicability [23, 81].

Genz [56] proposed to describe phosphate adsorption onto GFH by three mononuclear surface complexes, which had earlier been proposed for the adsorption of phosphate onto goethite (Equation 2.7). The description of adsorption edges recorded in this study was succesfull, but the model was not able to predict isotherm data determined under different experimental conditions.

To clearly identify the formed phosphate surface complexes at the GFH surface and the most suitable SCM is beyond the scope of this research. Instead, the surface complexes proposed by Genz [56] for phosphate adsorption onto GFH will be evaluated for their validity for the experimental data determined in this study. For simplicity and to enable comparison with Genz [56], the DDL model was chosen to describe phosphate and calcium adsorption onto GFH and tested against experimental equilibrium data. Ultimately, the aim is to predict adsorption capacity based on water quality analysis only, in order to improve the design of fixed-bed treatment systems.

4.2 METHODOLOGY

4.2.1 *pH adsorption edge*

A series of one-point isotherms developed at different pH values are also termed adsorption edge. Although limited to a fixed initial liquid-phase concentration, adsorption edges provide valuable information about the pH dependency of adsorption. Adsorption edges have been frequently used in combination with surface complexation models (SCMs) to derive surface complexation constants,

although any equilibrium data could be used as input for SCMs. In this study, adsorption edge data will be supplemented with isotherm data in the pH range relevant for GFH application (pH 6-8) and used for surface complexation modeling.

Adsorption edges were developed using GFH material of a grain size of 0.2 - 0.4 mm and a water content of approx. 40 %. Analogously to isotherm experiments, model solutions were prepared (DI water, 10 mM NaCl) with an initial phosphate concentration of 2.0 mg/L P and 15.4 mg/L of calcium. For single adsorbate experiments with calcium, an initial concentration of 24.6 mg/L Ca was set. Identical quantities of approx. 25 mg GFH were added to 200 mL solution (corresponding to a liquid-to-mass-ratio of 0.12 - 0.15 L/g) and different pH values were set by adding NaOH or HCl. After 96 h equilibration, samples were filtered and analyzed for phosphate and calcium. Since no buffer was used, pH values showed some variation until the end of the experiment and the final, equilibrium pH was measured.

4.2.2 *Parameter estimation with PHREEQC and PEST*

For fitting the adsorption edge of phosphate on GFH, the model-independent non-linear parameter estimation program PEST [52] is used in combination with PHREEQC-2 [91]. PEST fits calculated values with obervations by varying the value of one or more parameters in the input file of another program, in this case PHREEQC-2. The output file generated with PHREEQC-2 is read by PEST and compared with the observations. The parameter estimation process for nonlinear problems is an iterative process in which the Gauss-Marquardt-Levenberg algorithm is used [32].

PHREEQC-2 is a computer program designed to perform a wide variety of aqueous geochemical calculations, including speciation and surface complexation reactions. The DDL model [40] has been incorporated into PHREEQC-2 and three databases containing reaction constants are distributed with the program [91]. For the calculations in this study, the database minteq.v4.dat was used, which can be regarded as the most complete of the available databases. Among others, it contains reaction constants for dicalcium phosphate and hydroxylapatite, i.e. a potential precipitation interfering with SC formation is accounted for. The combined use of PEST and PHREEQC-2 for surface complexation modeling has been demonstrated by Appelo et al. [2].

4.2.3 *Surface Complexation Modeling*

The DDL model was tested against batch equilibrium data for GFH, either determined in this study or by Genz [56]. The speciation of the GFH surface was described as shown in equation 2.4-2.5 and the two acidity constants determined by Teermann [109] (pK_{a1}=6.3 and pK_{a2}=-9.4) were used. Adsorption of phosphate onto the ferric hydroxide surface was described by three mononuclear surface complexes as proposed by Genz [56] (Equation 2.7-2.9). Further input parameters are the concentration of solids in the batch experiments (in g/L) and the GFH surface site concentration (in mol/L), which can be calculated from the solids concentration and the total number of sites of 7.6×10^{-4} mol/g [109]. The determined BET specific surface area values (Table 6) were also used as input parameters.

4.3 RESULTS AND DISCUSSION

4.3.1 *Phosphate adsorption*

As a starting point, phosphate adsorption edges determined by Genz [56] were used to fit the DDL model. The resulting surface complexation constants (Table 8) are very close to the values determined by Genz. The difference is due to the different fitting procedures used. Whereas Genz [56] used FITEQL [123], PHREEQC-2/ PEST were used in this study. Compared to FITEQL, PHREEQC-2/ PEST has been found to be more stable, less prone to conversion problems in the iteration process and generally easier to use. Another important advantage of PHREEQC-2/ PEST over FITEQL is that PHREEQC-2 is not limited to a fixed L/m-ratio, which makes it possible to use adsorption isotherm data to supplement adsorption edge data. Figure 11 a) shows that the adsorption edge data can be described very good. PHREEQC-2 was then used to calculate adsorption edges as well as isotherms (Figure 8) determined in this study. Figure 11 b) shows that the adsorption edges cannot be predicted, but are both overpredicted by 10 - 20 %. Obviously, there is a discrepancy between the adsorption edge data determined by Genz [56] and in this study (Figure 11 a/b), especially in the pH range 6 - 9. Since both data sets are very limited, it is hard to find reasons for this difference and to identify potential errors in measurement. Other reasons for the different measurements might be the heterogeneity of the used GFH material as well as different characteristics of the GFH material used (different production batches). Without significantly more experimental data, this argument remains speculative. More research would be needed to clarify this, but this is beyond the scope of this study.

In a second parameter estimation run, the adsorption edge data determined in this study were used as input parameters. The results are shown in Figure 12. The input data (Figure 12 b) can be described successfully, but Genz' data (a) and isotherms (c) are significantly underpredicted.

Third, isotherm data (Figure 8) were used to supplement adsorption edge data and provide more input data for parameter estimation. The optimization results using both adsorption edge and isotherm data as PHREEQC-2/ PEST input are shown in Figure 13. Obviously, the isotherm data can be described very good. Both adsorption edge data sets are not perfectly described, but deviations are lower than in the previous attempts and phosphate adsorption onto GFH can be predicted reasonably well. The model slightly underpredicts Genz' and overpredicts the phosphate adsorption edge data from this study. This is because isotherm data (pH 6-8) were used to supplement the shown adsorption edge data and also used for fitting the DDL model. This puts more emphasis on the pH range relevant for most natural waters and waste waters. The model shows that at lower pH values, the uncharged surface complex $\equiv FePO_4H_2$ will be predominantly formed. Between pH 6 and 9.5, the dominating surface complex is $\equiv FePO_4H^-$. The formation of $\equiv FePO_4^{2-}$ at higher pH values is strongly hindered by the unfavourable conditions. Table 8 shows a summary of the calculated surface complexation constants.

In summary, phosphate adsorption onto GFH can in principle be described using the DDL model and three mononuclear surface complexes proposed by Genz [56]. However, the prediction of equilibrium data sets determined under different experimental conditions is difficult. It is, however, not clear, whether this is due to contradictory experimental results or to the modeling approach.

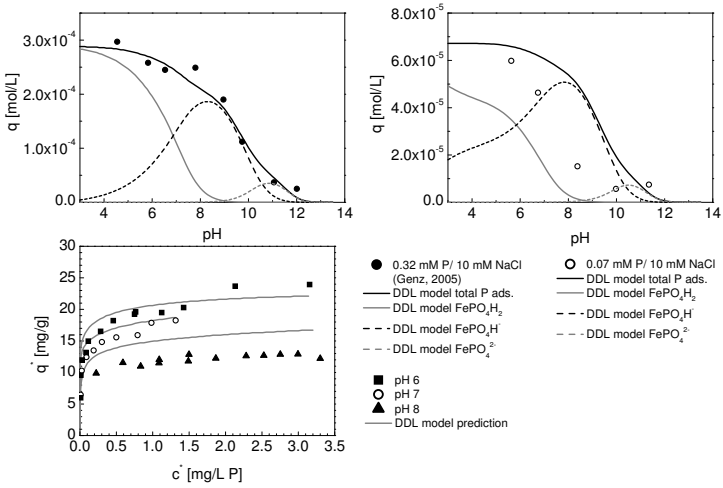

Figure 11: GFH-phosphate equilibrium data and DDL model prediction: a) adsorption edges determined by Genz [56], b) adsorption edges determined in this study, c) isotherm data (this study, cf. ch. 3); data set a) was used for fitting

4.3.2 *Interaction between calcium and phosphate adsorption*

Figure 14 shows adsorption edges for phosphate and calcium. In the presence of calcium, phosphate adsorption is significantly improved at pH $>$ 7. Whereas phosphate adsorption in the single-solute system decreases sharply between pH 7 and 9, this decrease is much less pronounced in the presence of calcium. In the single-solute system, calcium adsorbs at pH values above the pH_{PZC}, which is around pH 8. In the presence of phosphate, higher solid-phase concentrations of calcium are observed. Also, adsorption occurs below pH 8. Adsorption of negatively charged phosphate ions onto the GFH surface shifts the pH_{PZC} to lower values and improves adsorption of calcium, whereas adsorption of calcium cations shifts it to higher values, thus improves the adsorption of phosphate. Another

Table 8: GFH phosphate surface complexation constants for formation of three mononuclear surface complexes(Equation 2.7-2.9)

$pK_{a\,1}$ $\equiv FePO_4H_2$	$pK_{a\,2}$ $\equiv FePO_4H^-$	$pK_{a\,3}$ $\equiv FePO_4^{2-}$	Data used for fitting/ fitting procedure
32.32	28.03	19.70	Adsorption edge data [56], FITEQL
33.04±0.64	28.46±1.91	20.36±1.02	Adsorption edge data [56], PHREEQC-2/ PEST
31.37±2.30	25.55±1.28	19.48±3.89	Adsorption edge data (this study), PHREEQC-2/ PEST
32.40±0.24	27.21±0.28	19.68±1.75	Adsorption edge and isotherm data (this study), PHREEQC-2/ PEST

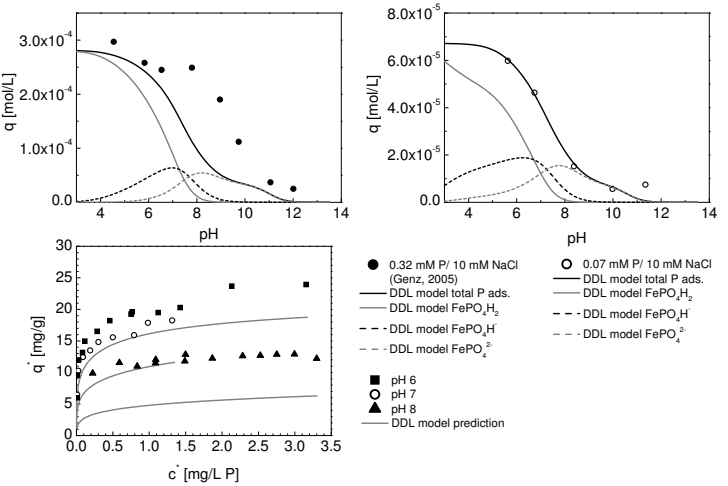

Figure 12: GFH-phosphate equilibrium data and DDL model prediction: a) adsorption edges determined by Genz [56], b) adsorption edges determined in this study, c) isotherm data (this study, cf. ch. 3); data set b) was used for fitting

explanation for the shown interaction is the formation of ternary P-Ca surface complexes. The shown results are in accordance with isotherm results, where addition of 0.9 mM calcium led to significantly higher phosphate adsorption capacities (Figure 8 b).

Calcium adsorption data in the single-adsorbate system could be satisfactorily fitted assuming the formation of a monodentate calcium surface complex:

$$\equiv FeOH + Ca^{2+} \quad \rightleftharpoons \quad \equiv FeOHCa^{+} + H^{+} \tag{4.1}$$

This reaction was proposed for calcium adsorption onto goethite by Gao and Mucci [53]. The PEST optimization routine calculates a pK value of 5.55 ± 0.52 for the ternary Ca-P surface complex.

Whereas the hypothesized surface complexes describe phosphate and calcium adsorption in the single adsorbate system quite well, the improved adsorption in the presence of calcium cannot be described with phosphate and calcium surface complexes only. Adsorption edge simulations using PHREEQC-2 for the Ca-P-GFH system are identical to the single adsorbate system, if only the described surface complexes are used. Also, the observed effect cannot be caused by Ca-P precipitation, as the PHREEQC-2 calculations show. To model the interaction between phosphate and calcium adsorption, two ternary calcium-phosphate surface complexes were hypothesized and tested:

$$\equiv FeOH + Ca^{2+} + PO_4^{3-} \quad \rightleftharpoons \quad \equiv FeOCaPO_4H^{-} \tag{4.2}$$

$$\equiv FeOH + Ca^{2+} + PO_4^{3-} + H^{+} \quad \rightleftharpoons \quad \equiv FeOCaPO_4H_2 \tag{4.3}$$

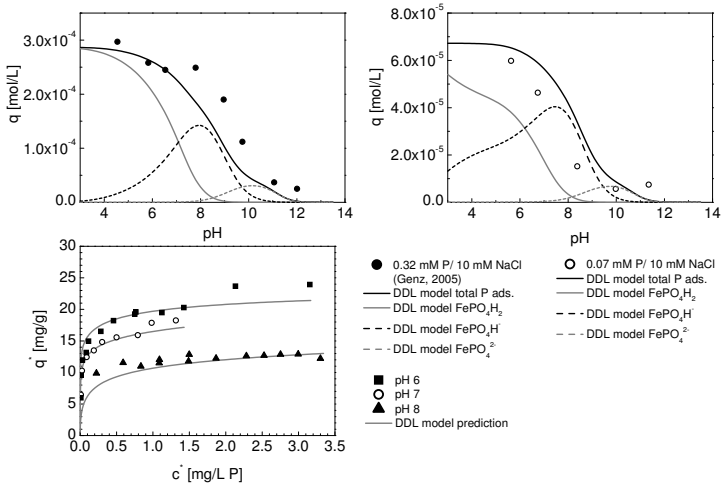

Figure 13: GFH-phosphate equilibrium data and DDL model prediction: a) adsorption edges determined by Genz [56], b) adsorption edges determined in this study, c) isotherm data (this study, cf. ch. 3); data set b) and c) were used for fitting

Gao and Mucci [53] formulated these complexes for phosphate adsorption onto goethite and could successfully describe phosphate-calcium interaction. However, using these complexes, the PEST optimization algorithm did not converge. Based on the presented experimental data, the interaction between phosphate and calcium adsorption cannot be described using the DDL model with the hypothesized surface complexes. Different conclusions might be drawn from this observation. First, these results put forward the statement of other researchers who have concluded that the observed calcium-phosphate interactions result purely from electrostatic effects without the formation of ternary surface complexes [94]. However, the available alternative, more sophisticated SCMs need to be tested with the presented data to confirm these results. Second, it cannot be ruled out that the used data set was not large enough to ensure a successful fitting with the DDL model. To provide insight into adsorption mechanisms, spectroscopic methods need to be used to obtain valid information on phosphate and calcium surface complex formation on the GFH surface.

Whereas the successful fitting with a SCM might be an indication for a specific mechanism such as ternary adsorption, it does not provide evidence. In this regard, the abundance of available literature belies the fact that the exact structure and formation of phosphate surface complexes remains unknown. In an earlier work, Thole [112] draws similar conclusions from batch experiments using amorphous ferric hydroxide and waterworks sludge. In this study, the presence of calcium led to an improved adsorption of phosphate, which was interpreted to be caused by compensation of the negative surface charge and also formation of calcium phosphate precipitates. In the present study, low calcium concentrations of 0.6 M

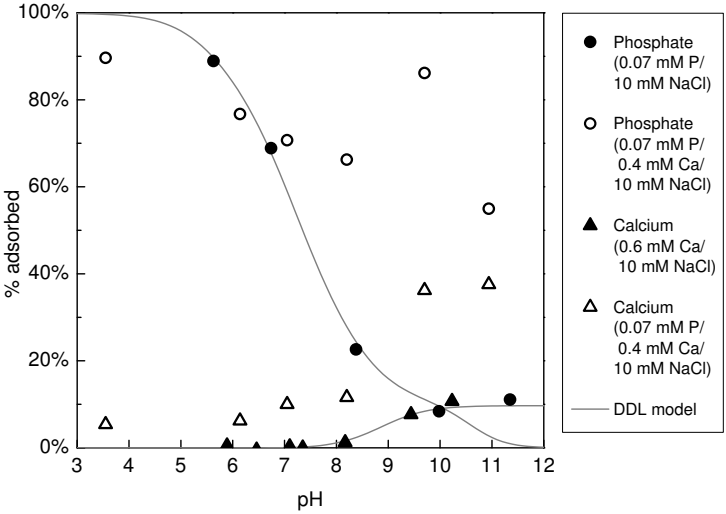

Figure 14: Adsorption of phosphate and calcium onto GFH in the single-solute system (filled symbols) and in the presence of the other ion (empty symbols)

were used. Using the minteq.v4.dat database, PHREEQC-2 calculations showed no precipitate formation. The formation of tricalcium and octacalcium phosphate precipitates is not included in the used database and cannot be ruled out. Using classical adsorption experiments, the limits of adsorption and precipitation are hard to define. In low concentration ranges, the formation of defined solid phases cannot be assumed. Instead, complex solid-phase equilibria can be expected, ranging from pure adsorption to heterogeneous surface precipitation [113].

However, the identification of the phosphate adsorption/removal mechanism was not the focus of this study. Instead, the objective was to describe the observed adsorption equilibrium data with existing SCMs in order to develop a tool for breakthrough prediction. From this more practical viewpoint, the use of SCMs to provide a prediction of adsorption equilibrium and thus the ideal breakthrough point of a GFH fixed-bed column based only on water quality data remains an ambitious goal for future research.

4.4 CONCLUSIONS

- In principle, phosphate adsorption onto GFH could be described using the DDL model under the assumption of three mononuclear surface complexes.
- Prediction of equilibrium data sets determined under different experimental conditions is difficult.

- An interaction between phosphate and calcium adsorption onto GFH was observed: presence of calcium significantly improved phosphate adsorption and vice-versa.

- Whereas the hypothesized surface complexes describe phosphate and calcium adsorption in the single adsorbate system quite well, the interaction between phosphate and calcium adsorption cannot be described using the DDL, not even using hypothesized ternary Ca-P complexes.

5

TREATMENT OF MEMBRANE CONCENTRATES: PHOSPHATE REMOVAL AND REDUCTION OF SCALING POTENTIAL

Alexander Sperlich[1], David Warschke[1], Christine Wegmann[1], Mathias Ernst[1] and Martin Jekel[1]

Water Science & Technology 2010, 61(2), 301-306.

ABSTRACT

The widespread application of nanofiltration (NF) and reverse osmosis (RO) membranes in wastewater reuse inevitably generates a concentrate stream. Due to high concentrations of phosphate and salts, disposal of membrane concentrates is a problem which seriously constrains the application of this technology, especially in inland applications. There is a need for technologies which facilitate an affordable and environmentally-safe disposal of membrane concentrates. The objectives of this study are to investigate appropriate treatment techniques to 1) increase the recovery of the membrane filtration thus minimising the volume of the concentrate stream, and 2) increase the concentrate quality to enable discharge into surface water bodies. The results show that both adsorption onto granular ferric hydroxide (GFH) and chemical precipitation are generally effective for phosphate removal from NF concentrates. Chemical precipitation by dosing of sodium hydroxide solution is rapid and removes more than 90 % of phosphate and calcium ions. By the removal of calcium ions, chemical precipitation can significantly reduce the scaling potential of NF and RO concentrates. This may allow for higher recoveries in the NF/ RO process.

5.1 INTRODUCTION

The reuse of treated municipal wastewater is already practiced in many parts of the world and continues to gain importance. The necessary advanced wastewater treatment for reclamation includes membrane filtration processes, which can provide an excellent barrier for pathogens and contaminants. However, high pressure membrane processes will inevitably generate a concentrate stream of 5 - 25 % of the feed volume. Management and disposal of membrane concentrates is a problem which might seriously constrain the application of this technology in inland communities [86], and also the widely practiced discharge into seawater has caused environmental concerns [116]. For inland applications, treatment options for membrane concentrates include discharge into surface water bodies, discharge into wastewater treatment plants, and deep-well injection. Due to the rejection of polyvalent anions by nanofiltration (NF) and reverse osmosis (RO) membranes, high concentrations of phosphate occur in membrane concentrates.

1 Technische Universität Berlin

Since even small phosphate concentrations can cause eutrophication, phosphorus-rich concentrate streams cannot be discharged into small to medium-sized surface water bodies. Consequently, both discharge into surface water and deep-well injection are difficult due to severe restrictions by water authorities. From a resource perspective, a potential recovery of nutrients from the concentrate stream might also be an interesting option. Discharge into the sewer system is not always possible and results in high costs. There is a need for technologies which facilitate an affordable and environmentally safe concentrate disposal. Where the above disposal options are not feasible, the alternative is zero liquid discharge (ZLD). In ZLD desalination, the concentrate is treated to produce desalinated water and essentially dry salts, which can be achieved by thermal desalination or evaporation ponds. This results in high energy or large land area demands [15].

The objectives of this study are to investigate appropriate treatment techniques to 1) increase the recovery of the membrane filtration and minimise the volume of the concentrate stream, and 2) increase the concentrate quality to enable discharge in surface water bodies (Figure 15). Volume minimisation requires the removal of scaling components, e. g. calcium ions. Chemical precipitation/ softening has been reported to be a potential treatment option for this purpose [66]. Since most concentrate brines are supersaturated with respect to calcium phosphate compounds, induced crystallisation of calcium phosphates using an appropriate seed material such as calcite [33] or tobermorite [12] might be another treatment option. The second objective could be met by the removal of phosphorus from membrane concentrates. Granular ferric hydroxide (GFH) has shown high capacities for arsenate and phosphate [44, 103] adsorption from aqueous solutions. This study investigates the suitability of GFH adsorption and chemical precipitation for phosphate removal from membrane concentrates and the reduction of scaling potential.

5.2 METHODS

5.2.1 *Materials and model solutions*

Granular ferric hydroxide (GFH) was obtained from the producer (GEH Wasserchemie, Osnabrück). GFH is predominantly akaganeite (β-FeOOH), a poorly crystallised iron oxide with a specific surface area of approx. 250 m^2/g [110, 96]. Calcite was obtained from Rheinkalk Akdolit (Pelm, Germany). The commercial product has a grain size range of 0.5 - 3.15 mm.

Membrane concentrate was produced from filtered secondary effluent and Berlin tap water using a nanofiltration pilot plant. A DOW NF270 membrane was operated in cross-flow mode with a water conversion factor (WCF) of 0.7 - 0.8. NF concentrate of filtered secondary effluent and tap water concentrate were produced discontinuously in a 200 L feed tank. NF concentrate was recycled to the feed tank, NF permeate was discarded.

To study the effect of concentrate water quality, RO concentrate from a full-scale RO application (the Torreele facility in Wulpen, Belgium) was also used. RO permeate of ultra-filtered secondary effluent is used for infiltration and reclamation [119]. The RO plant is operated using DOW Filmtec 30LE membranes at a WCF of approx. 0.75. Table 9 shows water quality data for the used concentrate solutions.

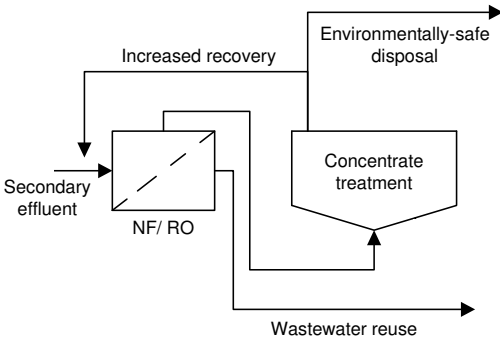

Figure 15: Investigated treatment scheme

RO concentrate data are in agreement with recently reported discharge water data [119].

Table 9: Water quality data of membrane concentrates used in this study

Parameter	NF concentrate of Berlin drinking water	NF concentrate of filtered secondary effluent	RO concentrate
pH [-]	7.5	7.0 - 8.5	8.1
Ca^{2+} [mg/L]	255	164 - 359	353
Mg^{2+} [mg/L]	37	26 - 44	41
PO_4^{3-}-P [mg/L]	0.1	0.4 - 1.3	1.3
DOC [mg/L]	19	27 - 52	34
SO_4^{2-} [mg/L]	336	369 - 574	268
Na^{+} [mg/L]	59	157 - 228	532
Cl^{-} [mg/L]	69	165 - 180	633

5.2.2 *Equilibrium isotherms*

GFH adsorption isotherms were developed using < 63 µm (ground) GFH, an equilibration time of 96 hours at room temperature (approx. 20°C). Different quantities of the adsorbent (4 to 80 mg dry matter) were added to 200 mL of solution. Prior to phosphate analysis, the samples were filtered using a 0.45 µm filter. For isotherm experiments, tap water concentrate was spiked with phosphate to a

concentration of 1.1 mg/L PO_4^{3-}-P. Initial PO_4^{3-}-P concentration of NF concentrate of tertiary effluent was 0.4 mg/L.

5.2.3 *Batch precipitation experiments*

In 2 L batches, different amounts of sodium hydroxide solution (3.1 - 22.5 mM NaOH) and calcite seeds were added to 1.6 L of NF and RO concentrates. After addition of NaOH, the solution was stirred for 2 h at 250 rpm. Samples were taken regularly, filtered (0.45 µm) and analysed for phosphate and other ions.

5.2.4 *Fixed-bed calcite column*

Three laboratory-scale columns were operated in series using NF concentrate of tertiary effluent. The columns had a diameter of 25 mm and 40 mm, respectively, and used a total dry mass of 600 g calcite as filter material. The total empty-bed contact time (EBCT) was adjusted to 25 minutes. The columns were operated for 165 h using a total volume of 200 L NF concentrate.

5.2.5 *Analyses*

Orthophosphate was determined using a flow injection analyzer (FIAstar 5000, Foss Tecator) according to ISO 15681-1. The standard deviation was determined to be 4.8 % at a mean concentration of 0.016 mg/L PO_4^{3-}-P and 0.77 % at 3.8 mg/L PO_4^{3-}-P with a detection limit of 3 µg/L. The concentrations of dissolved ions were analysed using Ion Chromatography (Dionex IonPac AS 11/14). DOC was analysed by thermal-catalytic oxidation using a High-TOC analyser (Elementar Analysensysteme, Germany).

5.3 results and discussion

5.3.1 *Adsorption*

Figure 16 shows adsorption equilibrium data for NF concentrates of filtered secondary effluent and drinking water. Solid-phase concentrations for NF concentrate of filtered secondary effluent and tap water at pH 7 are highly comparable. This is in agreement with the similar concentrations of calcium in tap water concentrate and secondary effluent concentrate. Competition of DOC seems to have only minor influence on the adsorption equilibrium. Adsorption capacity is significantly decreased at pH 8, confirming the decisive influence of pH for GFH adsorption [102]. Compared to isotherm data obtained from experiments using MBR effluent [44], the achieved capacities are lower, but in the same order of magnitude. Isotherm data clearly show that GFH can effectively remove phosphate from membrane concentrates.

Competition of DOC present in the membrane concentrate is compensated by the presence of divalent cations (Ca^{2+}, Mg^{2+}). These ions adsorb onto the metal oxide surface and increase the pH_{PZC} (point of zero charge), thereby promoting the adsorption of negatively charged $HPO_4^{2-}/H_2PO_4^-$ ions.

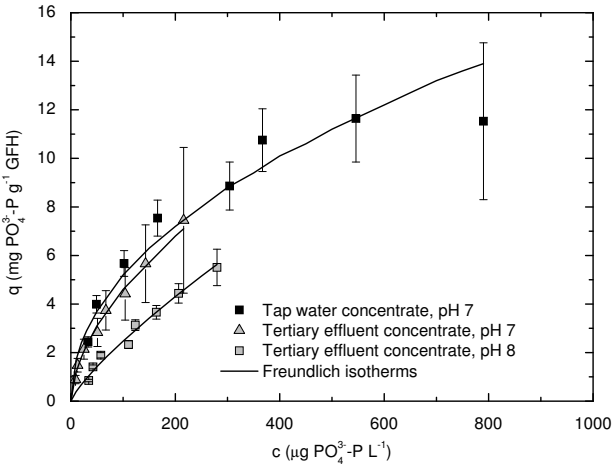

Figure 16: Phosphate adsorption equilibrium isotherms for NF concentrate of tap water (c_0 = 1 mg/L PO_4^{3-}-P, pH 7) and tertiary effluent concentrate (c_0 = 0.4 mg/L PO_4^{3-}-P, pH 7 and 8)

5.3.2 *Chemical Precipitation*

Figure 17 shows the removal of phosphate and other water constituents by induced precipitation by addition of NaOH. For the NF concentrate, a phosphate removal of 70 % is reached using 3.1 mM NaOH, corresponding to approx. pH 9.2. Higher dosages of NaOH (9.4 and 15.6 mM, respectively) increase the removal up to more than 90 %. For RO concentrate, a complete phosphate removal can already be achieved using 6.3 mM, corresponding to pH 9.2. Besides the removal of phosphate, chemical softening reduces the concentration of Ca^{2+} (removal of 50 - 90 %) effectively. At pH values higher than 10.5, the removal of Mg^{2+} is possible. This is due to the precipitation of $Mg(OH)_2$, which is known to occur at these pH values. The removal of K^+, Cl^-, SO_4^{2-} is negligible (lower than 10 %). The addition of NaOH to increase the pH and precipitate calcium carbonate and calcium phosphate, leads to an increased Na^+ concentration and therefore no reduction of TDS is achieved.

Figure 18 shows the calculated solubility index (SI) for calcium carbonate of the membrane concentrate solutions prior and after batch precipitation as a function of pH. The calculation is based on the water quality data shown in Table 9, chemical speciation calculations were done using the software MINEQL+. Obviously, both membrane concentrate solutions have a similar scaling potential as expressed in the SI_{CaCO_3}. Chemical precipitation using NaOH can significantly reduce the scaling potential and may facilitate higher recoveries in the membrane filtration step.

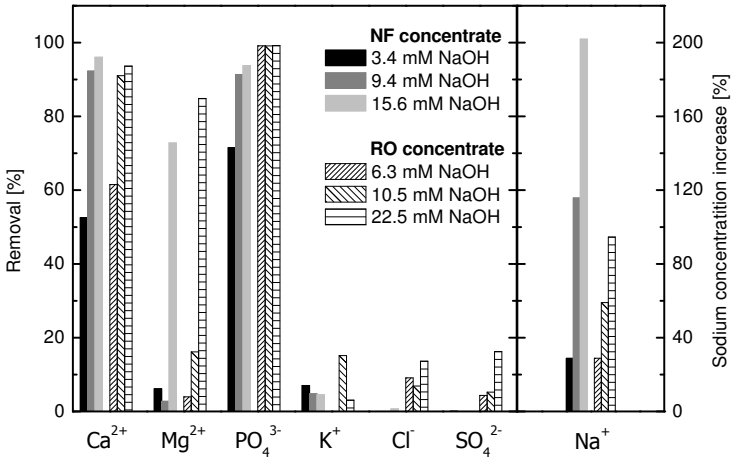

Figure 17: Removal of dissolved ions by chemical precipitation using different amounts of NaOH

Figure 19 shows the kinetics of the precipitation reaction. Phosphate and calcium removal is rapid, more than 90 % removal is reached within 0.5 minutes. The lowest dosage of 3.1 mM NaOH corresponding to pH 9.2 is not sufficient to achieve a comparable removal of phosphate and calcium. After an initial concentration decrease, a slight increase is observed after 5 to 10 minutes, before a slow concentration decrease can be observed until the end of the experiment. This might be explained by the kinetics of the precipitation reaction, which results in pH changes.

Calcite can provide a condensation surface for the precipitation of hydroxyl apatite. If calcite seeding material is added without addition of NaOH, phosphate and calcium removal can also be observed, but the precipitation is kinetically inhibited. After 30 h batch operation, only 40 % removal was observed (data not shown). These observations were confirmed by results from operation of a calcite fixed-bed column. Figure 20 shows an initially increased removal of phosphate, probably due to adsorption onto the calcite surface. After 70 h of operation, a steady state is reached. For an EBCT of 25 minutes the influent phosphate concentration of 600 µg/L PO_4^{3-}-P was reduced to 350 µg/L PO_4^{3-}-P, corresponding to a PO_4^{3-}-P removal of 37 %. A higher EBCT can most likely improve phosphate removal.

5.4 conclusions

- Both adsorption onto GFH and chemical precipitation have been shown to be generally effective for phosphate removal from NF concentrates.

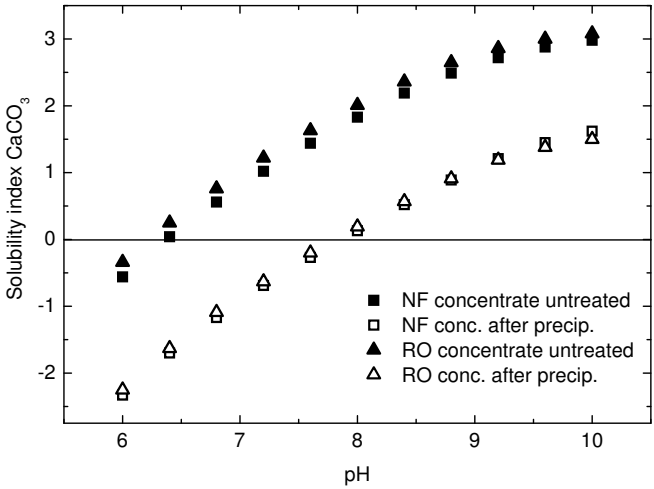

Figure 18: Calculated solubility index for calcium carbonate in the membrane concentrate solution prior and after treatment

- Chemical precipitation using NaOH is rapid and removes more than 90 % of phosphate and calcium.
- Induced crystallisation by addition of calcite seeds has been shown to remove phosphate (up to 40 %) and partially calcium, but the required contact times are high due to slow kinetics.
- Chemical precipitation significantly reduces the scaling potential and may therefore allow for higher recoveries in high-pressure membrane filtration.
- High removal of phosphate may permit environmentally-safe discharge into surface water bodies.

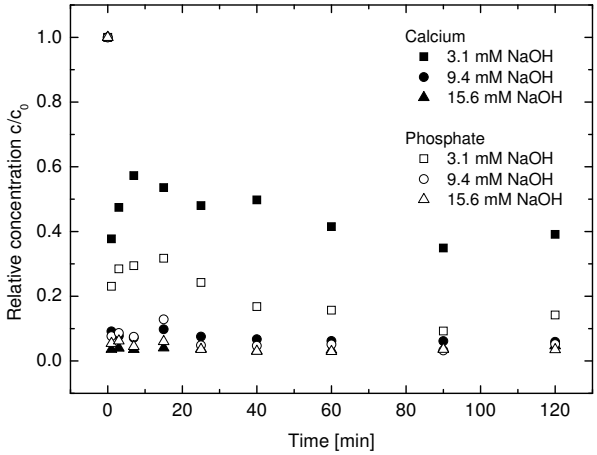

Figure 19: Precipitation kinetics; calcium and phosphate concentration decrease after addition of NaOH

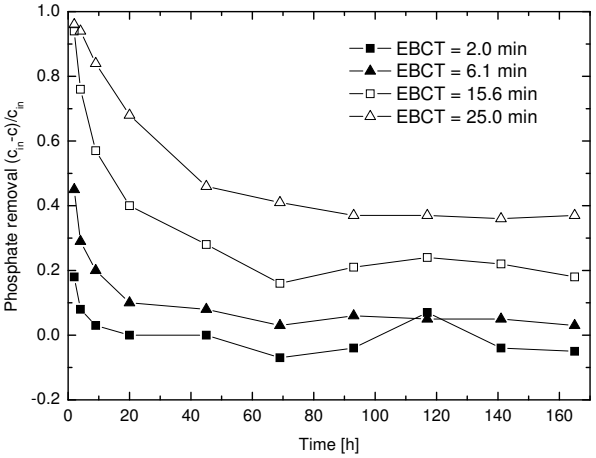

Figure 20: Phosphate removal in a calcite fixed-bed column crystalliser for different empty-bed contact times (c_0 = 0.587 mg/L PO_4^{3-}-P, pH 8.0-8.6

6

PREDICTING ANION BREAKTHROUGH IN GRANULAR FERRIC HYDROXIDE (GFH) ADSORPTION FILTERS

Alexander Sperlich[1], Sebastian Schimmelpfennig[1], Benno Baumgarten[1], Arne Genz[1], Gary Amy[2], Eckhard Worch[3] and Martin Jekel[1]

Water Research 2008, 42, 2073-2082.

ABSTRACT

Adsorption of arsenate, phosphate, salicylic acid, and groundwater DOC onto granular ferric hydroxide (GFH) was studied in batch and column experiments. Breakthrough curves were experimentally determined and modeled using the homogeneous surface diffusion model (HSDM) and two of its derivatives, the constant pattern homogeneous surface diffusion model (CPHSDM) and the linear driving force model (LDF). Input parameters, the Freundlich isotherm constants, and mass transfer coefficients for liquid- and solid-phase diffusion were determined and analysed for their influence on the shape of the breakthrough curve. HSDM simulation results predict the breakthrough of all investigated substances satisfactorily, but LDF and CPHSDM could not describe arsenate breakthrough correctly. This is due to a very slow intraparticle diffusion and hence higher Biot numbers. Based on this observation, limits of applicability were defined for LDF and CPHSDM. When designing fixed-bed adsorbers, model selection based on known or estimated Biot and Stanton numbers is possible.

6.1 INTRODUCTION

Granular ferric hydroxide is an effective adsorbent for removal of arsenate from groundwater (GW) [36]. Its suitability for the removal of various anions, e.g., phosphate and organic acids, is under current research [57, 58]. Investigated anions show a non-uniform behaviour during breakthrough in fixed-bed columns, resulting in different shapes of the breakthrough curves. From an engineering point of view, models are helpful for the appropriate design of fixed-bed filters. Surface complexation models are widely used to describe adsorption [40] in a state of equilibrium, but cannot predict the dynamic process of breakthrough of fixed-bed filters. For this purpose, models combining adsorption equilibrium data with mass transport are required. In this study, anion breakthrough is predicted using models which already have been established for trace organics adsorption onto granular activated carbon and are commonly available as PC software. Depending on the respective anion and the operational conditions, model selection and determination of input parameters are discussed.

1 Technische Universität Berlin
2 UNESCO-IHE, Delft
3 Technische Universität Dresden

6.2 MODELS

6.2.1 *Homogeneous surface diffusion model*

The homogeneous surface diffusion model (HSDM) consists of two partial differential equations (PDE), describing the mass transport through the adsorber (filter equation) and into the adsorbent grain (intraparticle equation). The following assumptions are incorporated in the HSDM: plug-flow conditions in the bed, linear liquid-phase mass transfer, solid-phase mass transfer only by surface diffusion, constant hydraulic loading rate and diffusion coefficients, spherical adsorbent grains, and the use of the Freundlich isotherm to describe the adsorption equilibrium. More details can be found in Sontheimer et al. [99].

A mass balance over an infinitesimal element of the filter leads to equation (6.1), where the first term represents the mass in the void fraction (pores), the second term reflects solute entering and exiting the element by advective transport, and the last term represents the sink, i. e., the mass of solute adsorbed by the adsorbent grains.

$$\epsilon_B \frac{\partial c}{\partial t} + v_F \frac{\partial c}{\partial z} + 3(1-\epsilon_B)\frac{k_L}{r_P}(c - c^*) = 0 \tag{6.1}$$

Intraparticle transport is described according to Fick's second law and is given in radial coordinates by:

$$\frac{\partial q}{\partial t} = D_S \left(\frac{\partial^2 q}{\partial r^2} + \frac{2}{r}\frac{\partial q}{\partial r} \right). \tag{6.2}$$

Dimensionless form, initial and boundary conditions

Equations 6.1 and 6.2 are transformed into a dimensionless form by introducing X, Y, Z, R, and T, dimensionless variables for the liquid-phase and solid-phase concentration, the axial position in the filter, the radial position in the adsorbent grain, and the time, respectively. The resulting dimensionless PDE for the fixed-bed filter is:

$$\frac{1}{D_g}\frac{\partial X}{\partial T} + \frac{\partial X}{\partial Z} + 3St\,(X - X^*) = 0, \tag{6.3}$$

where St is the dimensionless modified Stanton number, $St = k_L m/(r_P \rho_P Q)$, and D_g is the dimensionless solute distribution parameter, $D_g = \rho_B q_0/(\epsilon_B c_0)$. As an initial condition, the concentration at the beginning of operation is zero:

$$X_{T=0,Z} = 0 \tag{6.4}$$

A constant influent concentration serves as a boundary condition:

$$X_{T,Z=0} = 1 \tag{6.5}$$

The intraparticle PDE is written as:

$$\frac{\partial Y}{\partial T} = \frac{St}{Bi}\left(\frac{\partial^2 Y}{\partial R^2} + \frac{2}{R}\frac{\partial Y}{\partial R} \right), \tag{6.6}$$

where Bi is the dimensionless Biot number, $Bi = k_L r_P c_0/(D_S \rho_P q_0)$. Initially, the solid-phase concentration is zero:

$$Y_{T=0,Z,R} = 0 \tag{6.7}$$

The boundary condition for the particle center is symmetry:

$$\left.\frac{\partial Y}{\partial R}\right|_{R=0} = 0 \tag{6.8}$$

At the exterior adsorbent grain surface, the mass transported into the grain equals the mass transported through the stagnant liquid film. The resulting boundary condition for the particle surface is:

$$\left.\frac{\partial Y}{\partial R}\right|_{R=1} = Bi\,(X - X^*)\,, \tag{6.9}$$

which includes the description of the adsorption equilibrium by the Freundlich [51] equation:

$$Y_{R=1} = X^{*n}, \tag{6.10}$$

where n is the dimensionless Freundlich exponent.

Numerical solution

The finite differences method was applied to solve the set of partial differential equations in three steps:

1. Choice of grid (Discretization)
2. Substitute differential quotients by differences quotients
3. Solve resulting equations with regard to initial and boundary conditions and iteration to ensure that both PDEs are solved simultaneously

For the filter PDE (6.3), an explicit calculation scheme is derived using forward differences for temporal derivatives and backward differences for spatial derivatives, since mass transport in the filter is governed by advection. This method is also known as Forward Time Backward Space (FTBS). The resulting explicite calculation scheme for the dimensionless liquid-phase concentration is shown in Equation (6.11):

$$X_{i+1,j} = X_{i,j} - \alpha\left[X_{i,j} - X_{i,j-1}\right] - \beta\left[X_{i,j} - X^*_{i,j}\right], \tag{6.11}$$

with $\alpha = D_g \Delta T/\Delta Z$ and $\beta = 3StD_g\Delta T$. For the intraparticle equation, forward differences substitute the temporal derivatives, whereas central differences are used for the spatial derivatives (Forward Time Central Space-FTCS). This method is appropriate when the mass transport is thought to be mainly diffusion. The resulting explicite calculation scheme for the dimensionless solid-phase concentration then follows:

$$Y_{i+1,k} = Y_{i,k} + \gamma \cdot \left[\left(1 + \frac{1}{R}\right) Y_{i,k+1} - 2Y_{i,k} + \left(1 - \frac{1}{R}\right) Y_{i,k-1}\right], \tag{6.12}$$

with $\gamma = Ed\Delta T/\Delta R^2$. The boundary conditions (Eqs. 6.8 and 6.9) are transformed accordingly using a ghost-point method. The stability of the numerical algorithms strongly depends on the model parameters Bi, St, n, and the chosen grid width ΔZ, ΔT, and ΔR. To guarantee the stability and consistency of the numerical solution, the following criteria have to be met:

$$\alpha < 1.0, \tag{6.13}$$

$$\beta < 0.3, \tag{6.14}$$

$$\gamma < 0.5. \tag{6.15}$$

Using these equations, the optimal grid width can be calculated for every combination of the model parameters. For the HSDM calculations the software FAST 2.0 (Fixed-bed Adsorption Simulation Tool) was developed. For comparison, the software package AdDesignS 1.0 (Adsorption Design Software, Michigan Technological University) was used.

6.2.2 *Constant pattern homogeneous surface diffusion model*

In an attempt to provide an user-oriented tool to predict the breakthrough, Hand et al. [64] presented the constant pattern homogeneous surface diffusion model (CPHSDM). Using numerically derived solutions for the HSDM, a simple algebraic equation was used to approximate the model solution:

$$T(Bi, n, St_{min}) = A_0 + A_1 \cdot X^{A_2} + \frac{A_3}{1.01 - X^{A_4}} \tag{6.16}$$

The coefficients A_i used in Eq. 6.16 were published in data tables [64]. The CPHSDM offers a high calculation speed. As a trade-off, the model simulations do not represent true results of the HSDM and might differ substantially from those. Advances in the power of personal computers have made it possible to use the HSDM also in engineering practise, therefore reducing the need for approximations such as CPHSDM. CPHSDM calculations were performed using MS Excel and AdDesignS.

6.2.3 *Linear driving force model*

In order to reduce the amount of computation and increase the calculation speed, it is possible to simplify Eq. (6.2), e.g., by using approximations for the intraparticle diffusion rate. The most widely used approximation is a linear one, referred to as linear driving force (LDF), derived by Glueckauf [59]:

$$\frac{\partial \overline{q}}{\partial t} = \frac{15 D_S}{r_p^2} \cdot (q^* - \overline{q}), \tag{6.17}$$

where $\overline{q}$ represents the average solid-phase concentration in the adsorbent grain. This approximation is only valid for $D_S \cdot t/r_P^2 > 0.1$ [59]. In dimensionless form, this equation can be written as:

$$\frac{\partial Y}{\partial T} = 3St\,(X - X^*) = 15Ed\,(Y^* - Y) \tag{6.18}$$

$$X_{T=0,Z} = 0; Y_{T=0,Z} = 0 \tag{6.19}$$

$$X_{T,Z=0} = 1 \tag{6.20}$$

LDF model calculations were performed using the software LDF 1.3 (Eckhard Worch) and FAST 2.0.

6.3 PARAMETER ESTIMATION

To predict breakthrough of fixed-bed systems, the model input parameters have to be known. These values are either easily accessible (outer model parameters) or must be determined indirectly from accordingly designed experiments (inner model parameters). Since the parameters do not act independently to influence adsorber performance, they can be summarized in dimensionless groups (essential model parameters) to reduce the number of influencing parameters.

6.3.1 *Outer model parameters*

Outer model parameters, in contrast to inner model parameters, are usually known or can be determined easily. They represent operational conditions and/or adsorber geometry. Outer model parameters include the grain size, grain density, volumetric flow rate, influent concentration, adsorbent mass, and density of the adsorber bed. Although these parameters can be measured easily, some of them are not constant over the adsorber column. Hence, average values have to be used.

6.3.2 *Inner model parameters*

Inner model parameters cannot be easily measured but have to be determined in especially designed experiments. They can also be determined by empirical correlations from the literature or derived from column data. Adsorption equilibrium parameters, Freundlich n and K_F, the liquid-phase mass transfer coefficient k_L, and the surface diffusion coefficient D_S fall in this category. Adsorption equilibrium parameters were derived in two ways. First, batch equilibrium isotherms using ground material were performed. The smaller grain size allows for a short equilibration time. The resulting isotherm data were described by the Freundlich [51] equation. Second, breakthrough curves were evaluated: integration of a complete BTC provided a reliable isotherm point for the fraction used in the column experiment. Assuming a value for n, K_F can be determined. This approach is legitimate if the influence of n on the BTC is small or n is known from previous experiments.

Film diffusion coefficients were estimated by the Gnielinski [60] correlation. To validate this approach, k_L was determined using differential column batch reactor (DCBR) tests and the results were compared. In DCBR experiments operated at different HLRs of 14 to 75 m h^{-1}, it was also shown that external mass transfer is not predominant. The concentration decrease in the DCBR was independent from the chosen HLR. Also, variation of the film diffusion coefficient in the numerical application of the HSDM did not show differences in the resulting kinetic and breakthrough curves.

Surface diffusion coefficients were determined both independently from separate DCBR tests, as well as derived from laboratory-scale column experiments. In both cases, a best-fit D_S was determined by comparing HSDM model simulations to experimental data.

6.3.3 *Essential model parameters/ dimensionless numbers*

The influence of the dimensionless groups on the form of the BTC has been thoroughly investigated [99]. Hand et al. [64] successfully applied the HSDM for over 100 adsorbate-adsorbent (organic pollutant - activated carbon) systems. The 10 inner and outer input parameters defining the shape of the BTC can be transformed into four remaining dimensionless groups, Bi, St, D_g, and n. Therefore, these parameters are decisive when discussing model attributes or shortcomings.

6.3.4 *General (non-model) parameters*

General (non-model) parameters are not directly considered in the model equations, but influence the value of inner and outer model parameters and thus indirectly influence the breakthrough. Examples are the type of adsorbate, temperature, ionic strength and pH. In the investigated systems, pH is especially important. Previous studies have found that the adsorption equilibrium is strongly dependent on pH [58]. Literature suggests that surface diffusivity is a function of pH. Investigations on intraparticle diffusion of metal contaminants in microporous adsorbents [7] showed a decrease in D_S with increasing pH, attributed to a reduced metal affinity for the oxide and surface site density.

6.4 MATERIALS AND METHODS

6.4.1 *GFH and water composition*

GFH was obtained from the producer (GEH Wasserchemie, Osnabrück). GFH is predominately akaganeite, a poorly crystallised iron oxide. The specific surface area is reported to be 280 m^2 g^{-1} and its pH_{PZC} (point of zero charge) is between 7.5 and 8.0 [110]. More recent investigations determined a pH_{PZNPC} (point of zero net proton charge) of 5.7 and a pH_{IEP} (iso electric point) of 7.5 and comparable values for the specific surface area [96]. The commercially available material has a grain size range of 0.32 - 2.0 mm [38]. Different artificial model waters were prepared by adding either arsenate, phosphate or salicylic acid and NaCl (10 mmol L^{-1}) to deionized (DI) water or Berlin drinking (DW) water (pH 7.5, [DOC]=4.5 mg L^{-1}, [Ca^{2+}]=2.5 mmol L^{-1}), respectively. In the column experiments con-

cerning arsenate, arsenic(V)oxide hydrate was used. For isotherm and differential column batch (DCBR) experiments an arsenic standard solution (Titrisol) was used. Phosphate solutions were created using potassium dihydrogen phosphate. Salicylic acid solution was prepared by adding sodium salicylate (Merck) to DI water. All chemicals used were of reagent grade. To ensure constant pH conditions 2 mmol L^{-1} of a biological buffer were added to each model water in experiments focusing on arsenate or phosphate adsorption. The pH was adjusted using the biological buffers BES (N,N-Bis(2-hydroxy-ethyl)-2-aminoethane-sulfonic acid) to 7.1 and TAPS ((2-Hydroxy-1,1-bis(hydroxymethyl)ethyl)amino-1-propanesulfonic acid) to 8.4, respectively. In addition, GW from Füchtenfeld (Germany) was used (pH 7.8, [DOC]=9.4 mg L^{-1}).

6.4.2 *Equilibrium isotherms*

Adsorption isotherms were developed using < 63 µm (ground) GFH, an equilibration time of 96 h and a temperature of 20°C.

6.4.3 *DCBR tests*

Determination of the intraparticle diffusion coefficient was based on experiments using DCBRs as described by Sontheimer et al. [99]. The solution was pumped from a well-mixed reservoir through a bed of glass beads which maintains a thin layer of adsorbent particles. After flowing through the bed, the solution was returned to the reservoir. A peristaltic pump (ISMATEC Ecoline) was used to adjust the HLR to > 14 m h^{-1} to ensure that film diffusion would not be rate limiting. The adsorbent layer thickness was chosen to be 2 mm, corresponding to an adsorbent mass of 1 g. The experiments for arsenate and phosphate were carried out as long-term scaled tests (2500 h) with a relatively high reactor volume of 5 L to ensure that equilibrium conditions are reached within the experimental period. The resultant data were plotted as c/c_0 versus time and evaluated by use of the HSDM approach without simplification.

6.4.4 *Fixed-bed column experiments*

Laboratory-scale filter studies were performed using columns with a diameter of 25 mm and a dry mass of 30 to 50 g of GFH, corresponding to a media depth of 10 to 19 cm; the EBCT was adjusted to 3 to 6 minutes by experimental conditions (Table 11). For DCBR and filter studies, the adsorbent was sieved to a grain size of 0.8 to 1 mm.

6.4.5 *Analyses*

Arsenate samples were analysed using a Varian Techtron AA 400 spectrometer with hydride accessory VGA 76 and automated sampler PSC 56. The used method utilizes an on-line prereduction of As(V) to As(III) and continuous flow hydride generation [37]. Arsenic standard solutions were used for calibration. The practical working range extended from 1 to 50 µg L^{-1}. Samples containing higher concentrations of arsenic were diluted. The detection limit was 0.6 µg L^{-1}. Or-

thophosphate was determined using a flow injection analyzer (FIAstar 5000, Foss Tecator) according to ISO 15681-1. The standard deviation was determined to be 4.8 % at a mean concentration of 0.016 mg L^{-1} P and 0.77 % at 3.8 mg L^{-1} with a detection limit of 3 µg L^{-1}. Salicylic acid concentrations were determined photometrically at 230 nm using a Pharmacia Biotech Ultrospec 3000. pH was measured by a WTW pH 340-meter using a Sentix 41-electrode (WTW). DOC was analysed by thermal-catalytic oxidation using a High-TOC analyser (Elementar Analysensysteme, Germany).

6.5 RESULTS

6.5.1 *Adsorption equilibrium*

The investigated anions show different affinities to the GFH surface and corresponding equilibrium solid-phase concentrations (Table 10). GFH shows high capacities for arsenate and phosphate adsorption. DOC and salicylic acid also adsorb onto GFH, but show a comparatively poorer affinity to GFH. For arsenate and phosphate, equilibrium data from batch isotherm experiments were compared to the equilibrium data point calculated from the integration of the breakthrough curve. The corresponding Freundlich parameters were calculated assuming the same value of n. For phosphate, the calculated solid-phase concentrations match the data from isotherm experiments, whereas for arsenate, the isotherm data underestimate the breakthrough. DOC adsorption of GW NOM from Fuechtenfeld shows a non-adsorbable fraction of 1.45 mg L^{-1}. This fraction must be considered separately during subsequent modelling.

Table 10: Adsorption equilibrium for different adsorbates

Adsorbate	Water matrix	pH	Adsorption equilibrium constants K_F [L^n mg mg^{-n} g^{-1}]	n [-]	Data source
Arsenate	DW	8.0	32.3	0.29	Integration BTC
Arsenate	DW	8.4	23.4	0.29	Isotherm experiment
Phosphate	DW	7.7	14.9	0.19	Isotherm experiment
Phosphate	DW	8.2	14.9	0.19	Integration BTC
DOC	GW	7.8	8.0	0.62	Genz et al. [58]
Salicylic acid	DI	7.0	4.3	0.52	Sperlich et al. [101]

6.5.2 *Adsorption kinetics*

In Table 11, the determined surface diffusion coefficients are shown. Generally, diffusion coefficients are in the order of 10^{-14} to 10^{-15} m^2 s^{-1}, indicating a very slow intraparticle diffusion compared to values known from activated carbon. Although surface diffusivity is assumed to be constant in the equations of the transport models, it has been shown that D_S is a function of liquid- and solid-phase adsorbate concentration and also particle size [99]. D_S values from the literature can therefore only be used for identical adsorbate/ adsorbent pairs, particle size and initial concentration. Regarding the GFH/ arsenate system, few authors have published D_S values [8, 101].

Table 11: Adsorption kinetics for different adsorbates

Adsorbate	Water matrix	pH	Intraparticle diffusion coefficient D_S [$m^2\ s^{-1}$]	Data source
Arsenate	DI	8.4	$3 \cdot 10^{-15}$	DCBR
Arsenate	DW	8.0	$8 \cdot 10^{-15}$	Best-fit BTC
Phosphate	DI	8.4	$2 \cdot 10^{-15}$	DCBR
Phosphate	DW	8.2	$2 \cdot 10^{-14}$	Best-fit BTC
DOC	GW	7.8	$4 \cdot 10^{-14}$	DCBR
DOC	GW	7.8	$3 \cdot 10^{-14}$	Best-fit BTC
Salicylic acid	DI	7.0	$5 \cdot 10^{-13}$	DCBR
Salicylic acid	DI	7.0	$2 \cdot 10^{-13}$	Best-fit BTC

Badruzzaman et al. [8] found D_S values of approx. $6.4 \cdot 10^{-15}$ $m^2\ s^{-1}$ for a 10 x 30 mesh (0.6 - 2 mm) fraction of GFH and a corresponding Biot number of 19 in their experiments. This agrees well with the D_S values found in this study, which are slightly lower, but in the same order of magnitude. The determined values also fit in the range of surface diffusivities from 10^{-16} to 10^{-10} $m^2\ s^{-1}$ reported in the literature [7]. In another recent study [49] the GFH surface diffusivity for NOM was determined to be between 4 and $8 \cdot 10^{-15}$ $m^2\ s^{-1}$. DCBR tests [58] show values of the same magnitude. The column data presented here appear to show slightly higher diffusivities (Table 11). Compared to arsenate and phosphate, DOC and salicyclic acid are less strongly bound to the adsorbent surface, which results in higher diffusivities. In comparison to salicylic acid which shows comparable capacities, DOC represents a complex mixture of organic macromolecules and the molecular size might cause slower surface diffusion.

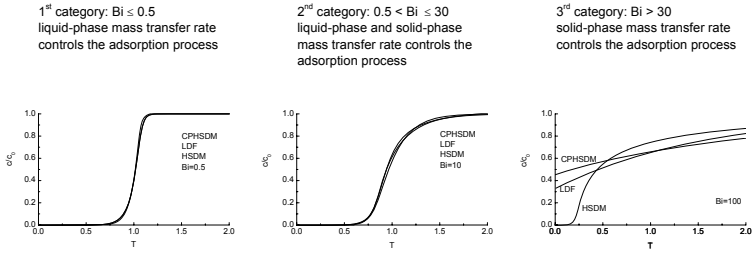

Figure 21: Categories defined by Hand et al. [64] and corresponding model simulations (St=5, n=0.2)

6.5.3 *Breakthrough Curves and Simulations*

Dimensionless groups analysis shows important differences between the performed breakthrough experiments, resulting in different breakthrough characteristics. According to Hand et al. [64], three categories of breakthrough curves were defined (Figure 21), corresponding to different Biot numbers. Whereas the BTCs for salicylic acid (Bi=16, St=7) and DOC (Bi=23, St=4) are in category 2, arsenic and phosphate breakthrough experiments were performed with higher Bi values

of 183 and 102, respectively, corresponding to category 3 (Table 12).

Table 12: Model input parameters

Adsorbate	Water matrix	Outer model (operational) parameters					Dimensionless numbers / Essential model parameters			
		c_0 [mg/L]	m_{GFH} [g]	v_F [m/h]	EBCT [min]	r_P [mm]	Bi [-]	St [-]	D_g [-]	n [-]
Arsenate	DW	4.5	51	3.0	3.6	0.45	182.5	9.7	24617	0.19
Phosphate	DW	2	46	3.0	3.3	0.45	102.1	10.0	20323	0.19
DOC	GW	9.4	42	1.4	6.6	0.38	23.3	3.9	8140	0.62
Salicylic acid	DI	8	27	1.0	6.3	0.39	16.3	6.9	4155	0.52

Figure 22 shows breakthrough curves for arsenate, phosphate, DOC, and salicylic acid and HSDM, CPHSDM, and LDF model simulations. For salicylic acid, all of the model simulations produce very similar results. The prediction of breakthrough is good. For DOC adsorption, CPHSDM is not able to predict the breakthrough correctly, but HSDM and LDF show identical model results and a good agreement with experimental data. This is especially remarkable considering that DOC is a mixture of various organic compounds. However, for simulation purposes, DOC is treated as a single substance with a non-adsorbable fraction. Phosphate and arsenate BTCs show different characteristics. Whereas the quality of the model simulations is acceptable, the shape of the BTC is difficult to simulate. For phosphate, all model simulations show slight differences, with LDF showing a better agreement with the data. The arsenate BTC shows breakthrough characteristics typical for category 3. The HSDM simulation shows some divergence from the monitored BTC, but correctly describes the initial phase and the asymptotic shape of the BTC. Both CPHSDM and LDF fail to predict the early steep incline of the BTC, but predict a instantaneous breakthrough.

BTCs in category 1 and 2 show sigmoidal breakthrough profiles and are most commonly found in organic pollutants adsorption onto activated carbon. These breakthrough curves can be successfully simulated using the LDF or the pure HSDM, but CPHSDM breakthrough predictions might fail, as the BTC for DOC shows. In contrast, arsenic and phosphate BTCs appear to commonly fall into category 3. This type of BTC is typical steep in the beginning, but concave downward with increasing operation time (i.e., bed volumes), asymptotically nearing complete breakthrough. Rarely encountered in activated carbon adsorption, this type of BTC has been frequently observed for adsorption onto GFH [35]. Problems modelling category 3 type BTCs have been reported earlier [101], where LDF was used to describe the BTC. However, it was generally concluded that rather simple homogeneous models are not able to describe the BTCs. It has been shown in this work that this type of BTC can be successfully predicted using HSDM. However, it is not possible to generally judge whether a category 3 BTC can be simulated using LDF or CPHSDM. Categorization solely based on the Biot number according to Hand et al. [64] does not seem to be a sufficient criterion for the suitability of a model. Therefore, a more detailed model comparison including the influence of the Stanton number and the Freundlich exponent n is presented in the following subsection.

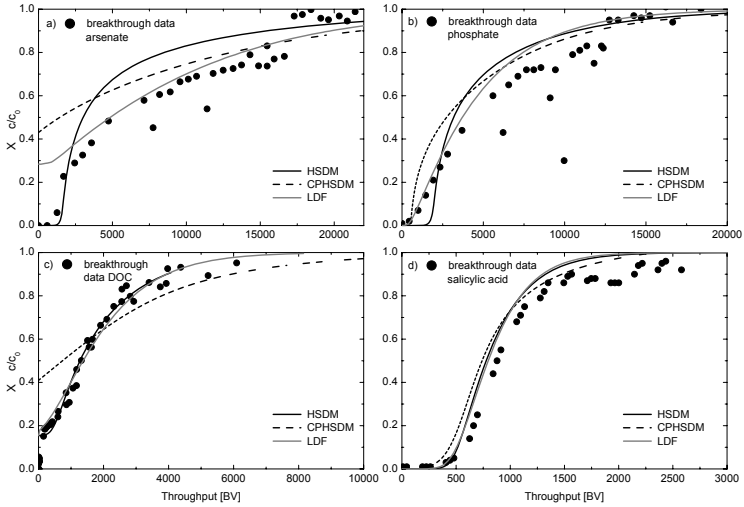

Figure 22: Breakthrough curves and model simulations for a) arsenate, b) phosphate, c) DOC and d) salicylic acid

Reasons for GFH BTCs often showing category 3 characteristics can be found in an extremely slow surface diffusivity D_S. Adsorption chemistry of actived carbon and GFH is fundamentally different: GFH is a metal oxide adsorbent, showing a highly pH-dependent surface charge. Adsorption of negatively charged arsenate or phosphate molecules leads to a shift of the pH_{PZC} towards lower pH values. Slower transport on the adsorbent surface may be caused by the negatively charged surface's electrostatical rejection of equally negatively charged oxyanions. DOC has a higher molecular weight in contrast to arsenate and phosphate, but shows a lower surface charge density. Slower transport may therefore be caused by sterical interactions by larger NOM molecules, affecting diffusion of smaller molecules or blocking GFH pores (97% are smaller than 4.5 nm) [58].

6.5.4 *Model comparison*

Using the same input parameters, the different model alternatives produce different simulations. The extent of model divergence, however, depends on the value of the essential model input parameters Bi, St, n and D_g. In the following, the HSDM was chosen as a reference and the differences to LDF and CPHSDM were quantified. In order to define limits of applicability for LDF and CPHSDM, a number of model simulations were performed using HSDM, LDF, and CPHSDM, varying the dimensionless input parameters. To measure the consistency of the model simulations, the match $(1 - \Delta\bar{X})$ was calculated for each data point (total number of data points N=200), as expressed in Eq. 6.21. All model calculations were performed in the interval $0 \leqslant T \leqslant 2$, corresponding to an operation time

of twice the stoichiometric breakthrough time. Since model comparisons were calculated for a dimensionless time scale (T), the results are independent of the solute distribution parameter, D_g, which is not influencing the shape of the BTC, but only the point of stoichiometric breakthrough.

$$1 - \Delta\bar{X} = 1 - \frac{1}{N}\sum_{i=1}^{N} |X(T_i)_{HSDM} - X(T_i)_{LDF/CPHSDM}| \tag{6.21}$$

The results for LDF are shown in Figure 23. Obviously, higher Biot numbers and low Stanton numbers (i.e., low value of Ed) lead to less consistency of both models, reaching a minimum at approximately Bi=100 and St=5. It is shown that both Biot and Stanton number influence the match, and a categorization based on the Biot number only is less exact. The simulation of experimental BTCs (Figure 22) is marked in Figure 23 (a to d). It is clearly shown that the arsenate BTC (a) is situated in a Biot-Stanton region where HSDM and LDF produce very different model results (match $1 - \Delta\bar{X} < 0.94$). On the other hand, the model results for salicylic acid BTC (d) differ negligibly, corresponding to a match of $1 - \Delta\bar{X} \approx 0.98$. Model simulations of phosphate and DOC BTCs (b and c) correspond to matches between 0.94 and 0.96, indicating a somewhat lesser model consistency. The influence of the Freundlich exponent n on the match ($1 - \Delta\bar{X}$) was found to be marginal. Exemplarily, results for $n = 0.2$ are shown.

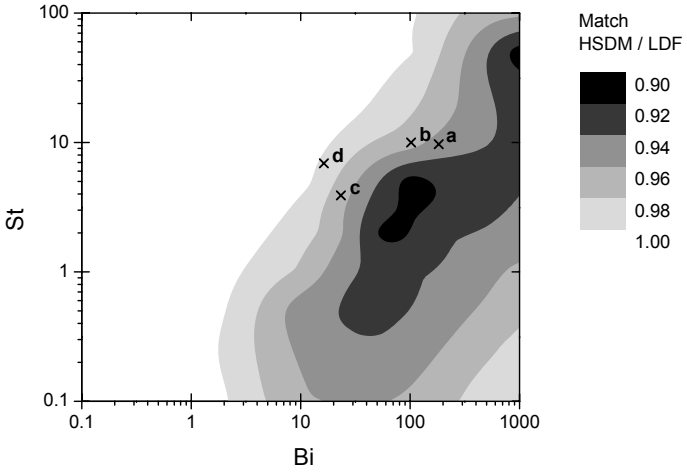

Figure 23: Match ($1 - \Delta\bar{X}$) between HSDM and LDF model simulations in dependence of Biot and Stanton numbers, n=0.2, a)-d) experimental data according to Figure (22)

Model comparison results for CPHSDM are shown in Figure 24. The differences between CPHSDM and HSDM are much more distinctive than the differences between LDF and HSDM. Here, low Stanton numbers lead to less consistency

of the models. In the literature, minimum Stanton numbers can be found to define the limits of applicibility of CPHSDM [64], which agree well with the limits found in this study. For Biot numbers higher than 10, the minimum Stanton number increases. Comparing the simulation of experimental BTCs (a to d), only the salicylic acid BTC (d) can be simulated using CPHSDM, with a match of $1 - \Delta\bar{X} \approx 0.98$. The other model simulations are situated in a Biot-Stanton region where CPHSDM cannot be applied, with arsenate showing the smallest match of $1 - \Delta\bar{X} < 0.90$, corresponding to very different simulation results (Figure 22).

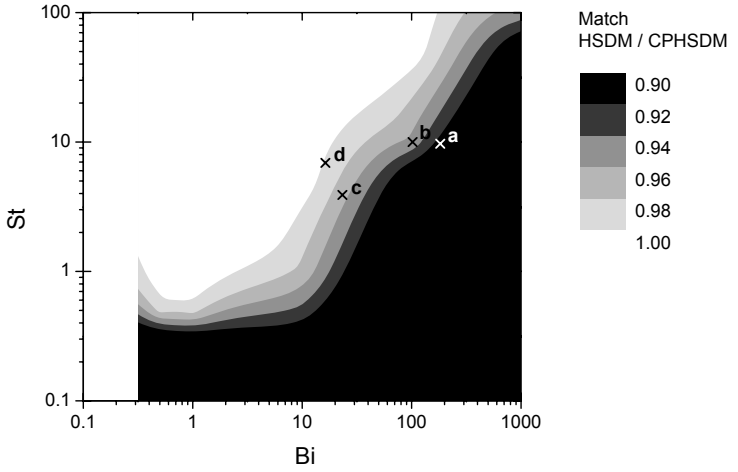

Figure 24: Match ($1 - \Delta\bar{X}$) between HSDM and CPHSDM model simulations in dependence of Biot and Stanton numbers, n=0.2, a)-d) experimental data according to Figure (22)

Hence, limits of applicability for LDF and CPHSDM can be given. Down to a match of approx. 0.97, model results do not differ substantially and LDF or CPHSDM might be favoured due to their high calculation speed. However, LDF might be preferred to CPHSDM, since it shows generally a higher correspondence to the unsimplified HSDM.

In order to choose the appropriate model when designing adsorbers, Biot and Stanton numbers should be determined beforehand. This might require an estimation of the mass transfer coefficients k_L and D_S, as well as the determination of adsorption equilibrium data, e. g., by isotherm experiments. Then, Figure 23 and 24 can be used to determine the required model. The categorization based on the Biot number only is less exact. In Figure 23 this corresponds to a Stanton number of approximately 10. Fixed-bed columns using GFH material were found to be outside the limits of applicability of LDF and CPHSDM. In these cases, HSDM must be used.

6.6 CONCLUSIONS

- Breakthrough curves for the adsorption of arsenate, phosphate, DOC, and salicylic acid onto granular ferric hydroxide (GFH) can be predicted using the HSDM.

- The applicability of LDF and CPHSDM (HSDM simplifications) is limited and depends on the values of the dimensionless Biot and Stanton numbers. Arsenate adsorption onto GFH shows very slow surface diffusion coefficients, leading to high Biot numbers. In most cases, LDF and CPHSDM are not able to describe arsenate breakthrough in GFH fixed-bed filters.

- Limits of applicability for LDF and CPHSDM were defined. When designing fixed-bed adsorbers, model selection based on known or estimated Biot and Stanton numbers is possible.

7

REGENERATION OF GRANULAR FERRIC HYDROXIDE ADSORPTION FILTERS FOR TRACE PHOSPHATE REMOVAL

Alexander Sperlich[1], Mathias Riechel[1] and Martin Jekel[1]

AS PREPARED FOR WATER RESEARCH

ABSTRACT

The regeneration and multiple use of Granular Ferric Hydroxide (GFH) which has shown high capacities for phosphate removal was investigated and compared to an alternative iron based adsorbent media (FerroSorp Plus, FS). Batch and fixed-bed column studies show that GFH is stable at high pH and can be efficiently regenerated using 1 M NaOH. Approximately 80 % of the initially bound phosphate can be eluated. However, the incomplete desorption leads to decreasing capacities with each additional use. Multiple uses are thus limited, but at least three operation cycles are feasible. FS shows lower total capacities than GFH and similarly decreasing desorption efficiency and capacity. Indications for the instability of FS at high pH and desorption of phosphate and organic matter from the unused adsorbent were observed. GFH desorption is fast and most of the desorbable phosphate could be eluated using 4 - 6 bed volumes of regenerant. A reuse of the regenerant solution is possible. Despite high phosphate concentrations in the regenerate, 61 - 85 % of the bound phosphate could be desorbed. A recovery of phosphate from the highly concentrated regenerant stream (up to 3.5 g/L P) is possible. Precipitation with lime water resulted in 90 % P removal and a plant available precipitate which might be used as a fertilizer. These results suggest that regeneration and multiple use of GFH can significantly increase operation times of fixed-bed adsorbers and be an economically favourable option compared to single use.

7.1 INTRODUCTION

Due to the adverse environmental impacts of phosphate discharges into surface waters and the increasing scarcity of mineral phosphate reserves, the development of appropriate techniques for phosphate removal and recovery has become an issue of common interest. Unlike traditional biological nutrient removal and chemical precipitation processes, fixed-bed adsorption onto metal oxides can reduce dissolved phosphate to near zero levels. This might be a requirement for advanced wastewater treatment due to increasingly stringent regulations on phosphorus discharge [11, 65] as well as for restoration of surface water bodies. Granular ferric hydroxide (GFH) is an effective adsorbent for removal of arsenate from groundwater [35]. Also, its suitability for the removal of phosphate [57, 104] and DOC has been investigated. An alternative iron based adsorbent (FerroSorp

1 Technische Universität Berlin

Plus, FS) which has also been shown to remove phosphate, arsenate and other anions [55, 100] was used for comparison in this study. Due to the potential creation of a toxic and hardly disposable concentrate stream, regeneration of arsenic loaden adsorbent material is neither investigated nor desired. However, if metal oxide adsorption is used for phosphate or DOC removal, regeneration can increase operation time and cost effectiveness. A regenerant solution containing phosphate is not toxic and could be safely disposed off, e. g., to wastewater treatment plants. Moreover, most phosphate removed from the (waste) water is concentrated in a relatively small volume of spent regenerant and might be converted into a solid fertilizer by precipitation. In several studies, sodium hydroxide (NaOH) solution has been shown as suitable regenerant for metal oxide adsorbents as well as hybrid anion exchange resins:

Donnert and Salecker [33] tested regeneration of activated alumina for phosphate adsorption by 0.5 M NaOH and recovery of phosphate by precipitation with $Ca(OH)_2$. In this study, 90 % of the phosphate was precipitated as calcium phosphate and the sludge contained 10 - 15 % P. Zhu and Jyo [131] used a zirconium loaded phosphoric acid chelating resin for phosphate removal. More than 90 % of the removed phosphate could be eluted within 20 bed volumes using 0.5 M NaOH. Phosphate adsorption behaviour was not adversely affected by repeated adsorption/ desorption cycles. Chitrakar et al. [19] used synthetic akaganeite for selective phosphate adsorption from seawater and regenerated with 0.1 M NaOH. Almost no loss in capacity after up to 12 adsorption/ desorption cycles was reported. Recently developed hybrid anion exchangers containing hydrated ferric oxide nanoparticles were reported to remove phosphate and showed much higher capacities than the parent material [14, 83]. Solutions of 2 - 4 % (0.5 - 1 M) NaOH and 2 % NaCl were found very effective to desorb phosphate and $>$ 95 % phosphate was desorbed after 12 bed volumes of regenerant. An economic assessment showed that the value of recovered phosphorus could not cover resin and regenerant costs, but potentially make adsorption and P recovery a favourable economic option compared to alternative treatments [83]. Genz et al. [57] studied phosphate adsorption from MBR effluents onto GFH and activated alumina followed by regeneration with 0.6 M NaOH and reported no decrease in capacity after three adsorption/ desorption cycles. A high regenerant to bed volume ratio (100 : 1) was used and a non-desorbable P fraction was supposed in long-term operation. In pilot-scale operation using tertiary effluent, NaOH has been applied successfully to regenerate GFH adsorption filters [104].

This work's objective was to study the regeneration and multiple application of GFH along with an economic use of the regenerant. Desorption and adsorption capacity were quantified over several consecutive adsorption/ desorption cycles. Precipitation of the desorbed phosphate and recovery of a plant-available P-fertilizer was also investigated.

7.2 MATERIALS AND METHODS

7.2.1 *Adsorbent media*

GFH was obtained from the producer (GEH Wasserchemie, Osnabrück, Germany). It is a synthetic, poorly crystallized iron(III) oxide-hydroxide and consists predominantly of akaganeite (β-FeOOH). The moisture content is approx. 50 %. The

pH_{PZC} (point of zero charge) is reported to be between 7.5 and 8.0 [109, 96]. In a grain size distribution analysis, the media was shown to contain particles ranging from < 0.2 mm to > 2 mm. The uniformity coefficient (d_{60}/d_{10}) was approx. 3.5, the effective grain size was 0.7 mm [100]. In the same study, the specific surface area was determined to be approx. 240 m^2/g, whereas earlier studies reported somewhat higher values of 280 m^2/g [38].

FerroSorp Plus, supplied by Zeolith Umwelttechnik GmbH (Waldsassen, Germany), is a granular adsorbent media based on ferric hydroxide. Manufacturer's (HeGo Biotec GmbH, Berlin, Germany) data specify a grain-size range of 0.5 - 2.0 mm and a water content of 10 - 15 %. An adsorption capacity for phosphate to be reached under optimal operational conditions of 12 - 16 g/kg P is stated. A specific surface area of 148 m^2/g was determined [100].

All results are presented on a dry mass basis after drying at 105°Cfor 12 h and cooling in a desiccator.

7.2.2 *Solutions*

Model waters

Model solutions for batch experiments and differential column-batch reactor (DCBR) tests were prepared using de-ionized (DI) water and NaCl to ensure an ionic strength of 10 mmol/L. Different concentrations of phosphate were set using KH_2PO_4. The pH was adjusted to 7.1 using 2 mmol/L of the biological buffer BES (N,N-Bis(2-hydroxy-ethyl)-2-amino-ethane-sulfonic acid), which was shown to not interfere with phosphorus adsorption in previous studies. The model solution for the rapid small-scale column test (RSSCT) was prepared using drinking water ($pH \approx 8$) without buffer addition but spiked with KH_2PO_4 to set a phosphate concentration of 2 mg/L P.

Regenerants

For the regeneration of the exhausted adsorbents, 1 M sodium hydroxide solution was used. In DCBR tests, the columns were regenerated with fresh NaOH after each adsorption step. In batch experiments, the NaOH solution contained KH_2PO_4 at concentrations of 0, 5, 10 and 20 mg/L P to simulate the regenerant's reuse. In a RSSCT, fresh NaOH was used for the first regeneration cycle and was reused for the following regenerations, initially containing 432 and 832 mg/L P.

Precipitants and citric acid

Different precipitants were used for phosphorus recovery directly out of the regenerant. Lime water (10 % calcium hydroxide solution) was used to precipitate calcium phosphate while solutions of magnesium chloride ($MgCl_2 \cdot 6H_2O$) and ammonium chloride (NH_4Cl) were used to precipitate magnesium ammonium phosphate (struvite) and potassium magnesium phosphate (potassium struvite), respectively. To determine the plant availability of the precipitated solid phosphates a 2 % citric acid solution (pH 2.5) was used.

7.2.3 *Single-point batch isotherms*

GFH and FS adsorption isotherms were developed using various samples of ground material of a grain size < 63 µm. Each sample was shaken with 200 mL of the model phosphate solution (DI water, ionic strength = 10 mmol/L, pH 7.1, c = 6 mg/L) for an equilibration time of 96 hours at room temperature (approx. 20° C). After 96 hours, the sample was filtered over a 0.45 µm filter. Each sample of loaded adsorbent was regenerated with 50 mL of 1 M sodium hydroxide solution being shaken for two hours.

7.2.4 *Differential column-batch reactor (DCBR) tests*

Choice of regenerant

In a preliminary test, spent GFH material used in column experiments with phosphate spiked DI water was tested with NaOH solutions of different strength and DI water. DCBRs containing approx. 1 g moist GFH media were operated using DI water and 0.01 M, 0.1 M and 1 M NaOH solution. After 2 h, the regenerate solution was neutralized and analyzed for phosphate.

Adsorption/ desorption tests

A set of six DCBRs were operated using GFH (grain size range of 0.8 to 1 mm) and FS (grain size range of 0.5 - 1 mm). Whereas for two pairs of duplicate columns of GFH and FS, a phosphate model solution (DI water, ionic strength 10 mmol/L, pH 7.1, c = 2 mg/L P) was used, a third pair of duplicates was operated using FS and DI water. The columns were operated for 144 h in the first and 96 h in the following two adsorption steps, each followed by a regeneration step using 200 mL of fresh, phosphate-free NaOH.

7.2.5 *Column experiments*

Rapid small-scale column test (RSSCT)

A fixed-bed filter of GFH material with a grain size range of 0.1 - 0.2 mm was operated with a phosphate solution (drinking water, pH $\approx$ 8.0, c = 2 mg/L P, EBCT = 0.6 min) until complete breakthrough. The column's output was discharged. After complete breakthrough, the column was regenerated with 200 mL of 1 M NaOH for one hour at a volumetric flow rate of 3.3 mL/min. To assess the efficiency of desorption and the capacity of regenerated GFH, the column was operated three times being regenerated with the same sample of NaOH after each breakthrough.

Desorption kinetics

Two GFH laboratory-scale columns (EBCT $\approx$ 3 min, 45 g dry matter of GFH) were operated using phosphate spiked Berlin drinking water (c $\approx$ 2 mg/L P). The breakthrough experiment is described in detail in Sperlich and Jekel [100]. After complete breakthrough, the columns were regenerated with 1 M NaOH solution at a volumetric flow rate of 10 and 2.5 mL/min, respectively.

Table 13: Regeneration of GFH fixed-bed columns

Experiment type	Water matrix	pH	c_0 [mg/L P]	EBCT [min]	Regenerant volume	Regeneration time	Data source
LC 1	DI	7 - 8	2.2 ± 0.1[1]	3.3	10 BV (1 L)	10 mL/min	[100]
LC 2	DW	7 - 8	2.0 ± 0.1[1]	3.0	20 BV (2 L)	2.5 mL/min	[100]
Pilot BXH	Tertiary effluent	7.2	0.3 ± 0.3[2]	6	10 BV (400 L)	20 - 45 L/h	[104]

[1] as PO_4-P
[2] as TP

After breakthrough of a GFH pilot column at Beijing's wastewater treatment plant Beixiaohe [104], the column was regenerated in the same manner using 400 L of 1 M NaOH solution. After 100 L of regenerant were put through at a flow rate of 20 L/h, regeneration was stopped overnight (≈ 12h). The remaining regenerant was put through at 45 L/h.

All column effluents were sampled in regular intervals, neutralized and analyzed for phosphate. The effluents were collected and the measured phosphate concentration was used to determine the total desorption. A summary of the column regeneration experiments is shown in Table 13.

7.2.6 *Phosphorus recovery*

Precipitation tests with P spiked NaOH solution

To examine the phosphorus recovery potential out of the regenerant of a fixed-bed adsorber, three different precipitation methods were tested. Lime water was added to three 200 mL batches of 1 M sodium hydroxide solution containing 10, 100 and 1000 mg P/L in a molar ratio Ca : P of 2.5 : 1. Another three batches contained 200 mL DI water spiked with KH_2PO_4 to set phosphate concentrations of 10, 100 and 1000 mg/L P. A pH of 9.0 [121] was adjusted by adding 0.1 M NaOH. Magnesium chloride ($MgCl_2 \cdot 6\ H_2O$) and ammonium chloride (NH_4Cl) were added in a molar ratio Mg : NH_4 : P of 1 : 1.5 : 1 to precipitate magnesium ammonium phosphate (MAP, $MgNH_4PO_4 \cdot 6\ H_2O$). The experiment was repeated with the exclusive addition of magnesium chloride ($MgCl_2 \cdot 6\ H_2O$) in a molar ratio K : Mg : P of 1 : 1.5 : 1 to precipitate potassium magnesium phosphate (KMP). All nine vessels were stirred for two hours, filtered and analyzed for phosphate to estimate the precipitation efficiency.

Precipitation tests with regenerate

To estimate the phosphorus recovery potential of lime water, 200 ml of a $Ca(OH)_2$ solution were added to the regenerant solutions in a molar ratio Ca : P of 2.5 : 1. All vessels were stirred for two hours and subsequently filtered.

Plant availability

To determine the plant availability of the different precipitated phosphate products, a standard method for the extraction of phosphorus soluble in 2 % citric acid was used [47]. The filtered precipitate of KMP, MAP and calcium phosphate from the highest concentrated (1000 mg/L P) batch was given into a vessel of 200 mL of a

2 % citric acid solution (pH 2.5). The vessels were stirred for 30 min to dissolve the solid phosphates before filtering the solutions using a 0.45 µm filter. Finally, the fraction of soluble phosphate was calculated to assess the plant availability of calcium phosphate, magnesium ammonium phosphate and potassium magnesium phosphate.

7.2.7 *Analyses*

Orthophosphate was determined using a flow injection analyzer (FIAstar 5000 Analyzer, FOSS Analytical, Denmark) according to ISO 15681-1. The standard deviation was determined to be 4.8 % at a mean concentration of 0.016 mg/L P and 0.77 % at 3.8 mg/L P with a detection limit of 3 µg/L. For pH measurement a WTW pH 340 with a Sentix 41 electrode (WTW, Germany) was used. Dissolved iron was determined by atomic absorption spectroscopy (Varian SpectrAA-300, VARIAN, USA) according to DIN 38 406-1. DOC was analysed by thermal-catalytic oxidation using a High-TOC analyser (Elementar Analysensysteme, Germany). UV absorption (254 nm) and color (436 nm) were determined using a Lambda 12 UV/VIS-spectrophotometer (Perkin-Elmer) with cuvettes of 1 cm length.

7.3 RESULTS AND DISCUSSION

7.3.1 *Capacity of the virgin adsorbent*

As a prerequisite to assess the regeneration of the adsorbent media, the capacity of the unused, virgin material needed to be determined. Single-point batch isotherm experiments using ground material aimed at complete use of the adsorption capacity. After an equilibration time of 96 h, adsorption capacity of GFH and FS was determined by a mass balance. For GFH, an average solid-phase concentration of 13.3 $\pm$ 0.4 mg/g P at an equilibrium concentration of 3.4 $\pm$ 0.1 mg/L P could be determined. FS showed a similar performance with 12.1 $\pm$ 0.3 mg/g P at an equilibrium concentration of 3.4 $\pm$ 0.1 mg/L P. Isotherm data for GFH and FS [100] show comparable values, although no direct comparison is possible since these isotherms were developed in a lower concentration range. In this range, capacities of FS are significantly lower than of GFH, which is much less pronounced at higher initial concentrations. A parallel control batch without adsorbent showed no concentration change.

DCBRs were operated using adsorbent material of 0.8 - 1.0 mm (GFH) and 0.5 - 2 mm (FS) grain size and thus would have needed a longer equilibration time to reach adsorption equilibrium. A solid-phase concentration of 7.4 $\pm$ 0.01 mg/g P for GFH was observed. For FS, the calculated solid-phase concentration was 3.6 $\pm$ 0.3 mg/g P. These values are significantly lower than the single-point isotherm data and do not represent adsorption equilibrium.

RSSCTs provide breakthrough data and allow direct assessment of operation time or throughput until breakthrough. For the described column, breakthrough, defined as an effluent concentration of $>$ 30 µg/L P, was reached after approx. 3600 bed volumes (BV). By integrating the breakthrough curve, the corresponding solid-phase concentration of 23.7 mg/g P was estimated. These significantly higher capacities are caused by the drinking water matrix. Very similar capacities were

determined in isotherm and RSSCT studies using drinking water and could be attributed to the presence of divalent cations, e.g., calcium [100].

7.3.2 *Choice of regenerant*

Figure 25 shows the desorption strength of NaOH solutions of different concentrations compared to DI water. Only 1 M NaOH solution contained considerably more phosphate than DI water. The phosphate found in DI water and less concentrated NaOH probably results from less strongly bound phosphate as well as liquid-phase phosphate in the pore volume, whereas the higher phosphate concentrations in 1 M NaOH represent a major part of the bound phosphate which desorbs from the adsorbent material. Obviously, the phosphate binding to the GFH surface is comparatively strong and very high pH values are needed to achieve considerable desorption of phosphate from GFH. For this reason, 1 M NaOH solution was chosen as regenerant and used in all of the experiments presented in this study.

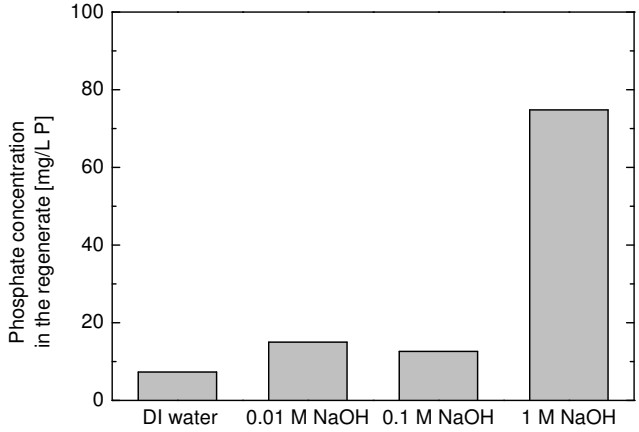

Figure 25: Desorption strenght of different regenerant solutions (2h regeneration using 200 mL regenerant

7.3.3 *Desorption and capacity of the regenerated adsorbent*

When assessing the regeneration of adsorbent media, it has to be distinguished between the amount of adsorbate which can be desorbed using the regenerant (desorption) and the newly available capacity of the regenerated adsorbent. Desorption and newly available capacity can be assumed to be closely connected, but do not necessarily have to be identical. For instance it cannot be ruled out that

the adsorbent's surface is modified during the regeneration process which might result in a change of the maximum available capacity.

In the single-point batch isotherm experiments, only desorption was investigated (Figure 26). For GFH, approx. 80 % of the bound phosphate could be desorbed using phosphate-free NaOH solution. Regeneration of FS using the same regenerant led to higher amounts of phosphate in the regenerant than was previously adsorbed. A desorption of 103 % was calculated and confirmed in later experiments. This indicates that fresh FS media already contains phosphate resulting from the production process. In contrast to GFH, which is pure, synthesized FeOOH, FS is produced from waterworks sludge.

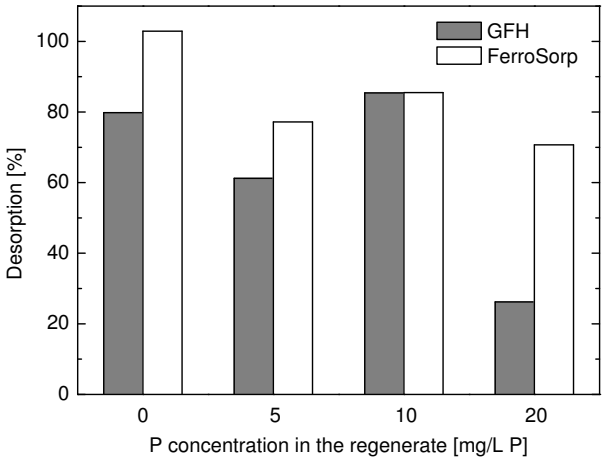

Figure 26: Desorption of phosphorus adsorbed onto GFH and Ferrosorp using 1 M NaOH of different initial phosphate concentrations as a regenerant

For an economic use of the regenerant, the reuse of NaOH solution is desired. Therefore, NaOH solutions of different phosphate concentrations were tested for their effectiveness as regenerant. For concentrations of up to 10 mg/L P in the regenerant, between 61 % and 85 % of the adsorbed phosphate could be desorbed from the GFH material. At a phosphate concentration of 20 mg/L P, desorption decreased to 26 %. It can be concluded that desorption is also possible when higher concentrations of phosphate are already present in the regenerant solution. The lowest desorption was observed at 20 mg/L P, but there was no linear correlation between desorption and phosphate concentration in the regenerant. A reuse of the regenerant solution appears feasible.

In the DCBR tests, both desorption and the capacity of the regenerated adsorbents were determined for three sequential operation cycles using phosphate-free NaOH (Figure 27). Arithmetic mean values of the duplicate results were calculated. For GFH, a desorption of 82.3 %, 84.4 % and 75.5 % of the mass of phosphate adsorbed in the preceding adsorption cycle were determined, respectively. In all

operation cycles, only a partial desorption was achieved, i.e. with each operation cycle adsorption sites were lost and the capacity of the regenerated material decreased continuously (Figure 27). The adsorption capacity after regeneration was 6.3 mg/g P and 5.2 mg/g P, respectively, corresponding to 84.9 % and 70.2 % of the initial capacity. The total adsorbed phosphate (newly adsorbed and not desorbable phosphate) is constant (7.4 - 7.6 mg/g P) over the three operation cycles.

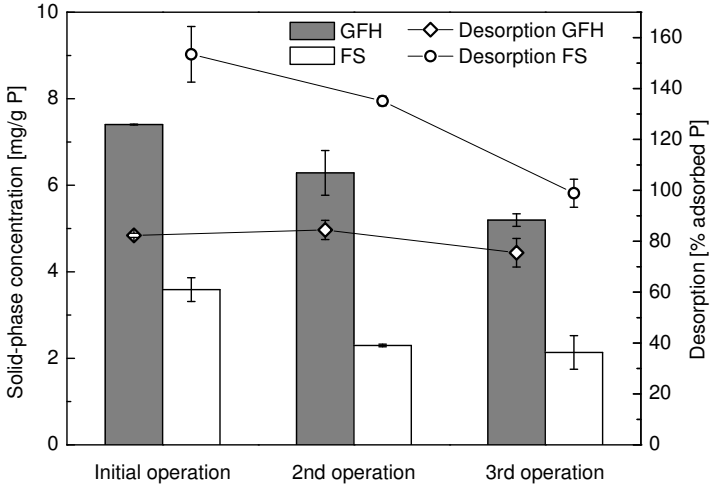

Figure 27: Solid-phase concentration reached and desorbed phosphate during operation and regeneration of DCBR tests using GFH and FerroSorp

In all cases, regeneration of FS showed more phosphate measured in the regenerant than adsorbed in the preceding adsorption cycle. Blind controls operated with phosphate-free DI water and regenerated with NaOH showed phosphate in the regenerant solution, corresponding to a solid-phase concentration of 2.2 - 2.5 mg/g P. Also, the regenerate solutions showed a yellowish/brownish color which indicates either dissolution of adsorbent media or desorption of organic matter such as humic and fulvic acids. The intense color may have led to higher phosphate measurements in the photometric method. The material is clearly unstable when treated with 1 M NaOH solution and was probably preloaded with phosphate and/ or natural organic matter during the production process. Based on the measured phosphate concentrations, 153 % (first regeneration), 135.1 % (second regeneration) and 98.9 % of the previously adsorbed phosphate was found in the regenerates (Figure 27).

The capacity of FS was significantly lower than of GFH and decreased from 3.6 mg/g P in the first to 2.3 and 2.1 mg/g P in the following operation cycles. This corresponds to 64.0 % and 59.5 % of the initial capacity. In contrast to the single-point isotherm data, FS' capacities are significantly lower than those of GFH, which might indicate slower adsorption kinetics, as the solid-phase concentrations seem to converge when the adsorption equilibrium is reached.

In RSSCTs, three operation cycles of adsorption/desorption were simulated and the regenerate solution (200 mL of 1 M NaOH) was reused. With each operation cycle, breakthrough occurs slightly earlier, as can be seen from the breakthrough curves (Figure 28). In the last two operation cycles, the throughput until breakthrough (30 µg/L P) decreased from 3600 to 2550 and 1500 BV, respectively. This corresponds to a 32 % and 43 % decrease of the operation time with each operation cycle. However, if higher relative effluent concentrations are chosen, the decrease in operation time is lower. For a breakthrough concentration of 1.8 mg/L P, the throughput until breakthrough decreased from 10700 to 10026 and 8662 BV, respectively, corresponding to a decrease of 6 and 14 % (Figure 29). This indicates that full use of the adsorbent which can be achieved by operation in series (lead-lag design) is also favourable if the material is regenerated. The estimated total capacity of the regenerated adsorbent (integration of the breakthrough curve) increased from 23.7 to 26.7 and 28.6 mg/g P. Due to the incomplete desorption, the newly available capacity is continuously decreasing, whereas the amount of non-desorbable phosphate increases (Figure 30).

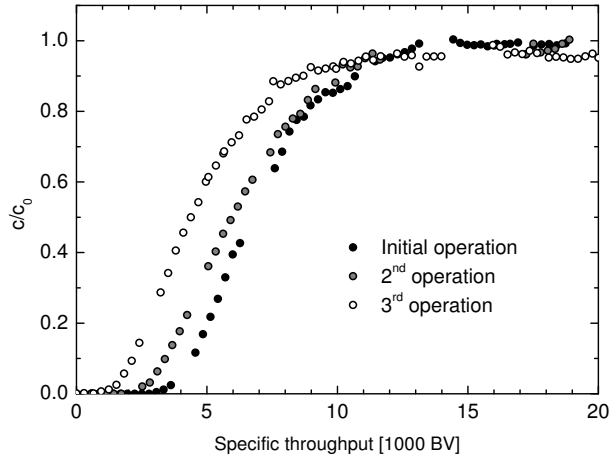

Figure 28: Breakthrough of a RSSCT column operated in three sequential operation phases and regenerated with one, reused batch of 1 M NaOH

Phosphate concentration measurements in the regenerate show an increase to 432 and 832 mg/L P after the first and second regeneration, respectively. While 86.3 % of the adsorbed phosphate could be desorbed in the first regeneration step, desorption in the second and third regeneration step decreased to 72.3 % and 71.0 % of the mass of phosphate adsorbed in the preceding adsorption cycle. Thus, a reuse of the regenerant solution seems to lead to less desorption of phosphate, but a partial desorption of 71.0 % of the bound phosphate is achievable, even with high phosphate concentrations in the regenerant solution (Figure 30).

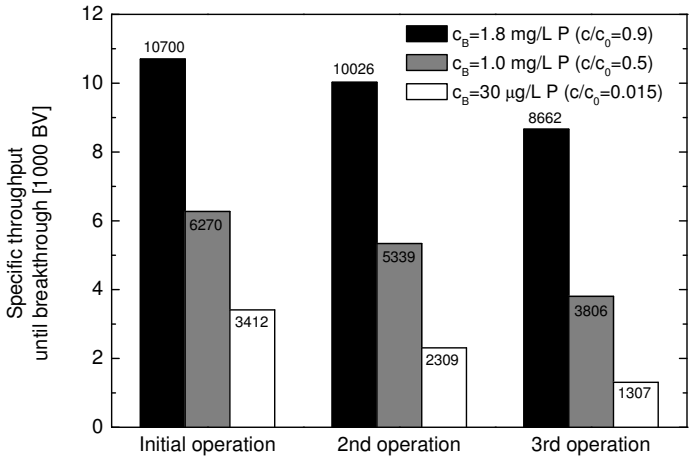

Figure 29: Specific throughput until breakthrough (operation time) of a RSSCT column operated in three sequential operation phases and regenerated with one, reused batch of 1 M NaOH depending on the target effluent concentration (c_B)

7.3.4 *Desorption kinetics*

Figure 31 shows the effluent concentration profile of two laboratory fixed-bed columns and a GFH pilot column during regeneration with 1 M NaOH solution. Although the conditions of operation and regeneration differed between these three columns, the effluent profiles are highly comparable. Obviously, desorption of phosphate is fast and most of the desorbable phosphate is desorbed after approx. 5 BV. Parallel batch experiments with spent GFH material showed no change in concentration over 2 h of regeneration. All of the desorbed phosphate was already in solution after approx. 10 min, confirming the negligible influence of mass-transfer on the desorption of phosphate.

7.3.5 *Characterization of the regenerate brine*

Regenerates from a GFH laboratory column operated with Berlin drinking water spiked with 2 mg/L P (LC 2, Table 13) were neutralized using HCl and analyzed for phosphate, DOC, UV_{254}, UV_{436} and dissolved iron. The strongly brown coloured solution showed high DOC concentrations of 97.3 mg/L along with high UV adsorption values of $> 300\ m^{-1}$ at 254 nm and 17.3 m^{-1} at 436 nm. Very low concentrations of 1.6 mg/L of dissolved iron were found in the regenerate after 2 h of regeneration with 1 M NaOH, confirming the adsorbent's stability at high pH.

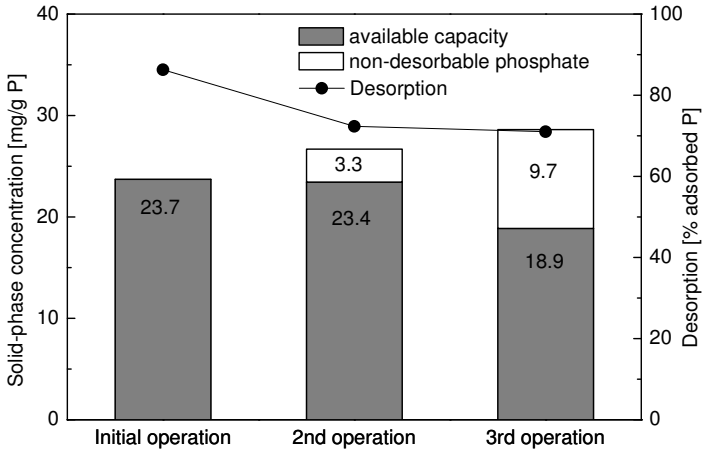

Figure 30: Phosphorus mass balance for three sequential adsorption/ regeneration phases of a RSSCT column: solid-phase concentration achieved in the adsorption step, remaining after regeneration and desorption of phosphate during regeneration

7.3.6 *Phosphorus recovery from the regenerate*

Besides the multiple use of NaOH solution for regeneration, a potential phosphorus recovery from the regenerate was tested, since a highly concentrated eluate appears ideal for nutrient recovery. Figure 32 shows phosphorus removal by precipitation from NaOH solutions of different phosphorus concentrations. Precipitation using lime water ($Ca(OH)_2$) showed a phosphorus removal of 93.7 - 99.9 %. Precipitation as struvite is only possible at a lower pH of 9 and showed less P removal. For MAP, 42.9 % of the dissolved phosphate in the highest concentrated batch (1000 mg/L P) could be precipitated, lower concentrated solutions showed only 15.2 % (100 mg/L P) and 17.6 % (10 mg/L P). KMP precipitation showed even less phosphorus removal with a maximum of 30.3 % removal from NaOH solution of 1000 mg/L P. This is significantly less than almost complete removal by MAP and KMP precipitation reported by Wilsenach et al. [125]. Since MAP and KMP precipitation are both quite pH sensitive, this might be due to unstable pH conditions during the experiment. Regarding a direct phosphorus recovery from the regenerate solution both MAP and KMP precipitation are no suitable technique even if optimal reaction conditions are met. The necessary decrease from pH 14 to pH 9 requires large amounts of acid and would prevent a possible reuse of the regenerant solution after filtration of the precipitates. Precipitation as calcium phosphate appears to be a promising technique for phosphorus recovery, since lime water can easily be dosed into the regenerate solution and no other chemicals are required. After precipitation and filtration, a solid product contain-

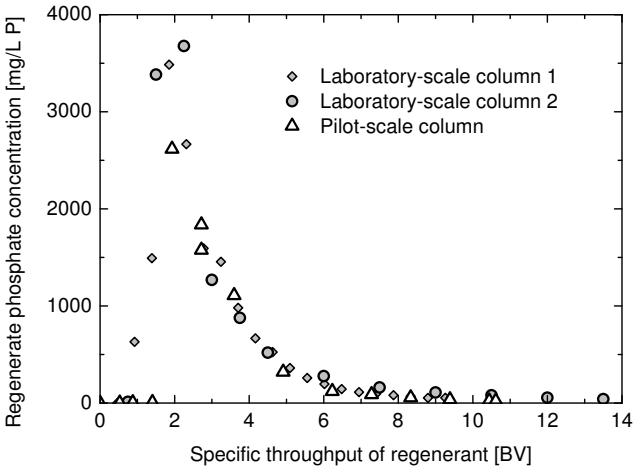

Figure 31: Phosphate elution curve of a laboratory-scale column regenerated with 1 M NaOH

ing approx. 10 - 15 % P [33] remains. A reuse of the filtered NaOH solution is possible, resulting in less NaOH consumption during operation.

Figure 32 also shows the precipitate's solubility in 2 % citric acid. For all investigated solids, high citrate solubility was found (68.9 - 84.1 %). It can be concluded that most of the precipitated phosphorus is plant available and all recycling products could be used as fertilizers.

Figure 33 shows phosphate removal from the regenerates of the DCBR tests. Addition of lime water at a molar Ca : P ratio of 2.5 : 1 led to almost complete removal of phosphate from all regenerates. The white precipitate formed is most likely calcium phosphate. Regenerates from FS columns which were operated with phosphate-free DI water (blind tests) showed only partial phosphate removal although phosphate concentrations of up to 10 mg/L P were detected. Whereas 24 % removal was observed in the first regeneration step, removal in the following regeneration steps decreased to 1 %. This indicates that FS eluates might contain coloured substances, probably organic matter, which is detected as P in the photometric method.

7.3.7 *Economic assessment*

While regeneration can extend the lifetime of a GFH fixed-bed adsorber, it will require both additional investment (storage tanks, pumps, etc.) and operating costs (regenerant). To make multiple use of the adsorbent economically feasible, saved material cost should trade-off additional costs for regeneration. Therefore, a simple economic assessment was carried out. Four scenarios of a typical full-scale operation (1000 m^3/d) were defined. A high influent concentration of 2 mg/L P

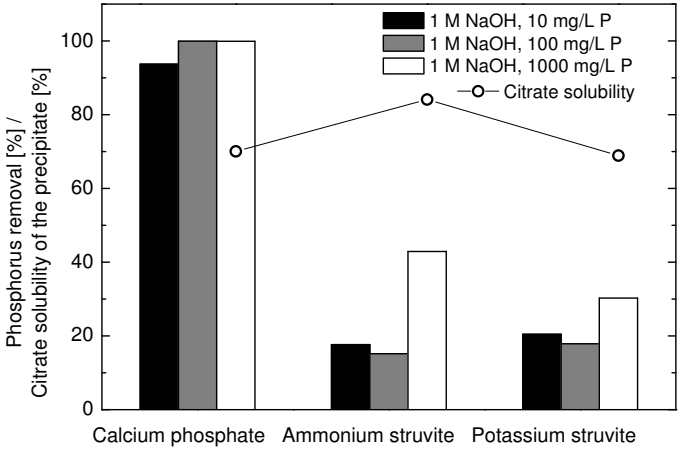

Figure 32: Phosphorus removal by precipitation as calcium phosphate (CP), struvite (MAP) and potassium struvite (KMP) from model regenerate solutions and citrate solubility of the precipitate

(Scenario 1 and 2), corresponding to the experiments in this study and a lower influent concentration of 0.2 mg/L P, representing a typical 'polishing' application (Scenario 3 and 4) were chosen. A target effluent concentration of 0.03 mg/L P represents a challenging effluent standard (Scenario 1 and 3), whereas scenario 2 and 4 were chosen to represent near to complete use of the adsorbent material ($c/c_0 = 0.9$) possible in serial operation (lead-lag design). The RSSCT breakthrough curve provided throughput until breakthrough data for the two high influent concentration scenarios. For the low influent concentration scenarios, this data was estimated from isotherm data. For scenario 3, a constant relationship between time until breakthrough ($>$ 0.03 mg/L P in the effluent) and time until ideal breakthrough was assumed. Based on current prices of GFH (4.4 €/kg), NaOH (252 €/t) and phosphate rock (72 €/t) [71], adsorbent and regenerant costs as well as the value of a fertilizer product was calculated (Table 14). This rough estimation shows that the high adsorbent cost can be reduced by 51 % in the single adsorber scenarios. In scenarios 2 and 4 (high effluent concentration, serial operation), the adsorbent costs could be reduced by 63 %. For arsenic removal from groundwater, GFH material and disposal costs have been estimated to amount to 60 - 70 % of the total annual costs [95]. Since very low influent concentration typical for arsenic removal applications were considered in this study, GFH costs in the presented scenarios for phosphate removal will probably make up an even larger share of the total annual costs. Consequently the potential savings could easily cover needed investment cost for regeneration. To estimate the potential of GFH adsorption for phosphate removal, a comparison to alternative phosphorus removal technologies such as coagulation/filtration is necessary. Dietze [31] reported specific total costs

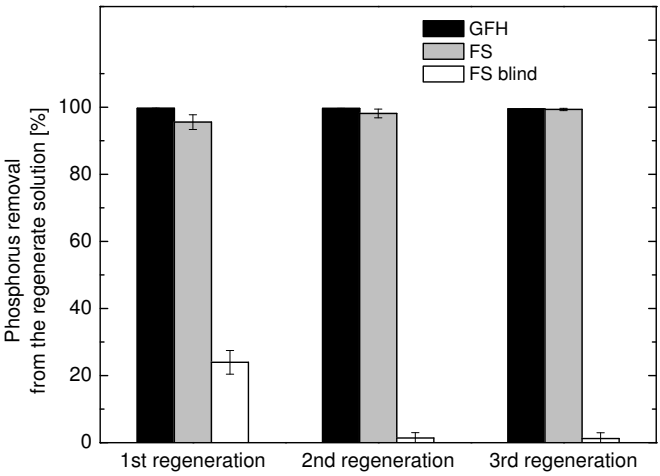

Figure 33: Phosphorus removal by precipitation as calcium phosphate from DCBR regenerates

of 0.13 Euro/m^3 for advanced phosphorus removal from surface water in Berlin. The costs of coagulation/filtration of wastewater effluents can be expected to be in the same range. GFH adsorbent costs calculated for low influent concentrations and/or serial operation are in a similar range, showing that phosphate adsorption onto GFH could be a promising treatment option if regeneration is included. RSSCT results also indicate that GFH could be regenerated more than three times, which would result in even lower specific adsorbent costs. Table 14 also shows, that the relative costs of the (reusable) regenerant are very low. Interestingly, the current value of potentially recovered phosphate is negligible in relation to the total operating costs. The necessary investment and operating costs to convert the regenerate into a marketable fertilizer product could probably not be covered. Also, existing legal and institutional barriers have to be considered. However, given the finite nature of mineral phosphate resources, this option might become more profitable in the future.

In summary, regeneration and multiple use of GFH can significantly increase operation times of fixed-bed adsorbers and thus decrease operating costs. The previously reported suitability of NaOH as regenerant solution [19, 33, 57, 104] was confirmed. Contrary to statements of Blaney et al. [14], GFH was shown to be chemically stable and suitable for multiple uses. Whereas Genz et al. [57] and Chitrakar et al. [19] did not report limits to regeneration and reuse, the present study, which is more detailed and close to real application (RSSCT), clearly shows limits of newly available capacity by regeneration. Attrition, which was not studied, might represent another, possibly more serious constraint to multiple use of GFH due to material loss during backwash and regeneration. Nevertheless, adsorption onto GFH offers a high potential for advanced phosphorus removal and recovery from wastewater.

Table 14: Operating cost assessment for a full-scale GFH adsorber (1000 m^3/d)

	Scenario 1	Scenario 2	Scenario 3	Scenario 4
Influent concentration [mg/L P]	2.0	2.0	0.2	0.2
Target effluent concentration [mg/L P]	0.03	1.8	0.03	0.2
BV treatable without regeneration	3,412[1]	10,700[1]	15,190[2]	38,767[2]
Adsorbent cost [cents/m^3 treated]	148	47	33	13
BV treatable in 3 operation cycles with 2 regenerations	7,027[1]	29,388[1]	31,283[2]	106,475[2]
Adsorbent cost [cents/m^3 treated]	72	17	16	5
Cost of regenerant [cents/m^3 treated]	0.86	0.21	0.19	0.06
P recovery [kg P/a], based on 80 % desorption	47	104	11	38
Value of recovered P [cents/m^3 treated]	0.01	0.03	< 0.01	0.01

[1] Based on RSSCT data (Figure 29)
[2] Estimated from isotherm data [100], assuming $t_{Breakthrough}/t_{stoich.}$ = const.

7.4 CONCLUSIONS

- Phosphate adsorbed on GFH can be desorbed using NaOH solution. Using 1 M NaOH, approx. 80 % of the initially bound phosphorus can be desorbed in the first regeneration step.

- Due to the incomplete desorption, capacities of regenerated GFH are lower compared to the unused adsorbent and decrease with each additional use. In DCBR tests, 85 % and 70 % of the initial capacity could be reached after the first and second regeneration, respectively. In a RSSCT, the calculated capacity decreased to 99 % after the first and 80 % of the initial capacity after the second regeneration. Although regeneration of the material is clearly limited, up to 3 operation cycles appear feasible.

- A reuse of the regenerant solution is possible. Even with high phosphate concentrations present in NaOH solution, 61 - 85 % of the bound phosphate can be desorbed.

- Desorption kinetics are fast. Most of the desorbable phosphate can be eluted using 4 - 6 BV of regenerant.

- A recovery of phosphate from the regenerate solutions is possible. Precipitation of calcium phosphate resulted in more than 90 % phosphorus removal. The precipitate is plant available and might thus be used as fertilizer.

- Parallel experiments with FerroSorp showed similarly decreasing desorption efficiency and capacity with each regeneration step. Although total capacities were lower compared to GFH, desorption of phosphate was higher due to a preloading of the material in the production process.

- Operating cost estimations show that regeneration can significantly decrease specific GFH costs due to longer operation times.

8

AN INTEGRATED WASTEWATER REUSE CONCEPT COMBINING NATURAL RECLAMATION TECHNIQUES, MEMBRANE FILTRATION AND METAL OXIDE ADSORPTION

Alexander Sperlich[1], Xing Zheng[1], Mathias Ernst[1] and Martin Jekel[1]

Water Science & Technology 2008, 57(6), 909-914.

PREFACE

The following chapter presents research carried out within the project "Sustainable water concept and its application for the Olympic Games 2008" funded by the German Federal Ministry of Education and Research (BMBF). Research in this project focussed around two major questions: 1) selective phosphorus removal by adsorption onto GFH, and 2) membrane fouling control by biofiltration prior to ultrafiltration. The latter aspects are not part of this thesis, but were included in the following article and are printed for completeness.

ABSTRACT

In a Sino-German research project, a sustainable water reclamation concept was developed for different applications of municipal water reuse at the Olympic Green 2008 in Beijing, China. Results from pilot-scale experiments in Beijing and Berlin show that selective nutrient removal by adsorption onto granular ferric hydroxide (GFH) after a membrane bioreactor (MBR) can maintain a total phosphorus concentration of < 0.03 mg L^{-1} P, thus preventing eutrophication of artificial lakes. Operation time of GFH adsorption columns can be extended by regeneration using sodium hydroxide solution. A subsequent ultrafiltration (UF) membrane after bank filtration creates an additional barrier for pathogens and allows for further urban reuse applications such as toilet flushing. Short term bank/ bio-filtration prior to UF is shown to effectively remove biopolymers and reduce membrane fouling.

8.1 INTRODUCTION

The 2008 Summer Olympics will be held in Beijing, China. Green Olympics is one concept of the Beijing Olympic Games and states the determination and ambition for environmental protection. However, the environmental problems of the mega-city Beijing are still tremendous. Above all the water sector is struggling with quality problems and declining groundwater levels. As a consequence the City of Beijing is striving for long term solutions for wastewater treatment and its reuse with a challenging and Olympic-oriented water program. The Olympic

1 Technische Universität Berlin

Green is intended to serve as a demonstration area for innovative, sustainable wastewater treatment and reuse technologies. The Park covers a total area of 1,215 ha, located north of the city centre. An area of 60 ha of constructed artificial lakes and channels will be filled with treated wastewater in the northern area of the Park. In the central area, a smaller lake of 15 ha with superior water quality will be operated with fountains; all waters supplied will be advanced treated municipal wastewaters. Further reuse applications are envisaged, including water for irrigation (not only in the Park, but also in neighboring areas) and urban water applications like toilet flushing and washing waters.

The present study summarizes the results of the Sino-German research cooperation project on a sustainable water concept and its application for the Olympic Games 2008 in the subproject "wastewater treatment and reuse". Project partners are the Beijing Drainage Group, the Tsinghua University in Beijing and the Technical University of Berlin. Moreover, a German small and medium-sized enterprise (SME) and a consulting company are involved. A combination of advanced wastewater treatment and nature-orientated technologies were realized in pilot-scale at the Beijing wastewater treatment plant (WWTP) Beixiaohe. The main objectives included advanced nutrient removal and eutrophication control of scenic impoundments, reuse for irrigation and urban reuse.

Based on the plans for the Olympic Green and the extension of the WWTP Beixiaohe, a reuse concept has been developed [44], including multiple barriers for contaminants and pathogens. Effluent of a membrane bio-reactor (MBR) with in-situ P-precipitation will be treated to two different qualities, depending on the use. In a first treatment step, phosphate as essential nutrient is removed by adsorption onto granular ferric hydroxide (GFH) and the water is pumped into an artificial lake. Here, the water is used for scenic impoundment, but also further treated by biological processes. Finally, lake bank filtration (BF) further removes organic compounds and serves as an additional pathogen barrier and effective pretreatment step for a subsequently operated membrane filtration. An ultrafiltration (UF) ensures a sufficient water quality for safe non-potable (urban) reuse.

Research on the developed treatment scheme focussed around two major questions. First, selective phosphorus removal by adsorption onto GFH and eutrophication control in the artificial lake was studied intensively. In previous laboratory-scale experiments, GFH has shown high capacities for phosphate removal from MBR filtrates [57] and wastewater effluents [44], despite potential competition by other wastewater constituents. A particle free influent and the goal of very low phosphorus concentrations in the effluent favors adsorption compared to other options of phosphorus removal, e.g. coagulation. Second, fouling of the ultrafiltration membrane and its control by biofiltration was investigated. Fouling is generally acknowledged as one of the main problems restraining the application of membrane filtration [6]. Polysaccharides and proteins have been found to be major foulants [74, 78]. Removal of these substances by biofiltration might therefore significantly reduce membrane fouling.

8.2 METHODS

The developed treatment scheme (Figure 34) was realized in pilot-scale at the Beijing WWTP Beixioahe. Effluent of a pilot membrane bioreactor, operated by the Tsinghua University, was used as influent for two GFH fixed-bed columns. Since

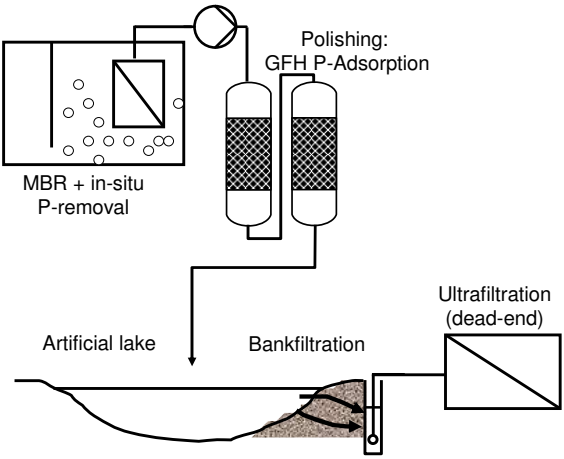

Figure 34: Wastewater reclamation and reuse scheme

MBR effluent P concentrations varied substantially, a flocculation step using poly-aluminium chloride (PAC, dosage of 8 - 16 mg L^{-1} Al) followed by sedimentation and rapid sand filtration was introduced before GFH adsorption. In large-scale application, this step could be substituted by in-situ precipitation or biological P removal in the MBR. The resulting modified treatment scheme for pilot operation in Beijing consisted of MBR effluent - flocculation/ sedimentation - rapid sand filtration - GFH adsorption - artificial lake - bank filtration - ultrafiltration.

To achieve effluent concentrations of less than 30 µg L^{-1} P, two fixed-bed adsorption columns were operated. Operational conditions and parameters are given in Table 15. To simulate the Olympic Lakes, a 30 m^2 large artificial lake was constructed and operated. At start-up, the lake was filled with 95 % drinking water, supplemented by 5 % secondary effluent. In order to facilitate the settlement of planktonic organisms, plankton samples were taken from four lakes in Beijing and the lake was inoculated. The dimensions of the lake were 5.5 m × 5.5 m × 2.5 m, the applied filtration materials were sand (d = 2 - 4 mm) and limestone (d = 3 - 6 mm) which were set up in two separated containers to form embankments. On the surface of each bank, a layer of textile was situated to ensure stability. The BF was operated with a filtration passage 1.7 m in depth, a filtration velocity of 1.55 m d^{-1} and a travelling time of about 1.1 to 1.5 days.

An UF pilot plant (W.E.T., Germany) was operated with a membrane module (INGE, Germany, membrane material: PESM, MWCO: 100 kD, dead-end filtration, membrane surface 4.5 m^2, operational flux: 60 - 140 L m^2 h^{-1}).

Following the pilot experiments in Beijing, a similar set-up was realized in Berlin's WWTP Ruhleben, Germany. Here, fine-screened secondary effluent was

Table 15: Operational parameters of two GFH fixed-bed columns at WWTP Beixiaohe

Parameter	Operation in series
Flow rate [$m^3\ d^{-1}$]	9
Empty bed contact time [min]	2×6
Empty bed volume [m^3]	2×0.038
Column diameter [m]	2×0.25
Bed depth [m]	2×0.76
Filtration rate [m h^{-1}]	7.6
Backwash	
Filtration rate [m h^{-1}]	25
Flow rate [$m^3\ h^{-1}$]	1.2
Volume [BV/m^3]	2/0.075

applied directly to four biofilters (slow sand filtration), operated at different hydraulic loading rates between 0.02 and 0.5 m h^{-1}. The filtration area was 0.018, 1 and 2 m^2, respectively. Filter height was approximately 0.72 m. As filter material, sand was chosen. The subsequently operated UF pilot plant was the one operated in Beijing before.

Water quality analysis included pH, turbidity, ammonia, total phosphorus, total coliforms, UV absorption at 254 and 436 nm, respectively. All analyses were performed according to standard methods [5]. Dissolved organic carbon in the water was characterized by size exclusion chromatography (LC-OCD with DOC/UVA online detection).

8.3 RESULTS AND DISCUSSION

Operation of the pilot adsorption columns was not constant during the operation period (July 28th to October 31st 2005). Start-up of the MBR pilot unit upstream resulted in strong variations of the influent concentration as well as shut-down periods. The measured effluent concentrations show a reliable and almost complete removal of phosphate by adsorption onto GFH. Despite highly variable influent concentrations (between 0.008 and 1.62 ppm P), the average effluent concentration was 0.023 ppm P, but always below 0.07 ppm P. After approximately 12,000 BV, breakthrough of the adsorber occurs (Figure 35). Following this, the first of two in series operated adsorbers was regenerated using 1 molar sodium hydroxide solution, thereby extending the operation time to more than 16,000 BV or 96 days, respectively. For regeneration, 400 L, equivalent to 10 bed volumes, of 1 molar sodium hydroxide solution were used. After a throughput of 100 L regenerant at 20 L h^{-1}, regeneration was paused for 12 h. The remaining 300 L regenerant were applied at 45 L h^{-1}. Figure 36 shows that after four bed volumes the major part of the bound phosphate is already desorbed. A total of 10.5 g P per kg dry matter GFH material could be desorbed. Corresponding lab-scale batch experiments show an average regeneration efficiency of 86 %, and marginal influence of operational time and pH.

By the effective removal of phosphate, which is the limiting nutrient for microbial growth, eutrophication of the artificial lake could be prevented. The mean concentrations in the operation period for chlorophyll A and total phosphorus

were 2.4 mg m^{-3} and 25.1 mg m^{-3}, respectively. Following the Vollenweider/ OECD model [120], the artificial lake can be classified as mesotrophic.

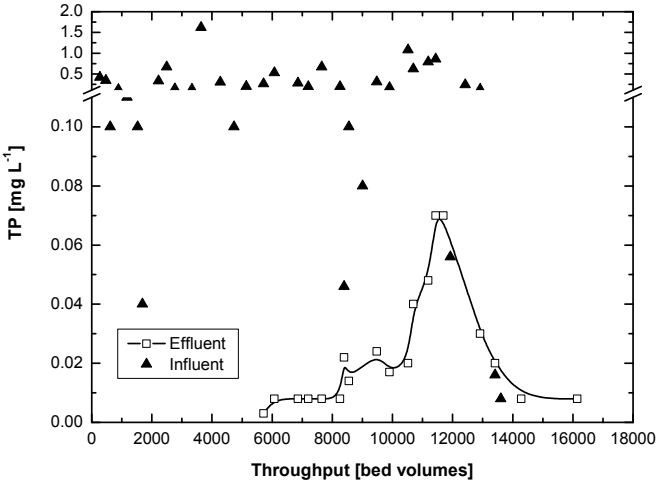

Figure 35: Breakthrough curve of GFH pilot columns at WWTP Beixiaohe

Table 16 shows the average water quality parameters of the lake water, sand filtrate and UF permeate. The reuse water quality after UF generally meets the Chinese reuse water standard for toilet flushing [44], in which chlorination is mandatory. This demonstrates the advantage of UF removing particles and bacteria in wastewater reuse.

During an operational period of more than 3 months (July - Nov. 2005) transmembrane pressure (TMP) of UF varied in different patterns depending on the characteristics of influents through different filtration media (Figure 37). In the first phase (July 27th to Aug. 15th) of the experiment, the influent to UF was a 50:50 mixture of sand and limestone filtered water. Because of impurities in the used limestone, effluent pH after limestone filtration was always higher than 10 and serious scaling was observed. In this phase scaling and organic fouling caused a steep TMP increase. In phase 2 (Aug. 16th to Sep. 12th), the influent to UF was exclusively effluent from sand filtration. TMP increased quickly, probably due to organic fouling. In this phase, organic foulants were not effectively removed, which can be explained by an insufficient adaptation of the biofilter. TMP increased much slower in phase 3 (Sep. 12th to Nov. 7th) compared to preceding phases. During this period, influent to UF was effluent from sand filtration only. Less organic fouling lead to a longer operation time and a moderate TMP increase of around 400 mbar within 55 days.

Figure 38 shows a LC-OCD diagram of the artificial lake water, bank filtration (limestone/ sand) effluent and ultrafiltration permeate. The liquid chromatogra-

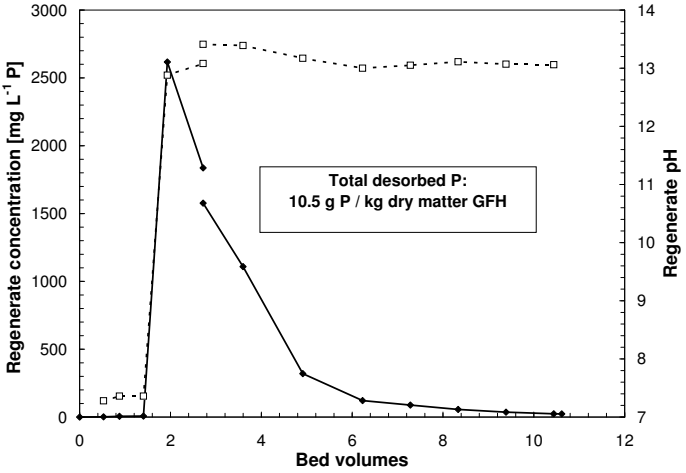

Figure 36: Phosphate desorption using 1 M NaOH as regenerant for fixed-bed GFH columns in WWTP Beixiaohe

phy unit separates organic compounds according to their molecular size through the size exclusion column. Online detection of organic carbon leads to three characteristic peaks, representing biopolymers, humic substances, and low molecular weight acids. It is shown that the artificial lake water contains high concentrations of biopolymers (first peak at a retention time of 40 min), but sand filtration effectively removes the biopolymer peak. Limestone filtration shows only slight reduction in biopolymer concentration, which explains the TMP development of the UF pilot plant (Figure 37). After an adaptation time (phase 2), biological processes in the filter material remove biopolymers.

Further investigations on the removal of biopolymers by biofiltration in Berlin's WWTP Ruhleben indicate a direct correlation between biopolymer concentration, filtration rate and fouling [130]. Figure 39 shows the removal of biopolymers by sand filtration at different filtration rates. The complete absence of a biopolymer peak in the UF permeate indicates that biopolymers are major foulants. Sand filtration reduces the biopolymer concentration, with lower filtration rates showing better removal and a higher filterability of the water sample.

Figure 40 shows the biopolymer removal by biofiltration for an operation time of 7 months (Nov. 2006 to May 2007), confirming that the filtration rate influences biopolymer removal. Biopolymer removal rate is improved from 32 % to 50 % on average when filtration rate is decreased from 0.5 m h^{-1} to 0.25 m h^{-1}, but as filtration rate sinks from 0.1 m h^{-1} to 0.05 m h^{-1}, the corresponding biopolymer removal rate increases only from 62 % to 65 % on average. This implies a need for technical optimization of the bio-filtration rate and the performance of the subsequent UF.

Table 16: Water quality after treatment steps (average values) and comparison to Chinese urban reuse water standards

	Water quality (Aug. 15th-Nov. 4th 2005)			Chinese urban reuse water standard (GB/T 18920-2002)
Parameter [mg/L]	Lake water	Sand filtrate	UF permeate	Toilet flushing
pH (n=36)	7.9±0.2	7.8±0.1	7.9±0.3	6 - 9
COD (n=20)	11±8	10±8	n.a.	-
BOD_5	n.a.	n.a.	n.a.	<10
TDS (n=36)	921±86	940±79	934±85	<1500
Turbidity (NTU) (n=36)	0.6±0.2	0.2±0.1	0.07±0.01	<5
NH_4-N (n=9)	0.8±0.9	0.6±0.9	0.5±0.8	<10
Total coliform [n/L] (n=19)	7000±4500	2000±1700	<3	<3
Residual chlorine		Without chlorination		>1 mg/L after 30 min chlorination
				>0.2 mg/L at point of use
UV_{254} [1/m] (n=22)	6.4±1.3	5.5±1.0	5.4±1.6	-
UV_{436} [1/m] (n=22)	24±15	20±13	17±13	- (colour 30 mg/L Pt)

8.4 CONCLUSIONS

- The Beijing pilot experiments have shown that the proposed reuse concept is a reasonable and feasible treatment option.
- The produced water quality is sufficient for scenic impoundment reuse (after phosphate removal) and urban reuse purposes (after membrane filtration).
- GFH adsorption shows high capacities for phosphate removal and its application produces effluents of very low phosphate concentrations for use in artificial lakes, thus preventing eutrophication.
- GFH material can be regenerated using sodium hydroxide solution, resulting in longer operation times of fixed-bed systems before the material needs to be replaced.
- Short term bank / bio-filtration prior to UF reduces the fouling potential by removing biopolymers, thus reducing the operational costs of UF membranes

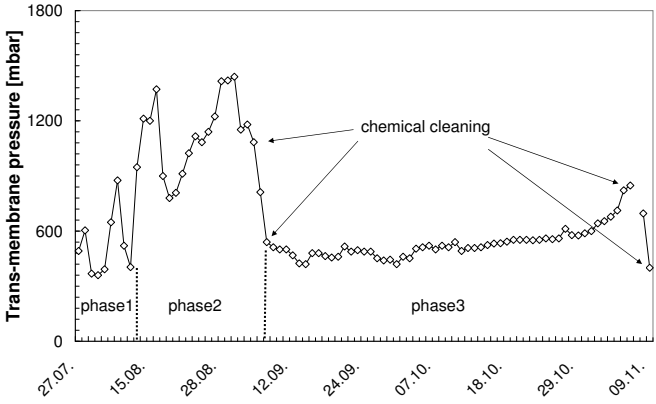

Figure 37: Trans-membrane pressure development during the experiment period in WWTP Beixiaohe (July 27th to November 09th 2005)

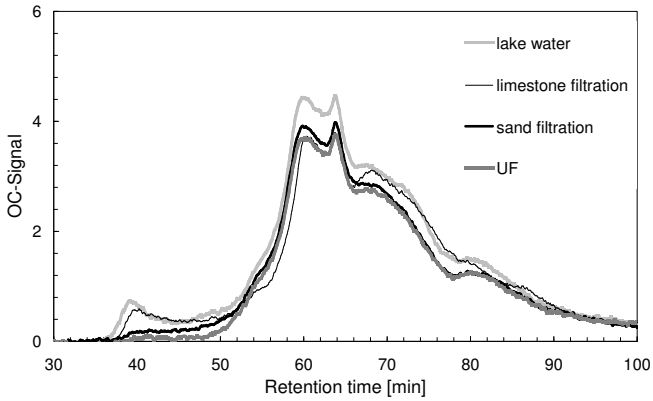

Figure 38: LC-OCD diagram of lake water, effluent after limestone and sand filtration and ultrafiltration permeate

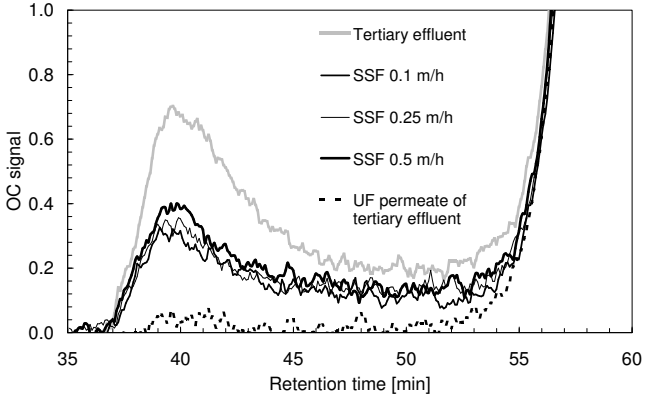

Figure 39: Bio-polymer peak of tertiary effluent, slow sand filtrates and UF permeate of tertiary effluent (WWTP Ruhleben) detected by LC-OCD

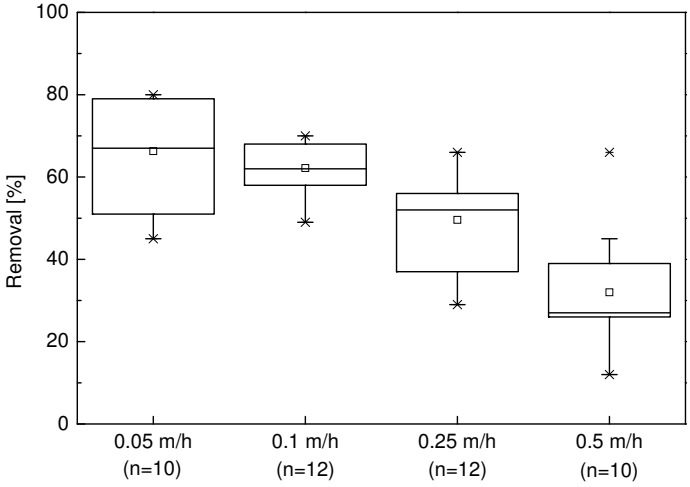

Figure 40: Biopolymer removal at different filtration rates (Nov. 2006 to May 2007 in WWTP Ruhleben)

9 GENERAL DISCUSSION

In the following, the results of the previous chapters are discussed in regard to their significance for the use of GFH adsorption as a treatment process for phosphate removal during advanced wastewater treatment. In this context, the suitability and the limits of this process alternative will be evaluated. Furthermore, a general procedure for the design of fixed-bed adsorbers will be developed and discussed.

9.1 GFH-PHOSPHATE ADSORPTION EQUILIBRIA IN DIFFERENT WATER MATRICES

Adsorption of phosphate onto GFH was studied and has shown high capacities of up to 24 mg/g P in the treatment relevant pH range 6-8. Phosphate adsorption onto GFH is strongly pH dependent: when pH was increased from 6 to 8, the observed capacities were approximately halved. This is typical for the adsorption of anions onto iron oxide surfaces near the pH_{PZC} [23]. Genz [56] observed phosphate adsorption onto GFH at pH values above the pH_{PZC} which confirms the strong affinity of phosphate to iron oxide surfaces, which has been described as ligand exchange [98]. This strong interaction is associated with a low influence of ionic strength on the adsorption equilibrium. These characteristics and hence the specific character of adsorption is confirmed by the significantly higher capacities observed in drinking and waste water as compared to DI water. Obviously, competitive adsorption of waste water constituents such as DOC is compensated by the presence of divalent cations which improves adsorption. The presence of calcium has been shown to strongly improve adsorption capacity and is supposed to be the main reason for higher capacities in drinking and waste water. Calcium may affect phosphate adsorption i) directly, through the formation of ternary surface complexes and ii) indirectly by changing the electrostatic properties of the surface, i.e. shifting the pH_{PZC} to higher values [23]. Regarding the nature of the interaction between phosphate and calcium adsorption onto iron oxides as well as the form of the phosphate surface complex, there is still debate in the scientific community [23, 81, 93, 94]. For clarification, studies involving advanced spectroscopic methods (FT-IR, EXAFS) are needed. However, the results of this study clearly show that phosphate adsorption onto GFH is a suitable process for advanced wastewater treatment and the wastewater matrix will not result in low capacities.

GFH phosphate adsorption from membrane concentrates shows lower capacities as compared to DI water. Competition of higher concentrations of DOC present in the membrane concentrate, the high ionic strength and lower initial phosphate concentrations lead to lower solid-phase concentrations. Although higher concentrations of calcium are also present, this cannot compensate for DOC competition. Since membrane concentrates are often supersaturated with respect to calcium carbonate and/or calcium phosphate compounds, this can lead to scaling and head loss in the fixed-bed column and GFH adsorption cannot be recommended for

membrane concentrate treatment. Chemical precipitation can effectively remove phosphorus and calcium ions and thus reduce the scaling potential of membrane concentrates. This may allow for higher recoveries in the NF/RO process.

9.2 ADSORBER DESIGN - FROM WATER QUALITY ANALYSIS TO BREAKTHROUGH PREDICTION

From an engineering point of view, a reliable prediction of operation time and thus breakthrough of GFH adsorbers based on easily accessible data is needed to design GFH fixed-bed columns. In figure 41, a general procedure for breakthrough prediction is shown. The traditional approach is a sequence of laboratory-scale experiments to determine the adsorption equilibrium (isotherm experiments) and mass transfer coefficients (DCBR/SFBR/CMBR experiments). Ultimately, the breakthrough of a GFH fixed-bed column can be predicted using mass transfer models, such as the homogeneous surface diffusion model (HSDM). In this study, breakthrough of arsenate, phosphate, salicylic acid and groundwater DOC could be predicted using models which already have been established for trace organic adsorption onto granular activated carbon. Breakthrough curves were experimentally determined and modeled using the HSDM and two of its derivatives, the constant pattern homogeneous surface diffusion model (CPHSDM) and the linear driving force model (LDF). Input parameters, the Freundlich isotherm constants, and mass transfer coefficients for liquid- and solid-phase diffusion were determined and analized for their influence on the shape of the breakthrough curve. HSDM simulation results predict the breakthrough of all investigated substances satisfactorily, but LDF and CPHSDM could not describe arsenate breakthrough correctly. This is due to a very slow intraparticle diffusion and hence higher Biot numbers. Based on this observation, limits of applicability were defined for LDF and CPHSDM. When designing fixed-bed adsorbers, model selection based on known or estimated Biot and Stanton numbers is possible. In addition, the determined isotherm data and mass transfer coefficients form the basis of a data base which can be used in future model simulations.

The knowledge of adsorption equilibrium data (isotherm constants or surface complexation constants) allows the calculation of the ideal (stoichiometric) breakthrough point, which describes the breakthrough if no mass transfer was present. It could be shown in this study that this procedure is viable for GFH adsorption and the determined ideal breakthrough points match the barycenters of experimentally determined breakthrough curves. Although GFH material was ground for isotherm experiments, batch equilibrium data are in agreement with capacities observed in fixed-bed column experiments and can provide a rough estimation of the breakthrough curve. The main drawback of this approach is the very slow mass transfer into the GFH particles which results in non-uniformely shaped breakthrough curves which deviate strongly from the ideal ones. It is possible to improve this prediction method by the determination of a correction factor based on dimensionless numbers which describes the deviation of the real BTC from the ideal BTC. In appendix B, the determination of these correction factors is shown.

Further research should aim on reducing the number of input parameters which have to be experimentally determined. A combination of models and database information for adsorbent, adsorbate, adsorption equilibrium data as well as mass transfer coefficients could enable prediction based on a water quality analysis for

the water to be treated, i.e. without experimental study. Surface complexation models are already used to describe the adsorption equilibrium of phosphate onto iron oxides. The diffused double layer model can in principle be used to describe phosphate adsorption onto GFH, but fails to describe simultaneous adsorption of phosphate and calcium. A number of more advanced SC models are available and further research is needed to improve surface complexation modeling of competitive adsorption of phosphate onto GFH. Kinetic parameters determined in this work could be used as the basis for a mass transfer coefficient database for GFH. Their validity under different conditions (pH, water matrix, etc.) has to be confirmed.

Future work should be directed to integrate SCM approaches into mass-transfer models (e.g., HSDM). Given the availability of mass transfer coefficients or their reliable estimation using known relationships, an integrated model could describe breakthrough curves using water quality data as input. The HSDM uses Freundlich isotherm coefficients as input parameters and the two partial differential equations in the HSDM are coupled by the Freundlich equation. Due to the non-linear coupling, an analytical solution is not available, but the equations have to be solved numerically. Introducing SCMs into the model would allow to eliminate this non-linearity and an analytical solution could be found, which would significantly reduce the calculation effort.

RSSCTs represent an alternative method to predict breakthrough of fixed-bed columns and have been shown to capture the shape of the breakthrough curve quite well. The constant diffusivity approach [24] has been found to be better suited to describe phosphate breakthrough in GFH adsorbers. In regard to a general procedure to design fixed-bed adsorbers, RSSCTs provide a powerful alternative, but require a significantly higher volume of water and time to produce results than batch isotherms. Given the limited breakthrough prediction strength of isotherms and the substantial experimental work to determine the input parameters for mass transfer models, RSSCTs might provide the preferred method for breaktrough prediction of GFH fixed-bed columns to date. Improved models could make breakthrough prediction less time consuming in the future.

9.3 OPERATION OF GFH FIXED-BED COLUMNS

Operation of two fixed-bed adsorbers at Beijing's wastewater treatment plant Beixiaohe was the first demonstration of GFH adsorption for phosphate removal from wastewater at larger than laboratory scale. In three months of pilot plant operation, a stable phosphate removal to less than 30 μg/L P was observed, despite very unstable influent concentrations and non-constant operation times. Appendix C shows strong variations of influent concentration and various shut-down periods. Nevertheless, effluent phosphate concentration were not detectable for $\approx$ 5000 BV and afterwards increased until breakthrough was reached at $\approx$ 12000 BV. Shortly after successfull regeneration, influent phosphate concentration decreased into the range of the target concentration due to operational changes in the WWTP plant. Due to the varying operational conditions, the pilot plant results cannot be compared to batch isotherm results or used for breakthrough simulation. Although influenced by operational problems upstream of the fixed-bed system, GFH operation was very stable and reliable. In GFH pilot tests for the surface water restoration of Lake Plötzensee [63, 70], algae growth on the adsorption

material caused head-loss of the filters and serious operational problems. In Beixiaohe, the adsorption columns were housed in a container, thus protected from light and similar problems were not observed. Also, the influent was filtered (turbidity $\approx$ 0.25 NTU) and a reduction by the GFH columns was not observed. The adsorbent material was backwashed after the initial filling of the columns, but did not require additional backwash in more than two months of operation until regeneration. During backwash, the low material strength of GFH led to abrasion and fine GFH particles were washed out. To avoid material loss, backwash of GFH fixed-bed columns should only be performed if head-loss is observed. If a low-turbidity influent is used, GFH adsorbers can be operated for several months. Handling of GFH adsorbers is easy and stable operation requires almost no maintenance. This is an advantage over phosphate precipitation where chemical addition, mixing, and solids separation make operation more complex. Further extended pilot-scale studies could provide more information about operational limits of GFH adsorption.

Operation of two GFH colums in series results in a more efficient use of the adsorbent. In RSSCT studies, 134 - 175 % higher specific throughputs were calculated for lead-lag design as compared to single adsorber design. A potential problem for GFH fixed-bed columns are anoxic conditions which might lead to dissolution of the material. Less relevant for wastewater applications, this problem might be more frequently encountered when GFH is used for surface water restoration. During pilot operation in Beixiaohe, no redox problems were observed. In the Lake Plötzensee pilot plant, high H_2S concentrations in the deep water of the lake led to formation of hardly soluble FeS_2 [70].

9.4 REGENERATION OF GFH

Regeneration and multiple application of GFH was investigated and shown to significantly increase operation times of fixed-bed adsorbers. GFH is stable at high pH and can be efficiently regenerated using 1 M NaOH. Batch and fixed-bed column studies show that approximately 80 % of the initially bound phosphate can be eluated. However, the incomplete desorption leads to decreasing capacities with each additional use. Multiple uses are thus limited, but at least three operation cycles are feasible. GFH desorption is fast and most of the desorbable phosphate could be eluated using 4 - 6 bed volumes of regenerant. A reuse of the regenerant solution is possible. Despite high phosphate concentrations in the regenerate, 61 - 85 % of the bound phosphate could be desorbed. A recovery of phosphate from the highly concentrated regenerant stream (up to 3.5 g/L P) is possible. Precipitation with lime water resulted in 90 % P removal and a plant available precipitate which might be used as a fertilizer. These results suggest that regeneration and multiple application of GFH can be an economically favourable option compared to single use.

9.5 FINAL REMARKS

The selection of the most suitable treatment process for a specific application is an engineering challenge and will always depend on the specific conditions of the application in question. Nonetheless, some general conclusions can be drawn regarding the suitability of GFH for phosphate removal. The main criteria for

process selection are costs, stability in terms of P retention and practicability of implementation.

GFH is an engineered, high-performance adsorbent, which is relatively expensive and offers high phosphate adsorption capacities. Competing phosphorus removal technologies include chemical precipitation, EBPR, and the use of low-cost adsorbents. The specific advantage of any fixed-bed adsorption processes is the ability to remove the target compound to near zero concentrations. In treatment scenarios which combine low influent concentrations and very low required effluent concentrations, GFH adsorption is the preferential treatment alternative. Low influent concentrations result in long operation times of GFH fixed-bed columns and thus lower adsorbent costs, which typically make up the majority of the total annual costs [95]. Operating cost estimations (Table 14) show that in low influent concentration (0.2 mg/L P) scenarios, GFH material costs amount to approx. 33 cents/ m^3. This is still considerably more than specific total costs of approx. 13 cents/ m^3 estimated for advanced P removal from surface waters by chemical precipitation/ filtration in Berlin [31]. Costs of chemical precipitation/ filtration of wastewater effluents are probably similar. Higher loads of influent phosphorus result in shorter operation times and thus higher adsorbent costs. In theses cases, chemical or biological phosphorus removal or the use of low-cost adsorbents will be the preferential alternative.

It was also shown that regeneration can increase operation times and reduce adsorbent costs to approx. 16 cents/ m^3 with almost negligible specific NaOH costs. However, operation complexity and investment costs will increase if storage tanks for NaOH as well as neutralization of spent caustic is considered. Operation of fixed-bed columns in series results in a more efficient use of the adsorbent. In low influent concentration scenarios with lead-lag design and regneration of spent material, specific adsorbent costs as low as 5 cents/ m^3 were estimated.

Other aspects to be considered when evaluating GFH adsorption as phosphate removal process include water quality parameters such as pH, redox potential, saturation, and turbidity. Lower pH values generally result in higher capacities and benefit GFH application. Although not relevant for treatment of most natural and waste waters, the limit is set at approx. pH 2, below which dissolution of GFH occurs. Adjustment of pH to improve capacities is possible but most probably not justified by the higher effort and costs needed for acid addition.

Instability under reducing conditions limits GFH application which especially has to be considered for surface water restoration applications, since anoxic conditions are frequently encountered in deep waters of eutrophic lakes. Supersaturated influents such as membrane concentrates can cause precipitation and head loss in the GFH filters and limit GFH application for this purpose. As for any adsorption process, low turbidity influents should be used for GFH fixed-bed systems. For wastewater applications, a conventional or membrane filtration step is therefore recommended prior to GFH adsorption.

These considerations limit potential application fields of GFH fixed-bed adsorption for phosphorus removal. GFH adsorption is not suited for use in municipal wastewater treatment plants to replace the widely used chemical precipitation and EBPR processes, since phosphorus influent concentrations and turbidity are high. However, the process is well suited to be used as a polishing step for effluents or side streams which require phosphorus removal to very low effluent concentrations. Chemical precipitation/ filtration prior to GFH polishing can ensure both

low influent turbidity and phosphorus concentration. Also, the easy handling and probably lower operating costs might be preferential to two-stage coagulation/filtration to achieve near zero effluent concentrations. Potential application fields include wastewater reuse in artificial lakes and advanced wastewater treatment for discharge into sensitive surface water bodies. GFH might also be used for restoration of eutrophic surface water bodies. Here, phosphorus loads can be quite high, but easy handling and no need for chemical addition or sludge disposal on site might be decisive points when selecting the suitable treatment technology. However, redox instability limits the use of GFH for anoxic deep water.

Interesting niche markets include nature oriented swimming pools as well as aquariums, where phosphorus concentrations need to be controlled and the easy handling of GFH overweights comparatively high price.

In conclusion, GFH adsorption is an effective and promising treatment technique to remove phosphorus from waste and surface waters. Economic use is limited to special applications where near zero effluent concentrations are required. Regeneration and serial operation prolonge operation times of fixed-bed columns and decrease the specific adsorbent costs.

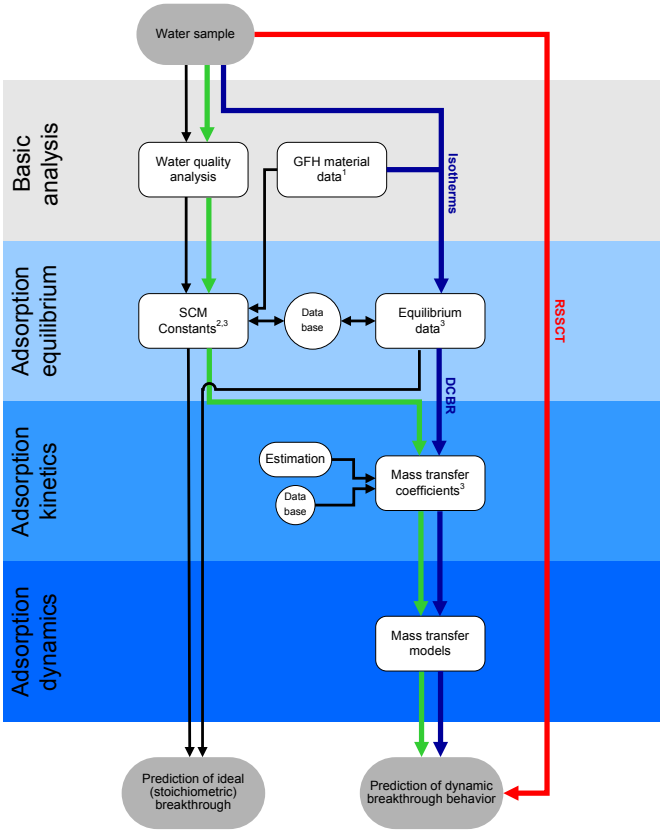

Figure 41: Procedure for breakthrough prediction of GFH fixed-bed adsorbers, and available input data from 1) Teermann [109], 2) Genz [56], 3) this work

APPENDIX

A

SUMMARY OF PHOSPHORUS ADSORBENTS AND THEIR PROPERTIES

Table 17: Summary of phosphorus adsorbents and their properties modified after Douglas et al. [34]

Adsorbent	Chemistry/ mineralogy	Occurrence	Phosphate uptake	Cost
Hydrotalcites	Double layer hydroxides, usually Mg and Al or Fe	Soils, synthetically prepared	High but with a strong pH dependence	Moderate to high
Allophane/ imogolite	Amorphous Al and Si with Al:Si ratio of approx. 1 : 1 - 2 : 1	Soils, synthetically prepared	High - strong pH dependence	Low (soils) to moderate (synthetic)
Iron oxides	Oxides/ hydrous oxides, e.g. goethite, ferrihydrite	Soils, synthetic, industrial waste	Low to high, depending on mineralogy	Low (waste material) to high (commercially produced)
Granular Ferric Hydroxide[1]	Akaganeite	Commercially produced	High	Moderate to high
Activated alumina	Al-oxide (Al_2O_3)	Commercially produced	High	High - synthesis and modification
Soils, sand, gravels	Generally contain Ca-, Fe- or Al-bearing minerals	Naturally occurring	Low to high depending on chemistry/ mineralogy	Generally low
Red mud	Complex Fe and Al oxides/ oxyhydroxides, hydrotalcites if modified	Waste product of alumina refining	Low to high, but depends on form and pretreatment	Low to moderate if pre-treated
Fly ash	Mullite, aluminosilicate glasses, zeolite, hydrotalcites if modified	Waste product of coal combustion	Low to moderate depending on chemistry and modification	Low to moderate if pre-treated
Expanded clay aggregates	Illitic clays and calcined carbonates	Industrially prepared by calcination	Low to moderate, related to Ca, Fe concentration	Moderate - industrial process
Blast/ arc furnace slag	Complex mineralogy of Ca, Fe oxides	Industrial (waste) by-product	Low to high, related to Ca, Fe concentration	Low as waste material
Rare earth modified clay	REE exchanged into high CEC clay	Synthetically prepared slurry	Moderate to high, depending on clay CEC	Moderate to high
Carbonates	Calcite, aragonite, dolomite etc.	Naturally and as industrial by-product	Low to high depending on form, surface area, etc.	Low (natural) to moderate (synthetic)

[1] this study

B

HSDM SIMULATION RESULTS DEPENDING ON ST AND BI

In the following, selected HSDM simulation results for different values of the dimensionless numbers Bi, St, and the Freundlich exponent n are shown. Simulated breakthrough curves are plotted as normalized effluent concentration c/c_0 vs. the dimensionless time coordinate T. Stoichiometric breakthrough corresponds to $T = 1$, thus correction factors for breakthrough prediction based on isotherm data can be derived as follows:

1. Estimation of St, Bi, and n for the adsorber to be designed,
2. Definition of a target breakthrough concentration c/c_0,
3. Determination of the value of T at the specific breakthrough concentration in the corresponding HSDM simulation.

The determined value of the dimensionless time coordinate value T can be directly used as a correction factor for stoichiometric breakthrough estimates.

Moreover, the plots show the influence of Bi, St, and n on the shape of the breakthrough curve and can thus be helpful when designing fixed-bed columns.

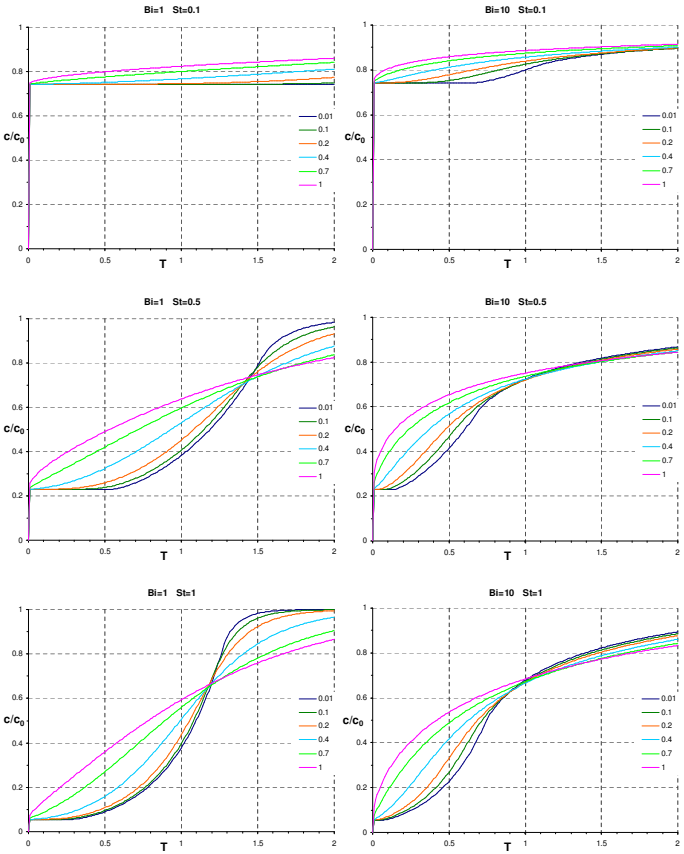

Figure 42: HSDM simulation results for Bi (1,10), St (0.1,0.5,1), and n (0.01,0.1,0.2,0.4,0.7,1)

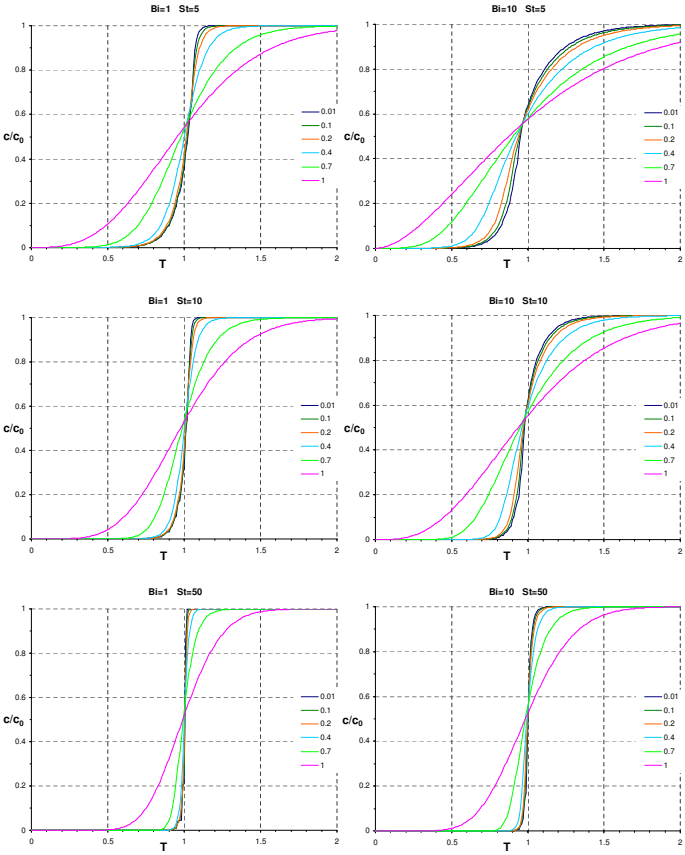

Figure 43: HSDM simulation results for Bi (1,10), St (5,10,50), and n (0.01,0.1,0.2,0.4,0.7,1)

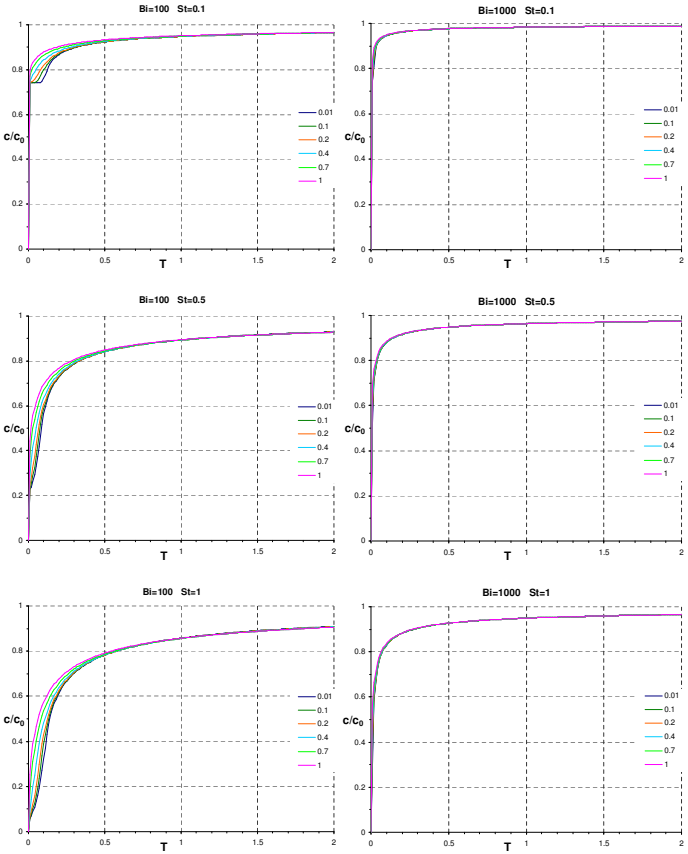

Figure 44: HSDM simulation results for Bi (100,1000), St (0.1,0.5,1), and n (0.01,0.1,0.2,0.4,0.7,1)

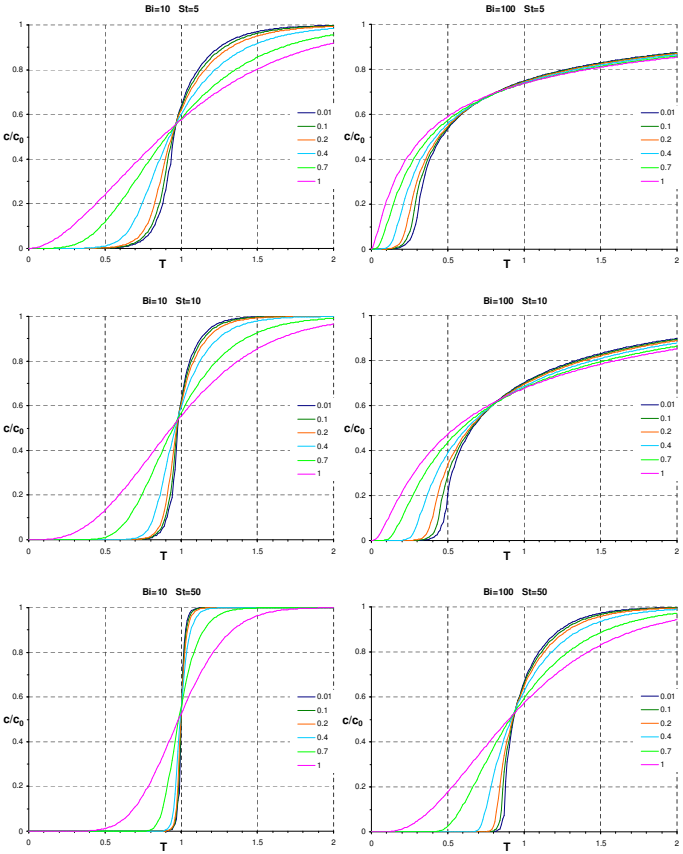

Figure 45: HSDM simulation results for Bi (100,1000), St (5,10,50), and n (0.01,0.1,0.2,0.4,0.7,1)

C

GFH FIXED-BED COLUMN OPERATION DATA FROM WWTP BEIXIAOHE

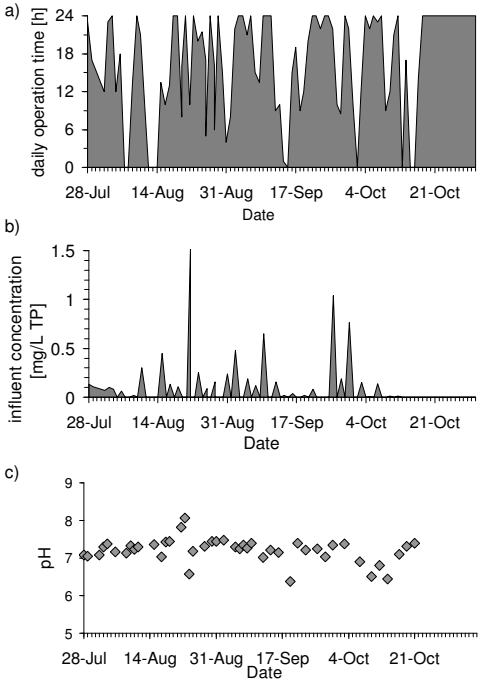

Figure 46: Daily operation time (a), phosphate influent concentration (b), and pH (c) during pilot operation of two GFH fixed-columns at the WWTP Beixiaohe

BIBLIOGRAPHY

[1] EN ISO 15681-1. Water quality - Determination of orthophosphate and total phosphorus contents by flow analysis (FIA and CFA) - Part 1: Method by flow injection analysis (FIA) (ISO 15681-1:2003), 2004.

[2] C. A. J. Appelo, M. J. J. Van der Weiden, C. Tournassat, and L. Charlet. Surface complexation of ferrous iron and carbonate on ferrihydrite and the mobilization of arsenic. *Environmental Science & Technology*, 36(14):3096–3103, 2002.

[3] Takashi Asano. *Water reuse issues, technologies, and applications*. McGraw-Hill, New York, 2007.

[4] ATV-DVWK. Bericht der ATV-DVWK Arbeitsgruppe Ak-1.1 Phosphorrückgewinnung. *Korrespondenz Abwasser*, 6, 2003.

[5] AWWA. *Standards Methods for the Examination of Water and Wastewater*. 20th edition, 1998.

[6] AWWA. Membrane Processes, AWWA Membrane Technology Research Committee Report. *Journal American Water Works Association*, 90(6):91–105, 1998.

[7] L. Axe and P. Trivedi. Intraparticle surface diffusion of metal contaminants and their attenuation in microporous amorphous Al, Fe, and Mn oxides. *Journal Of Colloid And Interface Science*, 247(2):259–265, 2002.

[8] M. Badruzzaman, P. Westerhoff, and D. R. U. Knappe. Intraparticle diffusion and adsorption of arsenate onto granular ferric hydroxide (GFH). *Water Research*, 38(18):4002–4012, 2004.

[9] C. Bahr. GEH Wasserchemie, Personal Communication, 2010.

[10] BDG. Research on environment safety and technology of reclaimed water supply for Olympic Park. Technical report, Beijing Drainage Group CO., LTD, 2005.

[11] H. Behrendt, D. Opitz, and M. Klein. Zielvorgaben für die Nährstoffbelastung von Spree und Havel aus gewässerökologischer Sicht. *Archives of Nature Conservation and Landscape Research*, 35:329–347, 1997.

[12] U. Berg, D. Donnert, P. G. Weidler, E. Kaschka, G. Knoll, and R. Nueesch. Phosphorus removal and recovery from wastewater by tobermorite-seeded crystallisation of calcium phosphate. *Water Science and Technology*, 53(3): 131–138, 2006.

[13] L. L. Blackall, G. Crocetti, A. M. Saunders, and P. L. Bond. A review and update of the microbiology of enhanced biological phosphorus removal in wastewater treatment plants. *Antonie Van Leeuwenhoek International Journal of General and Molecular Microbiology*, 81(1-4):681–691, 2002.

[14] L. M. Blaney, S. Cinar, and A. K. SenGupta. Hybrid anion exchanger for trace phosphate removal from water and wastewater. *Water Research*, 41(7): 1603–1613, 2007.

[15] R. Bond. Desalination with Zero Liquid Discharge. In *AWWA Water Quality Technology Conference*, Denver, 2006.

[16] J. W. Bowden, S. Nagarajah, N. J. Barrow, A. M. Posner, and J. P. Quirk. Describing the Adsorption of Phosphate, Citrate and Selenite on a Variable-Charge Mineral Surface. *Australian Journal of Soil Research*, 18(1):49–60, 1980.

[17] Stephen Brunauer, P. H. Emmett, and Edward Teller. Adsorption of Gases in Multimolecular Layers. *J. Am. Chem. Soc.*, 60(2):309–319, 1938.

[18] D. Bryant. The Chemistry of phosphorus. In E. Valsami-Jones, editor, *Phosphorus in Environmental Technology*. IWA Publishing, London, 2004.

[19] Ramesh Chitrakar, Satoko Tezuka, Akinari Sonoda, Kohji Sakane, Kenta Ooi, and Takahiro Hirotsu. Phosphate adsorption on synthetic goethite and akaganeite. *Journal of Colloid and Interface Science*, 298(2):602, 2006.

[20] Ingrid Chorus and Jamie Bartram. *Toxic cyanobacteria in water: a guide to their public health consequences, monitoring, and management*. E & FN Spon, London ; New York, 1999.

[21] P. Cooper, M. Day, and V. Thomas. Process Options for Phosphorus and Nitrogen Removal from Waste-Water. *Journal of the Institution of Water and Environmental Management*, 8(1):84–92, 1994.

[22] P. Cornel and C. Schaum. Phosphorus recovery from wastewater: needs, technologies and costs. *Water Science and Technology*, 59(6):1069–1076, 2009.

[23] R. M. Cornell and Udo Schwertmann. *The iron oxides: structure, properties, reactions, occurrences, and uses*. Wiley-VCH, Weinheim, 2nd, completely rev. and extended edition, 2003.

[24] J. C. Crittenden, J. K. Berrigan, and D. W. Hand. Design Of Rapid Small-Scale Adsorption Tests For A Constant Diffusivity. *Journal Water Pollution Control Federation*, 58(4):312–319, 1986.

[25] J. C. Crittenden, J. K. Berrigan, D. W. Hand, and B. Lykins. Design Of Rapid Fixed-Bed Adsorption Tests For Nonconstant Diffusivities. *Journal Of Environmental Engineering-Asce*, 113(2):243–259, 1987.

[26] J.C. Crittenden, P.S. Reddy, H. Arora, J. Trynoski, D.W. Hand, D.L. Perram, and R.S. Summers. Predicting GAC performance with rapid small-scale column tests. *Journal American Water Works Association*, 83(1):77–87, 1991.

[27] John C. Crittenden and Montgomery Watson Harza (Firm). *Water treatment principles and design*. John Wiley, Hoboken, N.J., 2nd edition, 2005.

[28] J. A. Davis and J. O. Leckie. Surface Ionization and Complexation at Oxide-Water Interface .2. Surface Properties of Amorphous Iron Oxyhydroxide and Adsorption of Metal-Ions. *Journal of Colloid and Interface Science*, 67(1):90–107, 1978.

[29] E. A. Deliyanni, E. N. Peleka, and N. K. Lazaridis. Comparative study of phosphates removal from aqueous solutions by nanocrystalline akaganeite and hybrid surfactant-akaganeite. *Separation And Purification Technology*, 52 (3):478–486, 2007.

[30] F. H. Denison, P. M. Haygarth, W. A. House, and A. W. Bristow. The measurement of dissolved phosphorus compounds: Evidence for hydrolysis during storage and implications for analytical definitions in environmental analysis. *International Journal of Environmental Analytical Chemistry*, 69(2): 111–123, 1998.

[31] A. Dietze. *Oberflächenwasseraufbereitung durch Membranfiltration*. Dissertation, Technische Universität Berlin, 2003.

[32] John Doherty. PEST - Model-Independent Parameter Estimation, 2004.

[33] D. Donnert and M. Salecker. Elimination of phosphorus from municipal and industrial waste water. *Water Science and Technology*, 40(4-5):195–202, 1999.

[34] G.B. Douglas, M.S. Robb, D.N. Coad, and P.W. Ford. A review of solid phase adsorbents for the removal of phosphorus from natural and waste waters. In E. Valsami-Jones, editor, *Phosphorus in Environmental Technology*. IWA Publishing, London, 2004.

[35] W. Driehaus. Arsenic removal - Experience with the GEH process in Germany. *Water Supply*, 2(2):275–280, 2002.

[36] W. Driehaus. *Arsenentfernung mit Mangandioxid und Eisenhydroxid in der Trinkwasseraufbereitung*. Dissertation. VDI Fortschrittsberichte Reihe 15 Nr. 133, Dissertation, Technische Universität Berlin, 1994.

[37] W. Driehaus and M. Jekel. Determination of As(III) and total inorganic arsenic by on-line pretreatment in hydride generation atomic absorption spectrometry. *Fresenius J Anal Chem*, 343:352–356, 1992.

[38] W. Driehaus, M. Jekel, and U. Hildebrandt. Granular ferric hydroxide - a new adsorbent for the removal of arsenic from natural water. *Journal of Water Supply Research and Technology-Aqua*, 47(1):30–35, 1998.

[39] A. Drizo, C. A. Frost, J. Grace, and K. A. Smith. Physico-chemical screening of phosphate-removing substrates for use in constructed wetland systems. *Water Research*, 33(17):3595–3602, 1999.

[40] D. A. Dzombak and F. M. Morel. *Surface complexation modeling: hydrous ferric oxide*. John Wiley & Sons, New York, 1990.

[41] EEA. Europe's environment: the second assessment. Technical report, 1998.

[42] U.S. EPA. Nutrient Criteria Technical Guidance Manual: Rivers and Streams, 2000.

[43] U.S. EPA. Nutrient Criteria Technical Guidance Manual: Lakes and Reservoirs, 2000.

[44] M. Ernst, A. Sperlich, X. Zheng, Y. Gan, J. Hu, X. Zhao, J. Wang, and M. Jekel. An integrated wastewater treatment and reuse concept for the Olympic Park 2008, Beijing. *Desalination*, 202(1-3):293, 2007.

[45] EU. Council Directive (91/271/EEC) concerning urban waste-water treatment, 1991.

[46] EU. Council Directive (99/31/EC) on the landfill of waste, 1999.

[47] EU. Regulation (EC) No 2003/2003 of the European Parliament and of the Council of 13 October 2003 relating to fertilisers, OJ L 304, p. 123, 2003.

[48] A.M. Farmer. Phosphate pollution: a global overview of the problem. In E. Valsami-Jones, editor, *Phosphorus in Environmental Technology*. IWA Publishing, London, 2004.

[49] J. Fettig. Modelling the uptake of natural organic matter (NOM) by different granular sorbent media. *Journal Of Water Supply Research And Technology-Aqua*, 54(2):83–93, 2005.

[50] G.M. Filipelli. The Global Phosphorus Cycle. In M.J. Kohn, editor, *Phosphates - Geochemical, Geobiological, and Materials Importance*, volume 48. Mineralogical Society of America, Washington, DC, 2002.

[51] H. Freundlich. Über die Adsorption in Lösungen. *Zeitschrift für physik. Chemie*, 57:385–470, 1906.

[52] Mark Gallagher and John Doherty. Parameter estimation and uncertainty analysis for a watershed model. *Environmental Modelling & Software*, 22(7): 1000–1020, 2007.

[53] Yan Gao and Alfonso Mucci. Individual and competitive adsorption of phosphate and arsenate on goethite in artificial seawater. *Chemical Geology*, 199(1-2):91, 2003.

[54] J. S. Geelhoed, T. Hiemstra, and W. H. Van Riemsdijk. Phosphate and sulfate adsorption on goethite: Single anion and competitive adsorption. *Geochim. Cosmochim. Acta*, 61(12):2389–2396, 1997.

[55] Hülya Genç-Fuhrman, Peng Wu, Yushan Zhou, and Anna Ledin. Removal of As, Cd, Cr, Cu, Ni and Zn from polluted water using an iron based sorbent. *Desalination*, 226(1-3):357–370, 2008.

[56] A. Genz. *Entwicklung einer neuen Adsorptionstechnik zur Entfernung natürlicher Organika mit granuliertem Eisenhydroxid*. Dissertation, Technische Universität Berlin, 2005.

[57] A. Genz, A. Kornmüller, and M. Jekel. Advanced phosphorus removal from membrane filtrates by adsorption on activated aluminium oxide and granulated ferric hydroxide. *Water Research*, 38(16):3523–3530, 2004.

[58] A. Genz, B. Baumgarten, M. Goernitz, and M. Jekel. NOM removal by adsorption onto granular ferric hydroxide: Equilibrium, kinetics, filter and regeneration studies . *Water Research*, 42(1-2):238–248, 2008.

[59] E. Glueckauf. Theory of Chromatography .10. Formulae for Diffusion into Spheres and Their Application to Chromatography. *Transactions of the Faraday Society*, 51(11):1540–1551, 1955.

[60] V. Gnielinski. Gleichungen zur Berechnung des Wärme- und Stoffaustausches in durchströmten ruhenden Kugelschüttungen bei mittleren und großen Pecletzahlen. *Verfahrenstechnik*, 12(6):363–367, 1978.

[61] R. Gnirss, B. Lesjean, C. Adam, and H. Buisson. Cost effective and advanced phosphorus removal in membrane bioreactors for a decentralised wastewater technology. *Water Science And Technology*, 47(12):133–139, 2003.

[62] A. E. Greenberg, G. Klein, and W. J. Kaufman. Effect of Phosphorus on the Activated Sludge Process. *Sewage and Industrial Wastes*, 27(3):277–282, 1955.

[63] D. Güssbacher and M. Klein. Nachhaltige Sanierung eines übernutzten Badegewässers am Beispiel Plötzensee in Berlin-Wedding. *Wasserwirtschaft Wassertechnik*, 1:29–35, 1997.

[64] D. W. Hand, J. C. Crittenden, and W. E. Thacker. Simplified Models For Design Of Fixed-Bed Adsorption Systems. *Journal Of Environmental Engineering-Asce*, 110(2):440–456, 1984.

[65] B. Hansen. Long-term plan seeks to reduce phosphorus in Spokane River. *Civil Engineering*, 76(10):24–25, 2006.

[66] S. G. J. Heijman, H. Guo, S. Li, and J. C. van Dijk. Zero liquid discharge: 99 In *7. Aachener Tagung Wasser und Membranen (AWM)*, Aachen, 2007.

[67] T. Hiemstra and W. H. VanRiemsdijk. A surface structural approach to ion adsorption: The charge distribution (CD) model. *Journal of Colloid and Interface Science*, 179(2):488–508, 1996.

[68] Herbert Hohl and Werner Stumm. Interaction of Pb2+ with hydrous [gamma]-Al2O3. *Journal of Colloid and Interface Science*, 55(2):281, 1976.

[69] Z. Hongshao and R. Stanforth. Competitive adsorption of phosphate and arsenate on goethite. *Environ. Sci. Technol.*, 35:4753–4757, 2001.

[70] M. Hupfer and B. Scharf. Seentherapie: Interne Maßnahmen zur Verminderung der Phosphorkonzentration. In Steinberg, Calmano, Klapper, and Wilken, editors, *Handbuch Angewandte Limnologie/*, pages 1–67. ecomed-Verlag, Landsberg, 2002.

[71] ICIS. ICIS pricing chemical price reports (January 29th, 2010), February 22nd, 2010 2010.

[72] IFA. Fertilizer Consumption Statistics. Technical report, 2002.

[73] ILEC/Lake Biwa Research Institute. Survey of the State of the World's Lakes. Technical report, International Lake Environment Committee, Otsu and United Nations Environment Programme, 1988-1993.

[74] C. Jarusutthirak, G. Amy, and D. Foss. Potable reuse of wastewater effluent through an integrated soil aquifer treatment (SAT) - membrane system. *Water Science and Technology: Water Supply*, 3(3):25–33, 2003.

[75] M. Jekel, A. Genz, and U. Stindt. Studies on phosphorus removal from fresh and sea water by commercial sorbents. Technical report, TU Berlin, Chair of Water Quality Control., 2002.

[76] L. Johansson. Industrial by-products and natural substrata as phosphorus sorbents. *Environmental Technology*, 20(3):309–316, 1999.

[77] R. Kümmel and E. Worch. *Adsorption aus wässrigen Lösungen*. Dt. Verl. für Grundstoffindustrie, Leipzig, 1. aufl. edition, 1990.

[78] C. N. Laabs, G. L. Amy, and M. Jekel. Understanding the Size and Character of Fouling-Causing Substances from Effluent Organic Matter (EfOM) in Low-Pressure Membrane Filtration. *Environ. Sci. Technol.*, 40(14):4495–4499, 2006.

[79] Irving Langmuir. The adsorption of gases on plane surfaces of glass, mica and platinum. *Journal of the American Chemical Society*, 40(9):1361–1403, 1918.

[80] L. Li and R. Stanforth. Distinguishing adsorption and surface precipitation of phosphate on goethite (a-FeOOH). *J. Colloid Interface Sci.*, 230:12–21, 2000.

[81] J. S. Loring, M. H. Sandstrom, K. Noren, and P. Persson. Rethinking Arsenate Coordination at the Surface of Goethite. *Chemistry-a European Journal*, 15(20): 5063–5072, 2009.

[82] B. A. Manning and S. Goldberg. Modeling competitive adsorption of arsenate with phosphate and molybdate on oxide minerals. *Soil Science Society of America Journal*, 60(1):121–131, 1996.

[83] B. D. Martin, S. A. Parsons, and B. Jefferson. Removal and recovery of phosphate from municipal wastewaters using a polymeric anion exchanger bound with hydrated ferric oxide nanoparticles. *Water Science and Technology*, 60(10):2637–2645, 2009.

[84] M. Maurer and M. Boller. Modelling of phosphorus precipitation in wastewater treatment plants with enhanced biological phosphorus removal. *Water Science And Technology*, 39(1):147–163, 1999.

[85] K. Moeller and J. Burgschweiger. Wasserversorgungskonzept für Berlin und für das von den Berliner Wasserbetrieben versorgte Umland (Entwicklung bis 2040). Technical report, Berliner Wasserbetriebe, 2008.

[86] M. M. Nederlof, J. A. M. van Paassen, and R. Jong. Nanofiltration concentrate disposal: experiences in The Netherlands. *Desalination*, 178(1-3):303, 2005.

[87] Adrian Oehmen, Paulo C. Lemos, Gilda Carvalho, Zhiguo Yuan, Jürg Keller, Linda L. Blackall, and Maria A. M. Reis. Advances in enhanced biological phosphorus removal: From micro to macro scale. *Water Research*, 41(11): 2271–2300, 2007.

[88] H. Ohashi, T. Sugawara, K. Kikuchi, and H. Konno. Correlation of Liquid-Side Mass-Transfer Coefficient for Single Particles and Fixed-Beds. *Journal of Chemical Engineering of Japan*, 14(6):433–438, 1981.

[89] R. L. Parfitt and R. J. Atkinson. Phosphate Adsorption on Goethite (Alpha-FeOOH). *Nature*, 264(5588):740–742, 1976.

[90] R. L. Parfitt, R. J. Atkinson, and R. S. C. Smart. Mechanism of Phosphate Fixation by Iron Oxides. *Soil Science Society of America Journal*, 39(5):837–841, 1975.

[91] D. L. Parkhurst and C. A. J. Appelo. User's guide to PHREEQC (Version 2) - A computer program for speciation, batch-reaction, one-dimensional transport, and inverse geochemical calculations. Technical report, 1999.

[92] S. A. Parsons and T. Berry. Chemical phosphorus removal. In E. Valsami-Jones, editor, *Phosphorus in Environmental Technology*. IWA Publishing, London, 2004.

[93] P. Persson and L. Lövgren. Potentiometric and spectroscopic studies of sulfate complexation at the goethite-water interface. *Geochim. Cosmochim. Acta*, 60(15):2789–2799, 1996.

[94] Rene P. J. J. Rietra, Tjisse Hiemstra, and Willem H. van Riemsdijk. Interaction between Calcium and Phosphate Adsorption on Goethite. *Environmental Science & Technology*, 35(16):3369–3374, 2001.

[95] A. Ruhland and M. Jekel. Concept for an integrated evaluation of arsenic removal technologies: demonstrated in a case study. In *2nd World Water Congress: Drinking Water Treatment*, volume 2 of *Water Science and Technology: Water Supply*, pages 267–274. IWA Publishing, London, 2002.

[96] B. Saha, R. Bains, and F. Greenwood. Physicochemical characterization of granular ferric hydroxide (GFH) for arsenic(V) sorption from water. *Separation Science and Technology*, 40(14):2909–2932, 2005.

[97] SenStadt. Abwasserbeseitigungsplan Berlin. Technical report, Senatsverwaltung für Stadtentwicklung Berlin, 2001.

[98] L. Sigg and W. Stumm. The interactions of anions and weak acids with the hydrous goethite (a-FeOOH) surface. *Colloids and Surfaces*, 2(2):101–117, 1981.

[99] H. Sontheimer, J.C. Crittenden, and R.S. Summers. *Activated Carbon for Water Treatment*. DVGW-Forschungsstelle am Engler-Bunte-Institut der Universität Karlsruhe, Karlsruhe, 1988.

[100] A. Sperlich and M. Jekel. Phosphate adsorption onto granular ferric hydroxide: isotherm and fixed-bed column studies. *Water Science and Technology (submitted)*, 2010.

[101] A. Sperlich, A. Werner, A. Genz, G. Amy, E. Worch, and M. Jekel. Breakthrough behavior of granular ferric hydroxide (GFH) fixed-bed adsorption filters: modeling and experimental approaches. *Water Research*, 39(6):1190–1198, 2005.

[102] A. Sperlich, B. Baumgarten, A. Genz, M. Ernst, and M. Jekel. Kinetic Aspects of Arsenate and Phosphate Adsorption onto Granular Ferric Hydroxide (GFH). In *The 2nd International Conference on Environmental Science and Technology*, Houston, Texas, USA, 2006.

[103] A. Sperlich, S. Schimmelpfennig, B. Baumgarten, A. Genz, G. Amy, E. Worch, and M. Jekel. Predicting anion breakthrough in granular ferric hydroxide (GFH) adsorption filters. *Water Research*, 42(8-9):2073–2082, 2008.

[104] A. Sperlich, X. Zheng, M. Ernst, and M. Jekel. An integrated wastewater reuse concept combining natural reclamation techniques, membrane filtration and metal oxide adsorption. *Water Science and Technology*, 57(6):909–914, 2008.

[105] A. Sperlich, D. Warschke, C. Wegmann, M. Ernst, and M. Jekel. Treatment of membrane concentrates: phosphate removal and reduction of scaling potential. *Water Science and Technology*, 61(2):301–306, 2010.

[106] I. Steén. Phosphorus recovery in the context of industrial use. In E. Valsami-Jones, editor, *Phosphorus in Environmental Technology*. IWA Publishing, London, 2004.

[107] W. Stumm, C. P. Huang, and S. R. Jenkins. Specific Chemical Interaction Affecting Stability of Dispersed Systems. *Croatica Chemica Acta*, 42(2):223–245, 1970.

[108] George Tchobanoglous, Franklin L. Burton, H. David Stensel, and Metcalf & Eddy. *Wastewater engineering: treatment and reuse*. McGraw-Hill, Boston, 4th / edition, 2003.

[109] I. Teermann. *Untersuchungen zur Huminstoffadsorption an ß-Eisenoxidhydrat*. Dissertation, Technische Universität Berlin, 2000.

[110] I. Teermann and M. Jekel. Adsorption of humic substances onto ß-FeOOH and its chemical regeneration. *Wat. Sci. Tech.*, 40(9):199–206, 1999.

[111] I. Tejedor-Tejedor and A. M. Anderson. Protonation of phosphate on the surface of goethite as studied by CIR-FTIR and electrophoretic mobility. *Langmuir*, 6:602–611, 1989.

[112] S. Thole. *Verwertung von eisenhaltigen Wasserwerksschlämmen zur Phosphatelimination aus kommunalem Abwasser*. Dissertation. VDI Fortschritts-Berichte Reihe 15 Nr. 117, Dissertation, Technische Universität Berlin, 1993.

[113] S. Thole, M. Borho, G. Voswinckel, and M. Jekel. Einfluß der Wassermatrix auf die Adsorption von Phospat an Eisenhydroxid und Wasserwerksschlamm. *Vom Wasser*, 79:313–321, 1992.

[114] M. Thomas, P. Wright, L. Blackall, V. Urbain, and J. Keller. Optimisation of Noosa BNR plant to improve performance and reduce operating costs. *Water Science and Technology*, 47(12):141–148, 2003.

[115] J. Torrent, V. Barron, and U. Schwertmann. Phosphate Adsorption and Desorption by Goethites Differing in Crystal Morphology. *Soil Science Society of America Journal*, 54(4):1007–1012, 1990.

[116] G. A. Tularam and M. Ilahee. Environmental concerns of desalinating seawater using reverse osmosis. *Journal Of Environmental Monitoring*, 9(8): 805–813, 2007.

[117] UBA. *Grundsätze und Maßnahmen für eine vorsorgeorientierte Begrenzung von Schadstoffeinträgen in landbaulich genutzten Böden*. Umweltbundesamt Texte 59-01. Berlin, 2001.

[118] E. Valsami-Jones. The geochemistry and mineralogy of phosphorus. In E. Valsami-Jones, editor, *Phosphorus in Environmental Technology*. IWA Publishing, London, 2004.

[119] E. Van Houtte and J. Verbauwhede. Operational experience with indirect potable reuse at the Flemish Coast. *Desalination*, 218(1-3):198–207, 2008.

[120] R. Vollenweider and J. Kerekes. Eutrophication of waters, monitoring, assessment, control. Technical report, Organisation for Economic Co-operation and Development (OECD), 1982.

[121] Jiansen Wang, Yonghui Song, Peng Yuan, Jianfeng Peng, and Maohong Fan. Modeling the crystallization of magnesium ammonium phosphate for phosphorus recovery. *Chemosphere*, 65(7):1182–1187, 2006.

[122] GEH Wasserchemie. GEH 102 - Technical Information 1, 2008.

[123] J. Westall and W. Schecher. MINEQL+ 4.50, 2001.

[124] C. R. Wilke and P. Chang. Correlation of Diffusion Coefficients in Dilute Solutions. *Aiche Journal*, 1(2):264–270, 1955.

[125] J. A. Wilsenach, C. A. H. Schuurbiers, and M. C. M. van Loosdrecht. Phosphate and potassium recovery from source separated urine through struvite precipitation. *Water Research*, 41(2):458–466, 2007.

[126] E. J. Wilson and C. J. Geankoplis. Liquid mass transfer at very low Reynolds numbers in packed beds. *Ind. Eng. Chem. Fundamentals*, 5:126–129, 1966.

[127] E. Worch. Fixed-bed adsorption in drinking water treatment: a critical review on models and parameter estimation. *Journal Of Water Supply Research And Technology-Aqua*, 57(3):171–183, 2008.

[128] E. Worch. Eine neue Gleichung zur Berechnung von Diffusionskoeffizienten gelöster Stoffe. *Vom Wasser*, 18:289–297, 1993.

[129] W. S. Yao and F. J. Millero. Adsorption of phosphate on manganese dioxide in seawater. *Environmental Science & Technology*, 30(2):536–541, 1996.

[130] X. Zheng, R. Mehrez, M. Jekel, and M. Ernst. Bio-filtration of treated domestic wastewater as a pre-treatment to ultrafiltration: effects on protein and polysaccharide related fouling. In *4th IWA International Membranes Conference*, Harrogate, UK, 2007.

[131] X. P. Zhu and A. Jyo. Column-mode phosphate removal by a novel highly selective adsorbent. *Water Research*, 39(11):2301–2308, 2005.